AD-A073 527 DEFENSE ATOMIC SUPPORT AGENCY WASHINGTON DC F/G 18/3

OPERATIONS NOUGAT AND STORAX IN SITU STRESSES IN ROCK, RAINIER --ETC(U)

SEP 64 L OBERT

UNCLASSIFIED DASA-WT-1869 NL

1 OF 2

AD A073527

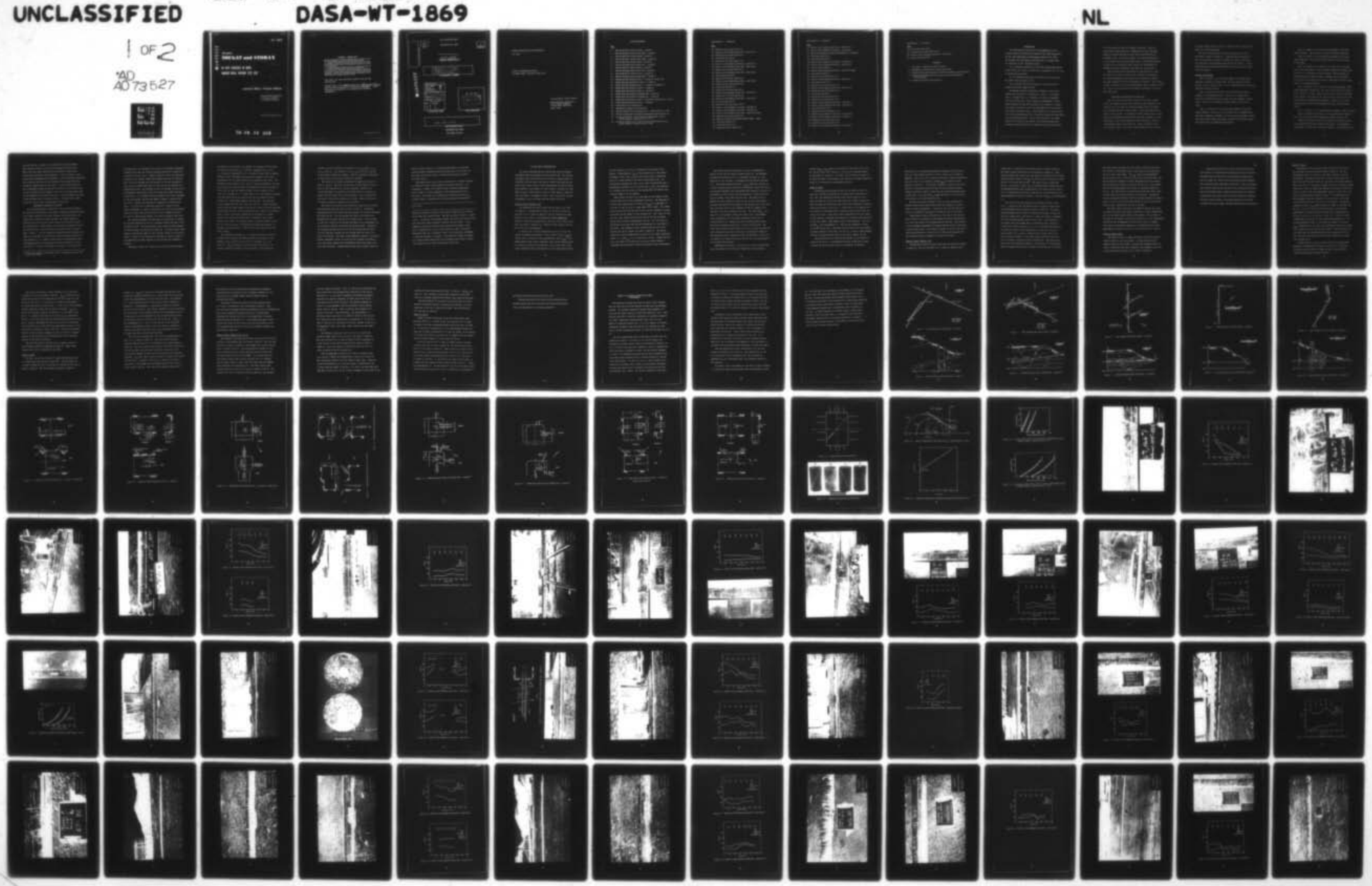

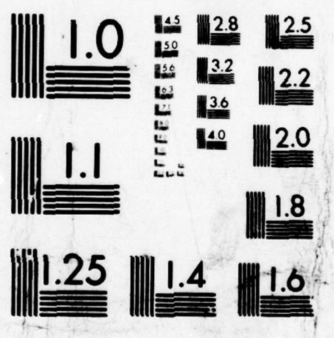

MICROCOPY RESOLUTION TEST CHART

NATIONAL BUREAU OF STANDARDS-1963-A

WT-1869

Operations

NOUGAT and STORAX

IN SITU STRESSES IN ROCK, RAINIER MESA, NEVADA TEST SITE

Leonard Obert, Project Officer

Applied Physics Laboratory
U. S. Bureau of Mines
College Park, Maryland

Issuance Date: September 11, 1964

This report has been reproduced directly from the best available copy.

Printed in USA. Price ~~$2.25~~ Available from the Clearing → now "NTIS" house for Federal Scientific and Technical Information National Bureau of Standards, U. S. Department of Commerce, Springfield, Va.

USAEC Division of Technical Information Extension, Oak Ridge, Tennessee

DATA PROCESSING SHEET

PHOTOGRAPH THIS SHEET

II

LEVEL

1

INVENTORY

DDC ACCESSION NUMBER

AD A073527

WT-1869

DOCUMENT IDENTIFICATION

DISTRIBUTION STATEMENT A

Approved for public release;
Distribution Unlimited

DISTRIBUTION STATEMENT

Accession For	
NTIS GRA&I	☒
DDC TAB	☐
Unannounced	☐
Justification per ltr. on File	
By	
Distribution/	
Availability Codes	
Dist.	Avail and/or special
A	

DISTRIBUTION STAMP

DDC
RECEIVED
SEP 6 1979
E

DATE ACCESSIONED

see Doc. cover

DATE RECEIVED IN DDC

PHOTOGRAPH THIS SHEET

AND RETURN TO DDA-2

OPERATION NOUGAT AND STORAX

WT-1869

IN SITU STRESSES IN ROCK, RAINIER MESA, NEVADA TEST SITE

Leonard Obert, Project Officer

Applied Physics Laboratory
U. S. Bureau of Mines
College Park, Maryland

April, 1964

ILLUSTRATIONS

Illustrations -- Continued

<u>Fig.</u>

Illustrations -- Continued

TABLES

INTRODUCTION

This investigation was made at the recommendation of the Lawrence Radiation Laboratory and funded by the Atomic Energy Commission under Memorandum of Understanding AT(29-2)-914, dated 14 September 1959 and amended by Modifications 9, December 1963. The objectives of this investigation were:

(1) To perform surveillance of the stress measurement made by Lucius Pitkin, Inc. (LPI), New York City, in Tunnels G, B, E, P, and N, Madison and Yuba Events;

(2) To determine the mechanical properties of the rock from the tunnel sites specified in (1);

(3) To analyze the results obtained in (1) and (2) and to prepare interim and summary reports.

The Lawrence Radiation Laboratory's interest in this investigation was specified in a telegram to L. Obert, O. H. Roehlke, and W. P. Bennett from J. E. Carothers, LRL, dated 12 September 1962, which stated that, "LRL's interest in measurements of overburden stresses with the APRL technique in our tunnels is to determine preshot conditions in the rock surrounding the shot rooms and at the massive concrete plugs. In the explosion of a nuclear device the cavity presumably grows until the pressure within the cavity falls to the overburden pressure. As the cavity vents into the tunnel, material will escape to the surface if the pressure exceeds the overburden pressure at the plug or between the shot room and plug,

or if the pressure exceeds the strength of the plug. With the limited data already available it appears that in situ overburden stresses in Rainier Mesa may be about those calculated from the lithostatic load. Our present interest is to have measurements of in situ stresses made in Rainier Mesa tunnels in sufficient quantity so that we can use the data to help improve our understanding of phenomena involved in effective containment of our explosions."

Interim letter reports dated March 4, 1963 and June 28, 1963 were sent to Dr. Roger G. Preston, LRL, reviewing the progress of the stress measurements made by LPI in which preliminary comments were made regarding the stress measurements in Tunnel G. This report includes an analysis of the stress measurements made in Tunnels G, B, E, P, and N, and also presents the mechanical properties of the rock from these sites.

SELECTION AND DESCRIPTION OF TEST SITES

The test sites were selected on the basis of several factors. First, and sometimes a factor that resulted in some compromise, the site had to be such that the drilling equipment would not interfer with the normal operation in the tunnel. Second, consideration was given to the rock type. An attempt was made to select areas in which the rock was relatively unfactured and reasonably competent. On the other hand, in the various tunnels an effort was made to include a representative range of the rock types. Third, usually one site was selected so that it was under a maximum depth of cover. Fourth,

the tunnel opening had to be of such a dimension that it would accommodate the drilling equipment.

The above conditions were reasonably satisfied at the sites indicated in figures 1 through 10. A detailed plan and section of each site are shown in figures 11 through 19, and the coordinates, floor elevation, and overburden depth are given in table 1. A brief description of the geology and petrology of each site is given below (from LPI report).

Geology and Petrology

Site 1 in tunnel G is in the lower member of the Indian Trail Formation of Miocene of Pliocene Age. The rock consists of moist zeolitic tuff or volcanic origin. It is a reddish-brown mass containing small white flecks of pumice.

Site 2 in tunnel G is in Bed A-3 of the Tertiary Oak Springs Formation - bottom member of TOS 3. The rock is a uniform red-brown tuff of uniform medium fine grain size with fragments of white pumice. The rock is wet-softer, and more shattered than that at site 1.

Site 1 in tunnel B is in the Survey Butte Member of the Piapi Canyon Formation. The rock is a soft, white tuff, non-welded vitric type with considerable jointing; it is fine grained and sandy, and contains black cherty nodules and larger inclusions of soft white pumice. The rock was wet, and indurated with moisture.

Site 2 in tunnel B is in the Survey Butte Member of the Piapi Canyon Formation. The tuff was soft, weak and severely fractured.

Site 3 in tunnel B is in the Survey Butte Member of the Piapi Canyon Formation. This rock was highly fractured, weak, and broke in thin discs.

Site 1 in tunnel E is in subunit H_2 of tunnel bed 4, the upper unit of the lower member of the Oak Springs Formation of Tertiary Age. The rock is a non-welded tuff with yellowish, zeolitized material, alternating with red patches giving a somewhat mottled appearance. It consists of fine lapilli sized pumice, phenocrysts and lithic fragments in a fine-grained matrix.

Site 1 of tunnel P is in subunit P-25 Survey Butte Member, Piapi Canyon Formation, Pliocene Age. The roof of this site was in subunit P-26. The rock is a hard, light tan vitric tuff, partially zeolitized and silcified. The grain size was fine to coarse, and the lower part of the walls was laminated white and brown. Subunit 26 is a soft, grayish green to white tuff interbedded with brown, gray and green chert.

Site 1 in tunnel N is in the Indian Trail Formation, Beds 3 or 4 (?).

Site 2 in tunnel N, main drift, is in the Indian Trail Formation bed. The rock is structurally bedded and contains zeolitic tuff.

Figures 11 through 19 also show the position and bearing of each of the stress-relief holes drilled at these sites. The designation and bearings of these holes are given in table 2. Not included in the

Plan and Sections, or table 2, are the NX and 5-5/8-inch diameter holes drilled to obtain solid cores for mechanical property tests. These cores were taken from holes drilled parallel to the stress-relief holes carrying the same designation. Of the 38 holes in which stress-relief measurements were attempted, 15 were considered nonfeasible, due to the fact that the rock was fractured to the degree that long enough core lengths could not be drilled. A part of this fracturing was of geological origin that naturally occurred in the rock and a part was due to either the low strength of the rock or the high stress level in the proximity of the stress relief hole. The low strength rock broke in some instances due to drilling vibration. The high stress levels caused the rock to "disc" as noted later in the report.

MECHANICAL PROPERTIES OF THE ROCK

The following mechanical properties of the tuff from the Madison and Yuba sites were measured: the uniaxial compressive strength (by LPI); the triaxial compressive and shear strength, the fracture angle, and coefficient of internal friction (by APL); the biaxial modulus of elasticity (by LPI); and the triaxial modulus of elasticity (by APL). The strength data, fracture angle, and coefficient of internal friction are given in table 1, and the biaxial and triaxial elastic property data, in table 2. The LPI compressive strength data were obtained from tests on 1D specimens cut from NX core using a procedure equivalent to that specified in U. S. Bureau of Mines Report of Investigations 3891, "Standardized Tests for Determining the Physical Properties of Mine Rock" (2).[1/] A total of 27 specimens were tested. The results show

1/ Underlined numbers in parentheses refer to references given at the end of this report.

that there was a 30 fold range in the inter-site unconfined compressive strength of the rock, the variation ranging from 402 psi in hole B-1-1 to 12,100 psi in hole P-1-2. However, except for Site P the intra-site variation in the uniaxial compressive strength was about ±20 percent. Thus, it can be concluded that the variation in the rock strength at a given site was comparatively small but the site-to-site variation was exceptionally large. The variation in the rock strength is even less if the sampling is restricted to that from a given hole rather than from a given site. It is probable that the strength of the tuff is dependent on the local geology, varying from member to member or possibly from bed to bed. However, the sampling was inadequate to establish this point. It should also be noted that there were a number of sites, termed non-feasible, in which a satisfactory core could not be obtained. The rock at these sites may have been even less competent than that at site B-1, which was the weakest of the rocks included in this test.

The triaxial strengths, fracture angle and coefficient of internal friction were measured by APL on 15 specimens selected and sent to the laboratory by LPI. The test equipment used in measuring the properties of these specimens are described by Obert (3). The axial stress, radial pressure, and fracture angle for each specimen, figure 20, are given in table 1. Three of the fractured test specimens are shown in figure 21. The compressive and shear strength of each specimen were obtained as follows:

Referring to figure 22; a Mohr's circle for the failure stresses

was drawn for each specimen, for example, for specimen N-1-4-28 inches the failure stresses were $\sigma_3 = 6{,}614$ psi, designated by σ_3'', and $p_o = 1{,}000$ psi, designated by σ_1''. The fracture angle θ was 37 degrees. A radius at $2\theta'' = 74$ degrees was drawn, and a tangent to the circle perpendicular to this radius (line AB) was extended to the τ-axis. The intercept of this tangent on the τ-axis is the shear strength of the rock ($S_o'' = 1{,}850$ psi), provided that the Coulomb-Navier theory of failure is valid, that is, that the tangent to Mohr's circle continues to the τ-axis as a straight line. A similar Mohr's circle was drawn for specimen N-1-4-260 inches (which was from the same hole as specimen N-1-4-28 inches) and a corresponding tangent (line CD) drawn. The intercept of this tangent with the τ-axis gives $S_o' = 950$ psi. A Mohr's straight line envelope was drawn tangent to the stress circles for the two specimens (line EF) and the value of the intercept with the τ-axis is $S_o = 1{,}000$ psi. Hence, a value of the shear strength can be obtained from a single triaxial test, although a better value is obtained if two or more specimens are tested. The envelope curve to a number of Mohr's circles may, for some rock types, curve downward and hence the intercept of a straight line envelope with a τ-axis will give the upper limit of the shear strength.

The compressive strength, C_o, of a triaxial specimen or group of specimens can be obtained by drawing a Mohr's circle tangent to the envelope, with σ_1 equal to zero, (which is equivalent to $p_o = 0$) figure 22. The σ_3 intercept of this circle with the σ-axis is the uniaxial compressive strength of the specimen(s). The compressive

strength can also be obtained by plotting on the $\sigma_1 \sigma_3$ plane, $p_o=\sigma_1$ and σ_3, figure 23. The intercept of the $\sigma_1 \sigma_3$ curve with the σ_3 axis is the uniaxial compressive strength. These two procedures should give the same values of the uniaxial compressive strength.

The values of the triaxial compressive strength C_o' are given in table 3, column 9. Note that the variation in these values is not as great as that obtained by the uniaxial procedure. However, the correlation between the uniaxial and triaxial values is such that it appears that the larger part of the difference is due to either local variations in the rock or specimen size or both. Again, the data are too meager to permit an appraisal of this effect.

The biaxial and triaxial secant modulus of elasticity of specimens from the Madison and Yuba sites are given in table 4. The biaxial measurements by LPI were made using the procedure and apparatus described by Fitzpatrick (1). In each specimen the modulus of elasticity was determined for two gage orientations 90 degrees apart. This was done to check the isotropy of the specimen (although the two measurements do not necessarily indicate the minimum and maximum values). Generally, the difference between the values of the two orientations was small and hence they were averaged and this average value was used in all stress calculations. The radial stress (hydraulic pressure = p_o) versus borehole deformation curves obtained from the specimens from tunnel G and P were linear, whereas the corresponding curves from tunnels B, E, and N were non-linear. Representative linear and non-linear curves are

shown in figures 24 and 25. In computing the modulus of elasticity from the borehole deformation data the secant slope of the curves was used, hence the biaxial modulus of elasticity data given in table 4 are secant values.

The maximum radial stress that can be applied to a biaxial specimen is limited by tensile strain strength in the axial direction. As a consequence, a number of the biaxial elastic constants measurements were not made at a stress comparable to that experienced by the in situ rock. This defect can be remedied by subjecting the cores to triaxial stress, a procedure that has been developed by Obert (4).[2]

2/ In press

Twenty-six specimens, similar to that shown in figure 21D, were tested by APL using the triaxial method. The data are given in table 4, columns 6 and 7. In general, the agreement between the biaxial and triaxial data were within the normal specimen-to-specimen variation range. If any difference existed the triaxial data usually gave the higher values. This is characteristic of the triaxial method as noted in the above-mentioned report and is probably a result of the additional confinement to which the specimen is subjected. The difference between the biaxial and triaxial secant modulii were not considered large enough to warrant any correction of the stress calculations made by LPI.

IN SITU STRESS DETERMINATIONS

The stress determinations were made by LPI using the borehole deformation-overcoring method described by Obert (5). The borehole deformation data, the procedure for selecting an average modulus of elasticity, and the stress calculations derived from these data are given in LPI reports titled, "Stress Measurements by Borehole Deformation Method in Tuff, Report No. 5608, Tunnel G, February 27, 1963; Tunnel B, May 7, 1963; Tunnel E, July 10, 1963; Tunnel N, August 12, 1963, and Tunnel P, September 9, 1963". These reports also include photographs of the cores taken from the various test sites.

Tunnel G, Site 1 (drift G .01)

The bearingsof the stress relief holes at Site G-1 are shown in figure 11. A representative section of the stress relief core from hole G-1-1 is shown in figure 26, and the secondary principal stresses S and T, that is, the maximum and minimum compressive stresses in the plane perpendicular to the axis of the stress relief hole, are given in figure 27 as a function of the distance from the face to the point of measurement.

In elastic rock a stress concentration occurs on or near the surface of underground openings. In this report the ratio S_{max}/S_{∞} will be used as a measure of this concentration, where S_{max} is the maximum value of the larger compressive stress (which usually occurs on or near the surface of the opening), and S_{∞} is the value of the larger compressive stress determined at a point sufficiently distant

from the opening so as not to be affected by the presence of the opening. Correspondingly, T_{max} is the maximum value of the smaller compressive stress, and T_{∞} is the value of the smaller compressive stress at a point outside of the stress concentration zone. The specification regarding the limit of the stress concentration zone is approximately satisfied if in an elastic rock S_{∞} and T_{∞} are measured at a distance from the surface of the opening twice the smaller cross sectional dimension of the opening.

These results from hole G-1-1 show that over the length of this hole the direction of S was approximately vertical. The magnitude of S varied from a maximum value of 1900 psi (S_{max}) at a gage depth of 20 inches, to 320 psi (S_{∞}) at a gage depth of 100 inches. This latter value is much lower than the value of the vertical component of stress calculated from the weight of the overlying rock. For a depth of 1180 feet and a unit weight for the rock of 120 lbs ft^3 the calculated gravity stress would be approximately 1075 psi. This low value was attributed to the fault zone that was intersected at a hole depth of 129 inches. The fragments of core recovered from the fault zone (between 129 and 150 inches) are shown in figure 28. The smaller compressive stress averaged about 50 percent of the larger compressive stress, i.e., $(S/T)_{av.} = 0.5$, a value that is normal. Between the face and a hole depth of 20 inches the rock was too badly fractured (presumably from blasting) to obtain satisfactory stress measurements.

The stress relief core from hole G-1-2 and a representative section of this core are shown in figures 29 and 30. The secondary principal stress data from G-1-2 is presented in figure 31. The direction of S was vertical, in agreement with the results from Hole G-1-1. The maximum compressive stress, S_{max}, (1670 psi) occurred at a point 30 inches from the surface of the opening, a value that also is in reasonable agreement with the maximum stress measured in hole G-1-1. S decreased with the distance from the opening to a value of 670 psi (S_{∞}) at a depth of 130 inches from the face. The latter value is greater than that obtained in hole G-1-1 but is still much smaller than that calculated from the weight of the overlying rock (1,075 psi). Thus, the stress field in the proximity of Site G-1 appears to be affected by the local geology in this area. The ratio $(T/S)_{av.}$ was about 0.6, a value that is within the normal range. The measured stress concentration for the larger compressive stress was 2.5 (1,675 psi/670 psi). Compared with the calculated gravity stress, the stress concentration would be 1.5 (1,670 psi/1,075 psi). The stress data from the vertical (down) hole G-1-3 is given in figure 32, and a representative section of the core is presented in figure 33. The maximum horizontal compressive stress (S) measured in hole G-1-3 at a depth of 40 inches from the face was 950 psi, and approximately in the north-south direction.

Summarizing the results from Site G-1, it can be concluded that near the surface of the opening the magnitudes of the secondary

stresses (S_{max}/, T_{max}) appear to be normal for the depth at this site, but that the stress field values (S_{∞}, T_{∞}) are low, presumably because of the effects of faulting in the area. The area does not appear to be under the effect of any tectonic force because the maximum compressive stress in all instances was approximately vertical.

Tunnel G, Site 2

A detailed plan and section of Site G-2 are given in figure 12, which also includes the bearings of the seven stress relief holes at this site. The secondary principal stress data for hole G-2-1 are given in figure 34, and the core from this hole is shown in figure 35. This core broke into relatively short pieces due to naturally occurring joints and fractures in the rock. S varied from 15 to 30 degrees from the vertical, an indication that a relatively small tectonic force was acting in the area. There was no stress concentration near the surface of this opening, a condition that indicates a relatively high plasticity in the rock, and/or a high degree of near surface fracture. The ratio of $(T/S)_{av.}$ was approximately 0.5. The vertical component of stress at the end of hole G-2-1, calculated from the ellipse for the secondary principal stresses at this point, was 500 psi, a value in good agreement with the calculated gravity stress at this point, namely, 540 psi.

Stress-relief hole G-2-5 was drilled parallel to, and within 24 inches of hole G-2-1. A representative section of the core is shown in figure 36, and the stress results are presented in figure 37.

The direction of S averaged approximately 15 degrees from the vertical and in the same general direction as that in hole G-2-1, as would be expected. Also, as in G-2-1, there was virtually no stress concentration near the surface of the opening, although S_{max} was lower than that measured in hole G-2-1. The vertical component of stress at the end of hole G-2-5, calculated from the ellipse for the secondary principal stresses, was 435 psi which is lower than the calculated gravity stress at this point. The ratio $(T/S)_{av.}$ ranged from about 0.3 at the collar of the hole to 0.7 at the end of the hole.

The other five holes attempted at this site were declared non-feasible because stress-relief cores broke into lengths too short to permit a stress determination. A section of the core from hole G-2-4 figure 38, exemplifies the degree of fracture in the rock at Site 2.

Summarizing the results from Site G-2, the rock at this Site was either inelastic or fractured to the degree that stress concentrations on or near the surface of the opening had been relieved. The direction of S was averaged approximately 15 degrees from the vertical indicating a small tectonic force. The vertical component of stress at the end of stress relief holes G-2-1 and G-2-5 was in fairly good agreement with the calculated vertical component of stress at this point.

<u>Tunnel B, Site 1 (drift B .01)</u>

The bearing of the five stress relief holes at Site B-1 are given in figure 13. The core from hole B-1-1 is shown in figure 39 and a

closer view of a section of core from this hole is shown in figure 40. The stress results from hole B-1-1 are presented in figure 41. These results indicate that, except near the surface, the direction of the stress field was almost vertical, and S_{max} was 660 psi, which occurred at a depth from 40 to 50 inches from the face. The value of S_{∞}(150 inches) was 480 psi, a value that is lower than the computed gravity stress (650 psi). The maximum measured stress concentration, at 45 inches from the surface, was 1.4, although this value may be high because of the low value of the stress measured at the end of the hole. The ratio $(T/S)_{av.}$ was approximately 0.5.

Hole B-1-2 was drilled parallel to and within 24 inches of hole B-1-1. A section of the core from this hole is shown in figure 42 and the corresponding stress results are given in figure 43. The stress results obtained from this hole are essentially the same as those from hole B-1-1 except that S_{∞} was 530 psi, a value more nearly in agreement with the calculated gravity stress at this point. Also, because of this higher value the maximum stress concentration which occurred at a depth of 60 inches was smaller, viz., 1.2. Horizontal paralled holes B-1-3 and B-1-4 were drilled perpendicular to holes B-1-1 and B-1-2. The core from B-1-4 is shown in figure 44 and a closer view of this core is shown in figure 45. The stress results from holes B-1-3 and B-1-4 are given in figures 46 and 47, respectively. The results from these holes are essentially identical. The direction of S was approximately 45 degrees from vertical at depths from the face up to 80 inches,

but became almost horizontal from 100 inches to the end of the hole. This rotation of the maximum stress often occurs in the proximity of faults or major joint planes. The S_{max} varied from approximately 900 psi near the face, to 400 to 460 psi at the end of the hole. The measured vertical component of stress (determined from the secondary stress ellipse) at a depth of 140 inches was 450 psi, a value smaller than the calculated gravity stress which, as previously noted, was 650 psi. This lower value also may result from the fact that a fault or major joint occurred near the ends of these holes. The maximum stress concentration determined from the measured stresses was approximately 2, but this value may be high because of the low value of the vertical stress measured near the end of the hole.

The stress results from hole B-1-5 (drilled vertical up), given in figure 48, indicate that there is virtually no stress concentration near the horizontal (roof) surface of the opening. From a depth of 60 inches to the bottom of the hole the direction of S was approximately north-south and the magnitude of S was 260 psi, which is somewhat lower than the north-south component of S estimated from the stress measuremrnts in holes B-1-1, B-1-2, B-1-3, and B-1-4, viz., 325 psi.

Tunnel B, Sites 2 and 3

Test Sites B-2 and B-3, plans and section of which are given in figures 14 and 15, were non-feasible. In these areas the cores generally broke into thin wafers, indicating an extremely weak rock and/or a relatively high stress compared to the strength of the rock. A part of the core from hole B-2-1 is shown in figure 49.

In general the tuff from all of the tunnel B sites was non-linear-elastic as indicated by the hydraulic pressure versus bore-hole deformation results from a representative specimen from Site B-1, figure 50. These curves are similar to those obtained from specimens taken from Sites B-2 and B-3. This non-linearity may account in part for the low stress values obtained at Site B-1. Most of the biaxial elastic constant determinations were made at comparatively low stress levels, and as the modulus of elasticity increases with the stress, it is possible that the in situ elastic constant of the rock is higher than that determined in the laboratory.

Tunnel E, Site 1

The bearings of the six stress relief holes drilled at Site E-1 are indicated in the site plan and sections, figure 16. The core from parallel holes E-1-2 and E-1-5 are shown in figures 51 and 52, respectively. The texture of the rock is shown in the annular cuts made at 43 and 180 inches, figure 53. The stress results from parallel holes E-1-2 and E-1-5 are given in figures 54 and 55. This pair of holes intersected a fault (or shear zone) between a hole depth of 60 and 180 inches, as shown in the core photographs, figures 51 and 52, and in the sketch of the geological structure, figure 56. No satisfactory bore-hole deformation data were obtained in this fault zone. The stress relief results from holes E-1-2 and E-1-5 are similar. The maximum compressive stress, S_{max}, which occurred at a depth of 60 inches, was 800 psi. At the end of these holes (240 inches) S_{∞} was inclined approximately 20 degrees from the horizontal and its magnitude was 640 psi in hole E-1-2, and 515 psi in hole E-1-5. Thus, the stress concentration in this pair of holes averaged approximately 1.3. The minimum compressive stress, T, was within ±20 degrees of vertical. T_{max}, averaged for the two holes, was approximately 600 psi at a depth of 60 inches, and T_{∞} was 380 psi at 240 inches. The latter value was much lower than the calculated gravity stress, which was 1100 psi. This low value was probably due to the close proximity of the fault zone to these holes.

Parallel holes E-1-3 and E-1-6 were drilled in the horizontal direction, and perpendicular to holes E-1-2 and E-1-5. The cores from these holes are shown in figures 57 and 58, and the stress results are presented in figures 59 and 60.

The results were similar to those obtained in E-1-2 and E-1-5. S tended to lie in the horizontal direction. S_{max} occurred within 20 inches from the face and its magnitude was 850 psi in hole E-1-3 and 620 psi in hole E-1-6. S_{∞} was 360 psi at a depth of approximately 200 inches from the face in both holes. T, which was in the approximate vertical direction, varied over the length of the hole. T_{max} was 570 psi at 48 inches in hole E-1-3 and 440 psi at 108 inches in hole E-1-6. At a depth of 200 inches in both holes T_{∞} was approximately 230 psi, a value mucy lower than the calculated gravity stress at this point. From all indications both holes E-1-3 and E-1-6 are affected by the proximity of the fault that runs approximately parallel to this hole and at a distance of 9 feet to the west. It cannot be concluded that the larger horizontal component of stress was due to a regional tectonic action because of the inordinately small values that were measured in the vertical direction.

The core from vertical (up) hole E-1-4 is shown in figure 61 and the stress results are presented in figure 62. These results indicate that S and T increased with the depth.

Tunnel P, Site 1

The plan and section of Site T-1 includes the bearings of the six stress-relief holes drilled at this site. The core from P-1-1 is shown in figure 63, and a closer view of a section of this core is shown in figure 64. The stress results are given in figure 65.

In hole P-1-1 S_{max} was 1,200 psi at a distance from the face of 40 inches and S decreased erratically to a value of 960 psi at the bottom of the hole (approximately 190 inches from the face). The direction of S in the bottom 80 inches of the hole was within 20 degrees of horizontal. Correspondingly, T_{∞} was within 20 degrees of vertical and its value was 740 psi. The vertical component of stress calculated from the ellipse for the secondary stresses was approximately 750 psi, a value that is in fair agreement with the calculated gravity stress at this point, which for a depth of 780 feet is 650 psi. $(T/S_{av.})$ was approximately 0.75. Thus, at this site and in the horizontal direction approximately normal to hole P-1-1 there is evidence of a tectonic force which caused the stress in the horizontal section to be larger than that in the vertical direction.

The core from horizontal hole P-1-2 which was perpendicular to hole P-1-1, is shown in figure 66. This core was more strongly fractured than that from P-1-1 as indicated in the section shown in figure 67. The stress results from hole P-1-2 are given in figure 68. In this hole the S was very close to vertical, and at all points the vertical component of stress was much larger than the horizontal component. S_{max} was 1,680 psi which occurred at a depth of 160 inches from the face. S dropped to 1,160 psi at a depth of 250 inches, a value that is much higher than the computed gravity stress at this point, which is 650 psi. The cause of this abnormal high stress is

not known but it may be associated with jointing that obliquely intersected the core from this hole at frequent intervals. T_∞ was 470 psi, which is somewhat higher than the computed vertical gravitational stress.

The modulus of elasticity data for the rock from both holes P-1-1 and P-1-2 indicated a very linear-elastic material. Also, this rock was the strongest that was encountered in any of the Madison and Yuba sites, although LPI compressive tests on 1D NX specimens indicated that the core from hole P-1-2 averaged about 70 percent greater than that from hole P-1-1. Two attempts were made to drill vertical (up) holes at this site but both were unsuccessful as the core fractured along the axis of the core at frequent intervals, as illustrated in figure 69.

Tunnel N, Site 1 (drift L.O.S. No. 2)

The bearings of the seven stress-relief holes drilled at Site N-1 are given in the detailed plan and section, figure 18. The core from hole N-1-1 is shown in figure 70, and enlarged views of this core are shown in figures 71 and 72. The discing which was evident in this core, especially near the surface indicated that the stress level was high compared with the rock strength. In the areas where the core disced no stress data could be obtained, but it is probable that the stress values in these areas were higher than the maximum values measured in the adjoining rock. The stress results from parallel holes N-1-1 and N-1-2 are given in figures 73 and 74. The direction of S and T in both was virtually identical, and invarient

over the length of the holes. Also, S_∞ and T_∞ were essentially the same in both holes, the average values being 1210 psi and 570 psi, respectively. S_∞ was within 20 degrees of horizontal and greater than twice the vertical components of stress, which was 580 psi (calculated from the stress ellipse). The vertical component of stress is in good agreement with the calculated vertical gravity stress, which is 560 psi. Hence, a tectonic force appears to be acting in this area. The ratio $(T/S)_{av.}$ was approximately 0.5. The stress results from hole N-1-1 and N-1-2 differ in that in hole N-1-1 there was a near surface stress concentration of 1.3, with S_∞ equal to 1620 psi at a hole depth of 60 inches, whereas in hole N-1-2 the magnitude of both S and T was almost constant over the length of the hole.

The bearings of parallel holes N-1-4 and N-1-5, which were drilled at right angles to N-1-1 and N-1-2 are given in figure 18. The core from hole N-1-4 is shown in figure 75 and an enlarged view of the section of core from 85 inches and 140 inches is shown in figure 76. The stress results for both holes N-1-4 and N-1-5 are shown in figures 77 and 78, respectively.

Both the magnitude and direction of S and T in parallel holes N-1-4 and N-1-5 (which were perpendicular to holes N-1-1 and N-1-2) were essentially identical over the length of these holes. There was no stress concentration at or near the surface, although both S and T varied along the length of the hole. S_∞ and T_∞ for both holes averaged 640 psi and 450 psi, and the vertical component of stress was 510 psi

compared with the vertical gravity stress of 560 psi. $(T/S)_{av.}$ was about 0.7. The inclination of the larger compressive stress from vertical is probably caused by the tectonic force acting in this area.

Horizontal hole N-1-3, up hole N-1-6, and down hole N-1-7 were declared non-feasible because of excessive core fracture, in fact a large part of the core in these holes disced. The core from hole N-1-6 is shown in figure 79.

Tunnel N, Site 2

Figure 18 shows the bearings of the four stress-relief holes drilled at Site N-2. A section of the core from hole N-2-1 is shown in figure 80 and the corresponding stress results are given in figure 81. In hole N-2-1 the direction of S was approximately vertical and there was no stress concentration on or near the surface of the opening. At a depth of 230 inches S_∞ was 440 psi, as compared with the computed vertical gravity component of stress which was 580 psi.

The core from hole N-2-2 is shown in figure 82 and an enlarged section of the core is shown in figure 83. The stress results from hole N-2-2 are given in figure 84. These results are similar to those from hole N-2-1, which was perpendicular to hole N-2-2. There was no near surface stress concentration and the direction of S was within 15 degrees of vertical. S_∞ was 480 psi at a depth of 260 inches, as compared with the computed vertical gravity stress of 580 psi. $(T/S)_{av.}$ was approximately 0.5. In both holes N-2-1 and N-2-2 the stress values varied erratically from point to point, a result that is attributed to

the natural fracture that occurred in this rock.

Vertical down holes N-2-3 and N-2-4 were declared non-feasible because the core from both holes disced and fractured. The core from hole N-2-3 is shown in figure 85.

SUMMARY OF MECHANICAL PROPERTY AND STRESS MEASUREMENTS

The mechanical property data given in tables 3 and 4 indicate that the tuff from the various Madison and Yuba sites was extremely variable. The uniaxial compressive strength range amounted to 30 fold, and the biaxial modulus of elasticity range was 20 fold. Thus, the tuff from Site P-2 would be classified as a relatively competent rock with a compressive strength greater than 11,000 psi and a modulus of elasticity greater than 2×10^6 psi, whereas the uniaxial compressive strength of the tuff from Site B-1 averaged less than 500 psi and the corresponding modulus of elasticity averaged 0.33×10^6 psi.

The stress measurements made in the Madison and Yuba sites are summarized in table 5. At Sites G-2, P-1, and N-1 there is an indication of tectonic forces acting in the horizontal direction, in fact, at Site N-1 the horizontal component of stress is greater than twice the vertical component of stress, and the vertical component of stress is in reasonable agreement with the value calculated from the weight of the overlying rock (a condition necessary to satisfy static equilibrium). At Sites G-1, B-1, E-1, and N-2 there was no indication of tectonic forces acting in the horizontal directions, and hence the stress field is presumed to be that due to only the gravitational load. However, the vertical component of the stress

field, S_∞, was in most instances less than the computed vertical component of stress. As the measurements at these sites were made in fractured, jointed, and faulted areas, it is possible that these low stress values resulted from these geological factors, and that in adjoining areas higher vertical stresses are present such that the average stress in the vertical direction is equal to the gravity load.

Although the stress distribution curves showed that in most instances the secondary principal stresses varied erratically with the gage depth, and sometimes between wide limits, the fact that almost identical results were obtained in ajoining and parallel holes shows that this erratic variation is not a consequence of measurement inaccuracies. Rather, these stress variations are presumably due to jointing and fracturing in the rock. It is interesting to note that the direction of the secondary principal stresses is not as variable as the magnitude. This observation is consistent with that obtained from measurements in other rock types.

With one exception the stress concentration on or near the surface of openings was less than 2.5. The exception was in hole G-1 in which the stress concentration was 6 but in which the magnitude of S_∞ was inordinately small and presumably affected by local geology.

In general, stress concentration on the walls of tunnel openings of a rectangular shape would be greater than 3 and possibly as high

as 5 or 6 (the exact value depending on the geometry of the opening). The fact that these high values were not found indicates that there has been a strong near-surface stress relaxation which may be due to a loosening of the surface rock from blasting or other mining operations, or to plastic and/or viscoelastic properties of the rock that permit a time-dependent movement and a corresponding stress relaxation in the rock. In both the biaxial and triaxial elastic constant determinations it was noted that there is a tendency for the tuff from the Madison and Yuba sites to creep when subjected to a constant load and hence the latter factor is considered to be the more likely cause of the low stress concentrations.

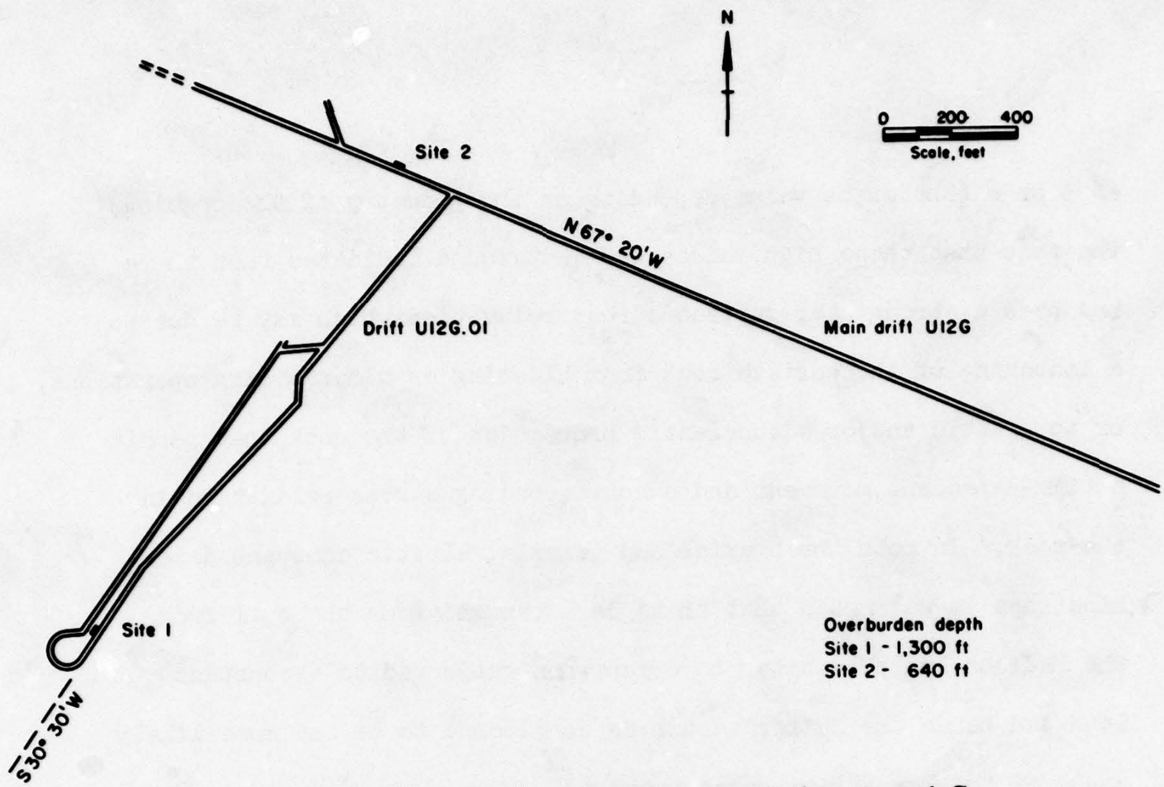

Figure 1 - Site locations for stress-relief -- tunnel G

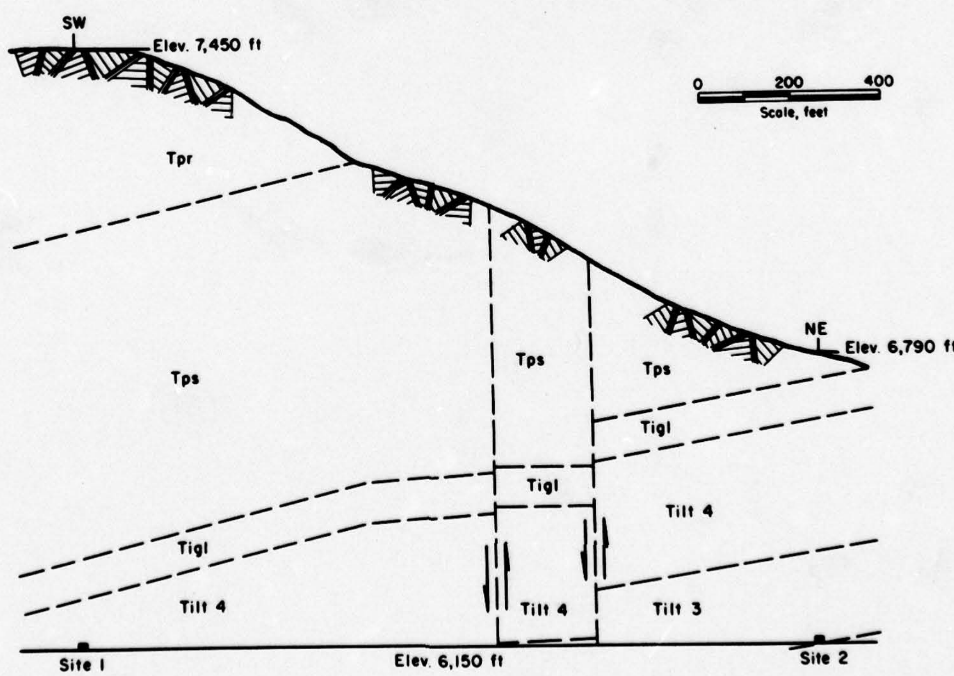

Figure 2 - Section through stress-relief sites -- tunnel G

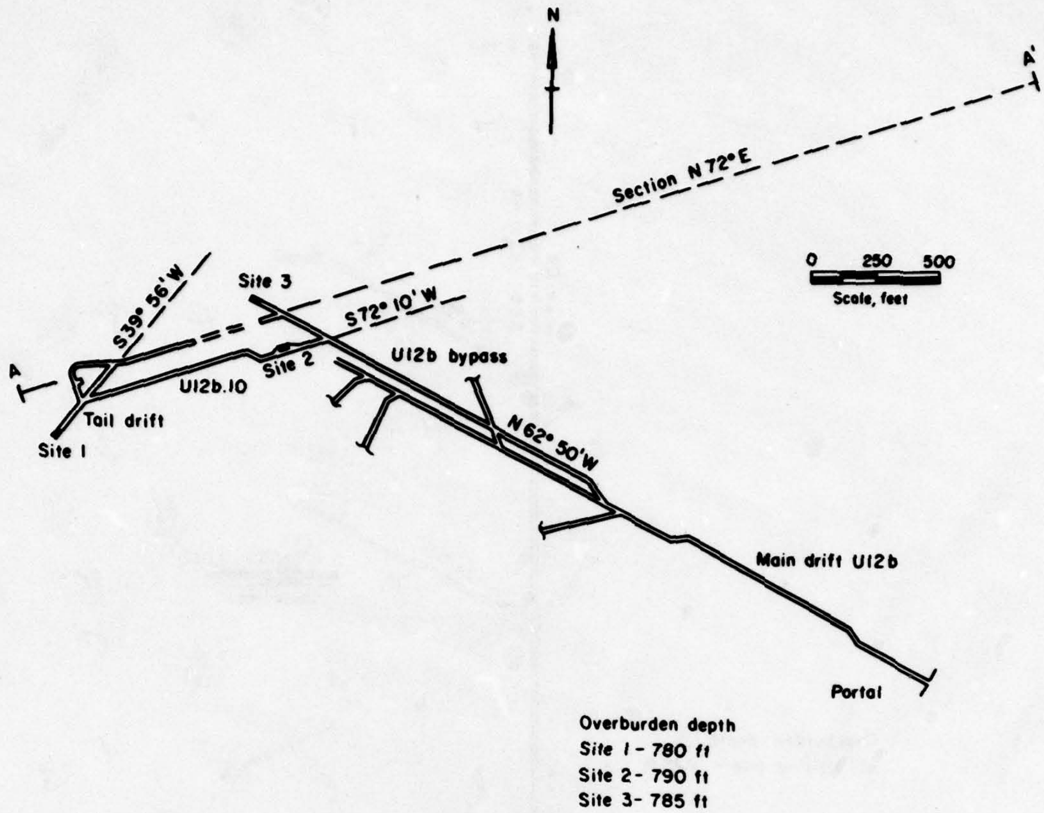

Figure 3 - Site locations for stress-relief --tunnel B

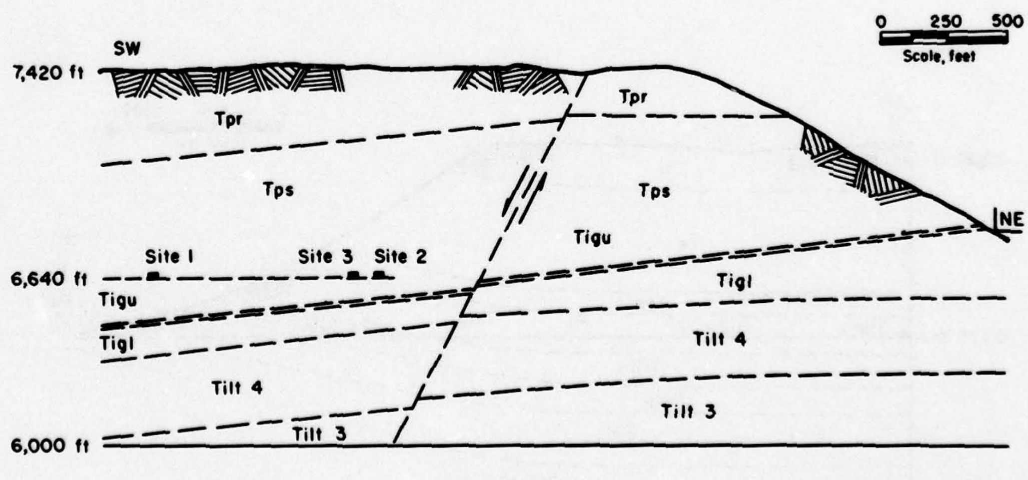

Figure 4 - Section through stress-relief sites -- tunnel B

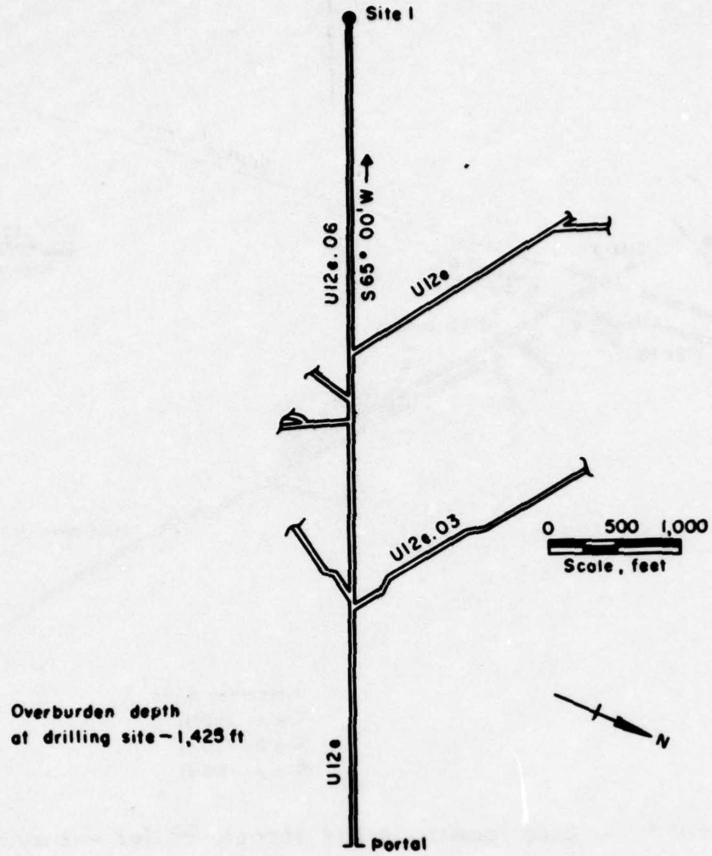

Figure 5 - Site location for stress-relief -- tunnel E

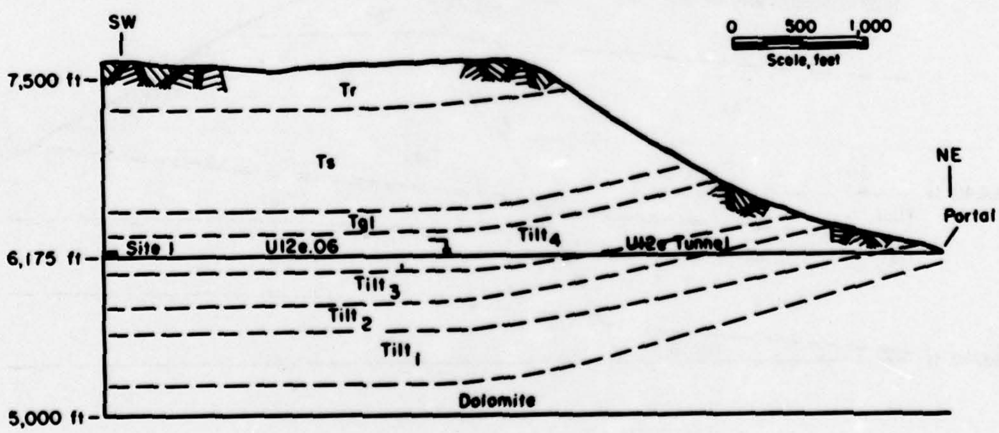

Figure 6 - Section through stress-relief site -- tunnel E

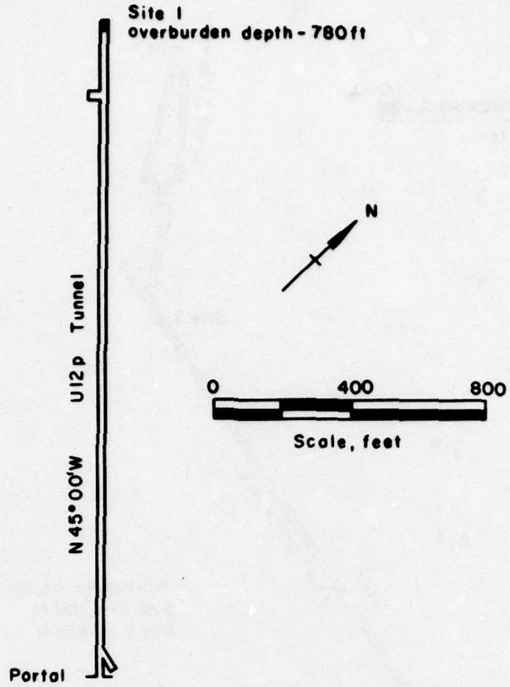

Figure 7 - Site location for stress-relief -- tunnel P

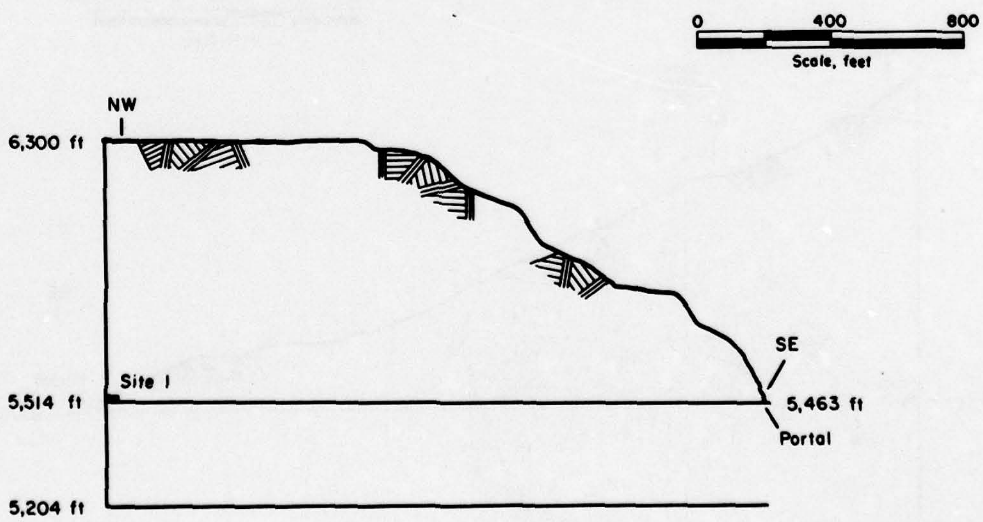

Figure 8 - Section through stress-relief site -- tunnel P

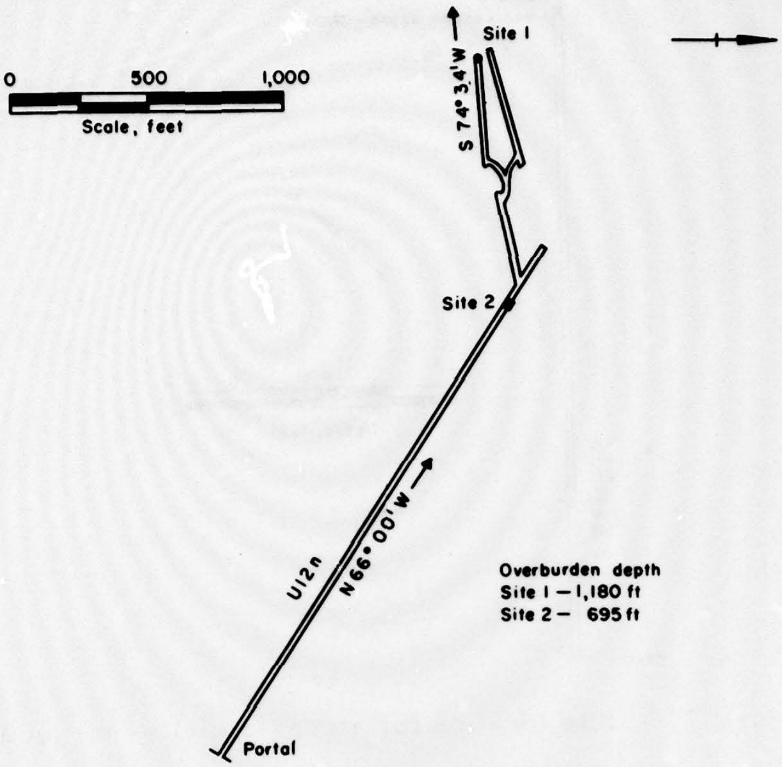

Figure 9 - Site locations for stress-relief -- tunnel N

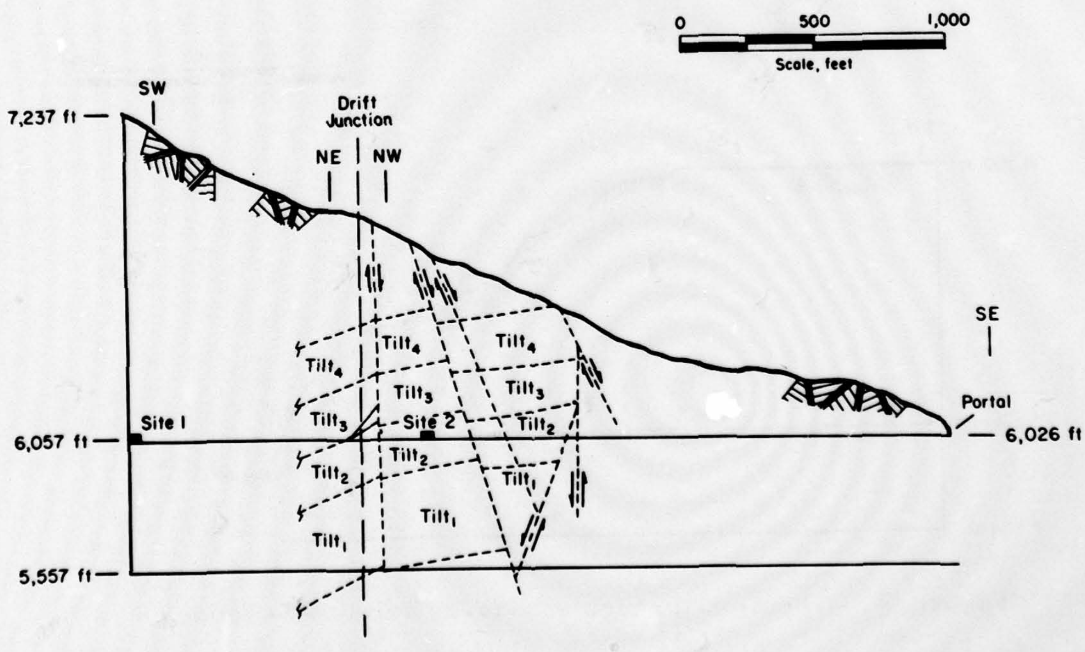

Figure 10 - Section through stress-relief sites -- tunnel N

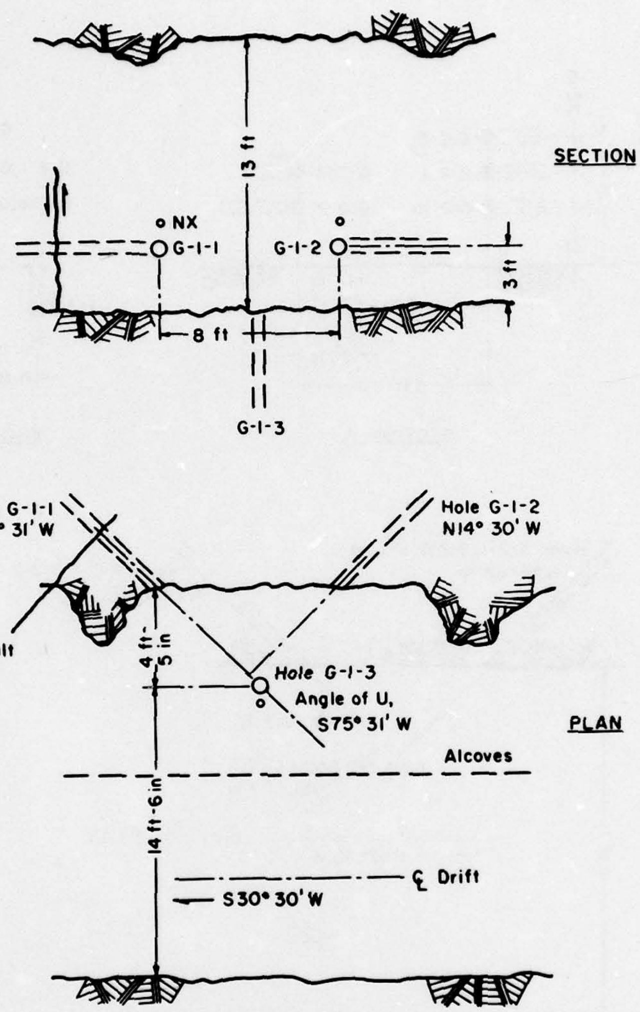

Figure 11 - Detail plan and section of site 1 -- tunnel G - drift G.01

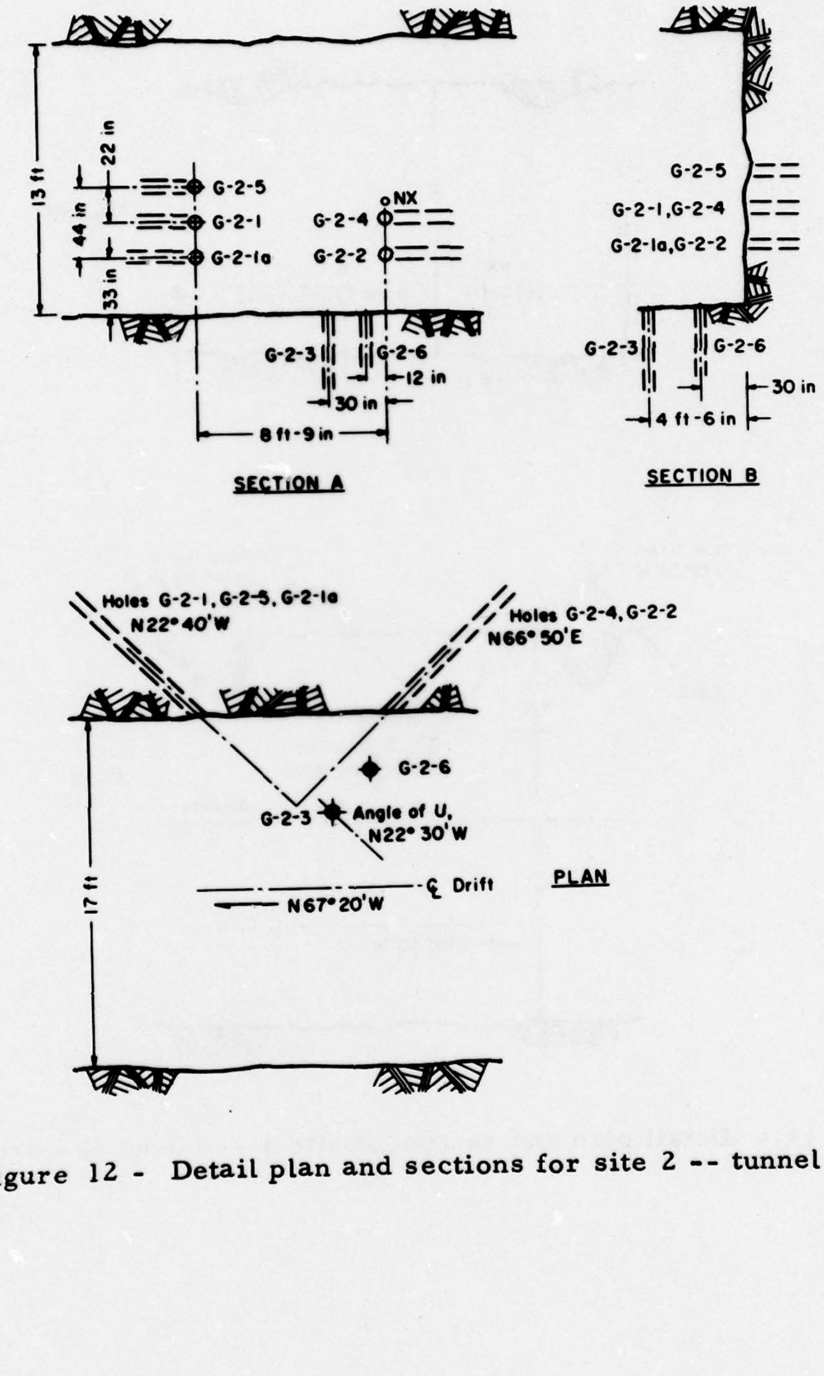

Figure 12 - Detail plan and sections for site 2 -- tunnel G

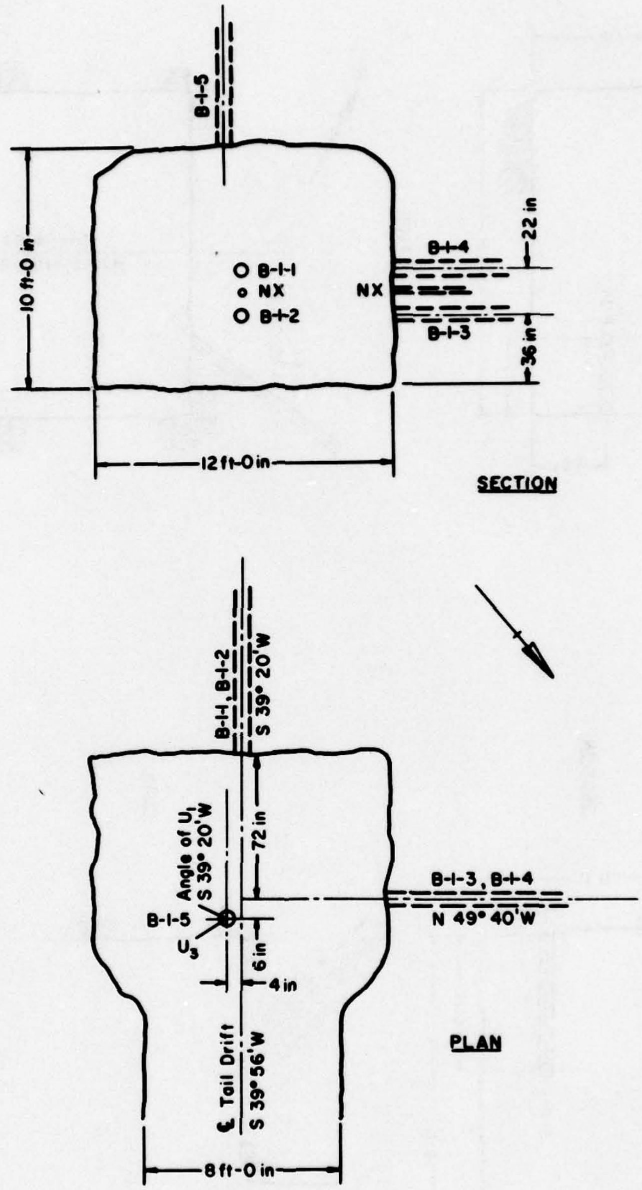

Figure 13 - Detail plan and section of site 1 -- tunnel B - drift B.01

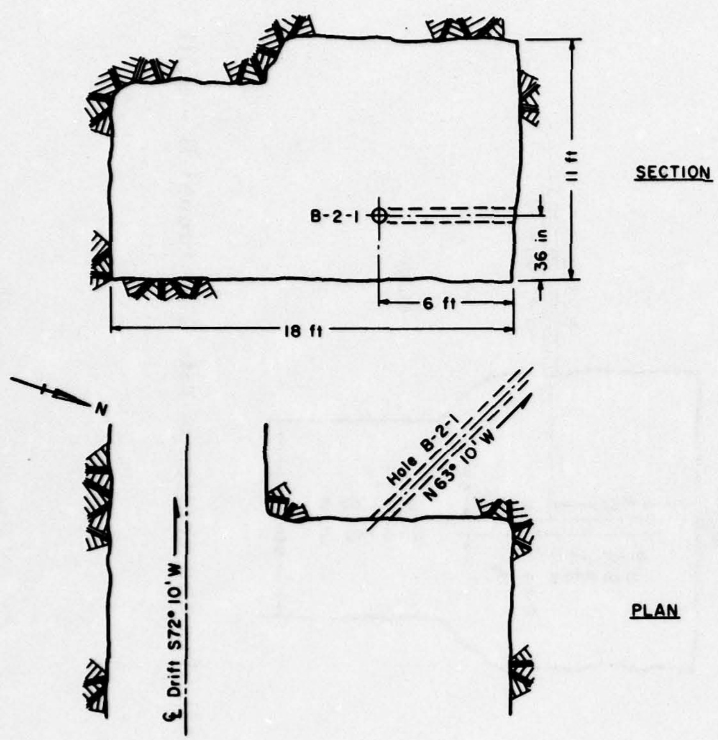

Figure 14 - Detail plan and section of site 2 -- tunnel B

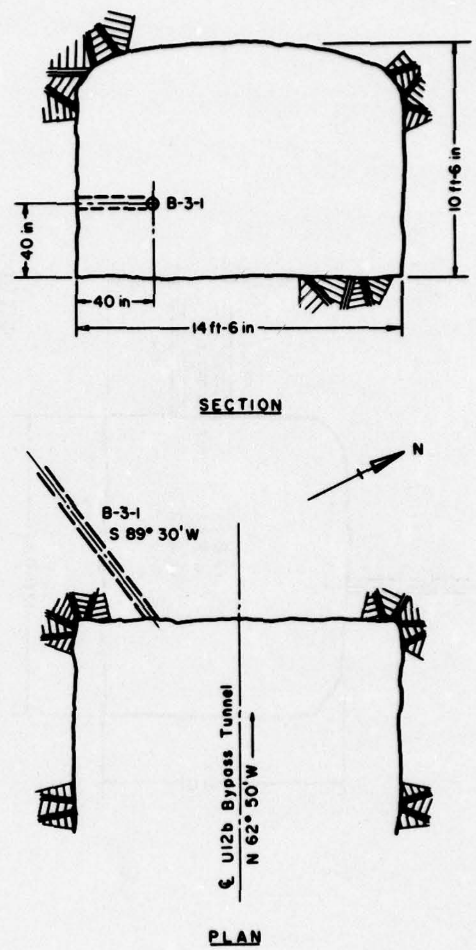

Figure 15 - Detail plan and section of site 3 -- tunnel B

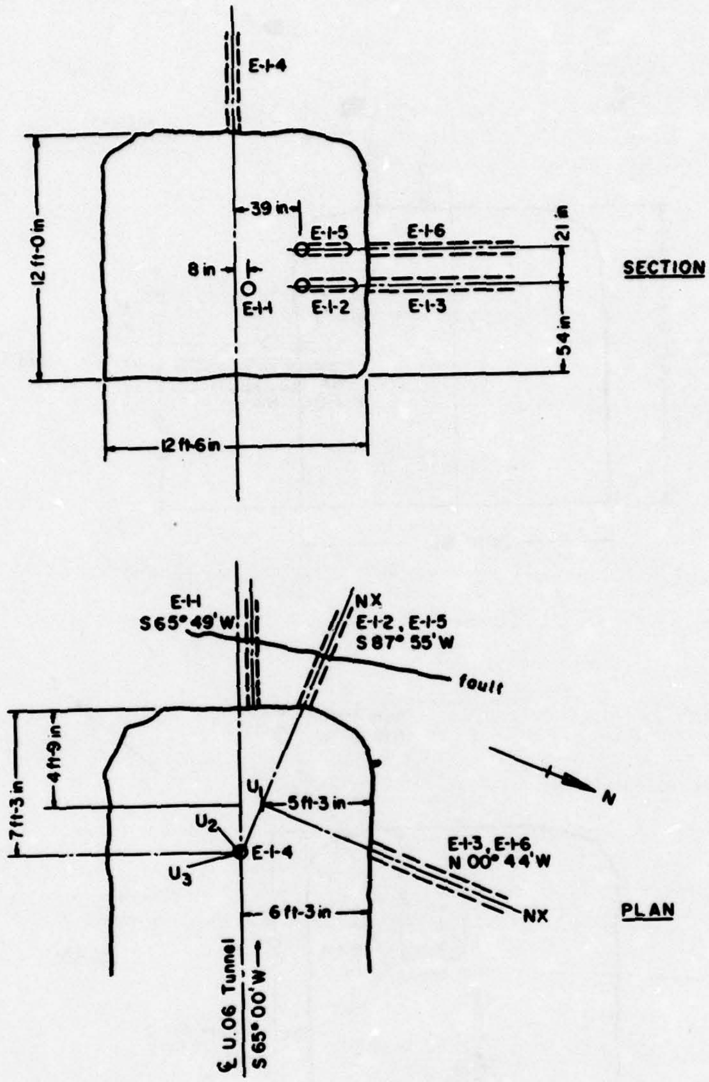

Figure 16 - Detail plan and section of drilling site -- tunnel E

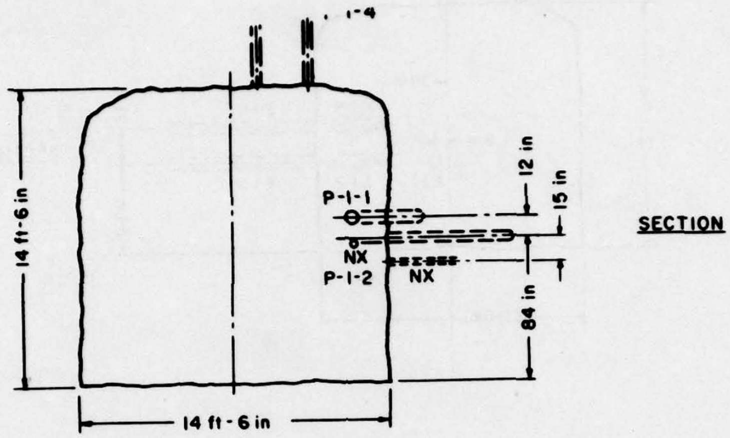

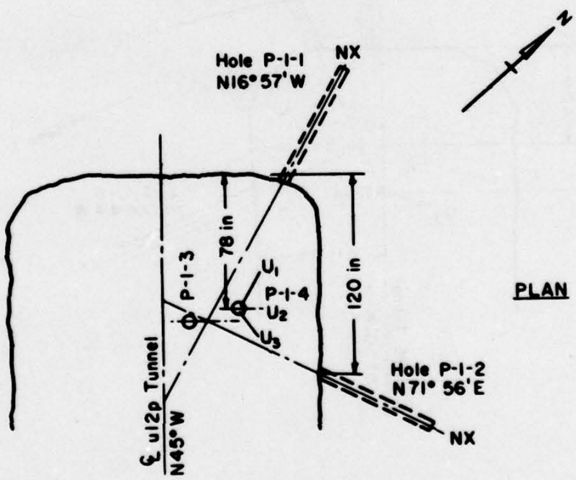

Figure 17 - Detail plan and section of drilling site -- tunnel P

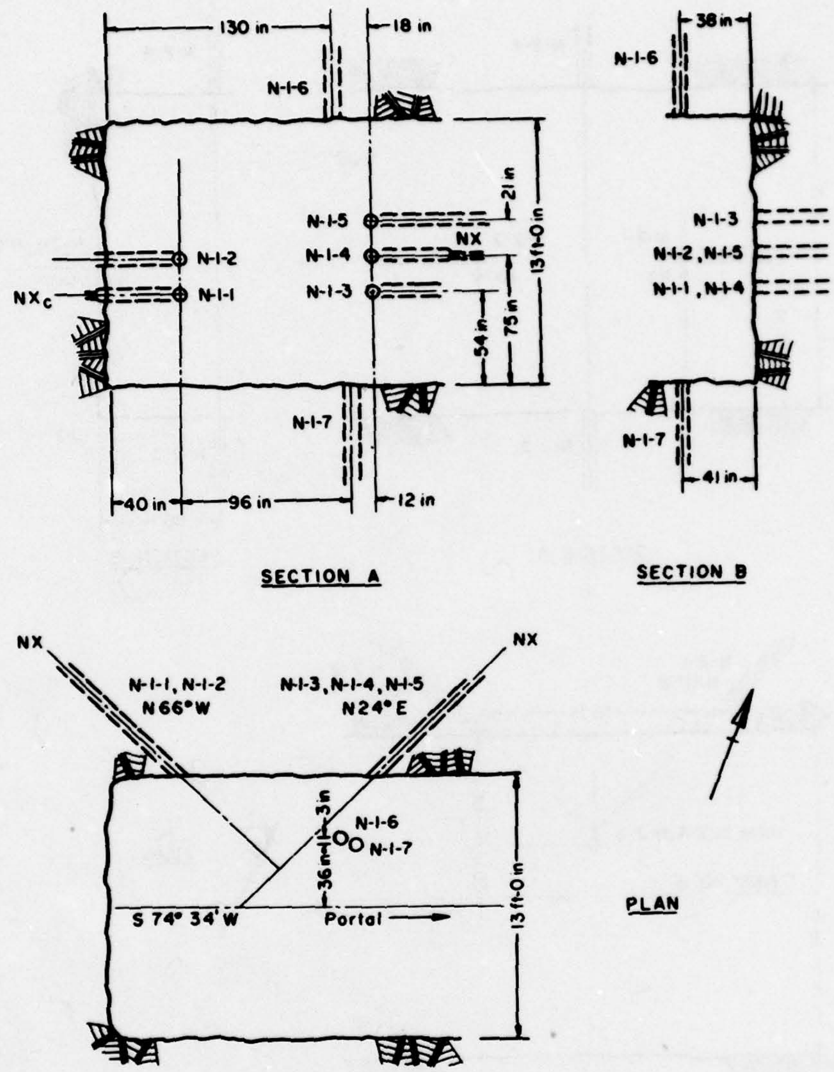

Figure 18 - Detail plan and section of site 1 -- tunnel N - (drift L. O. S. No. 2)

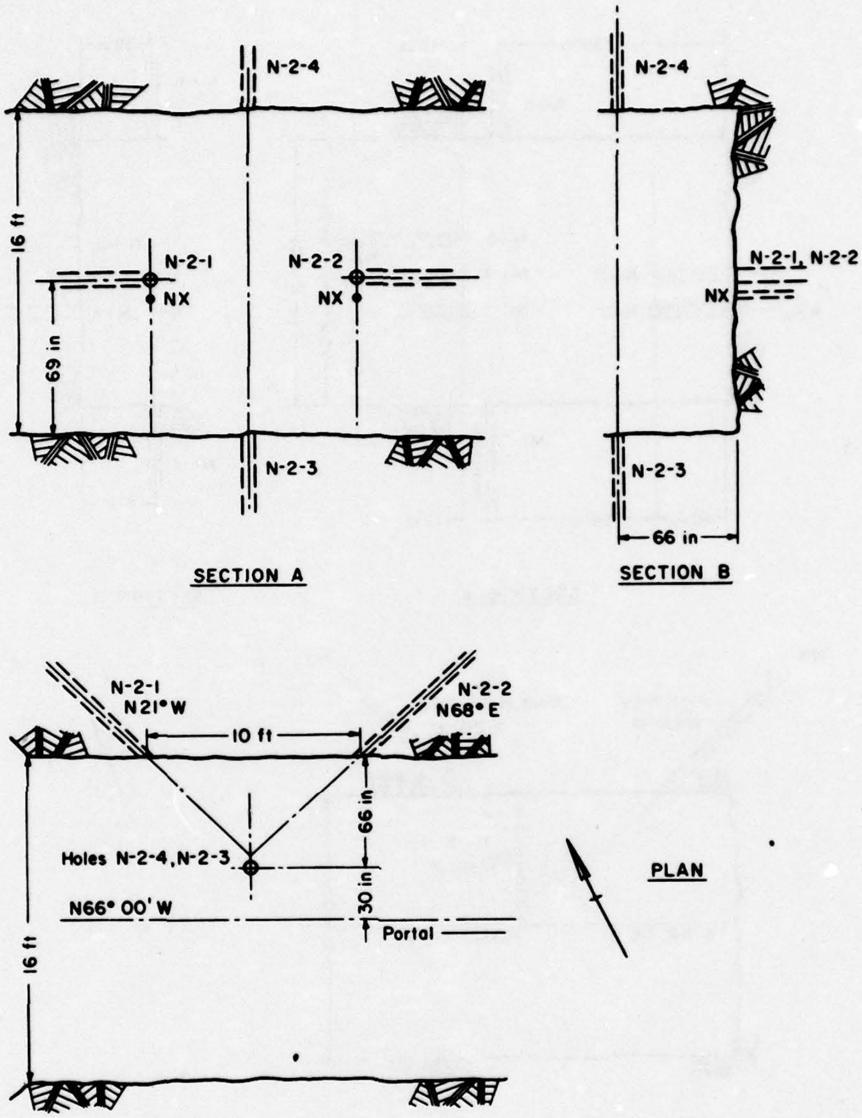

Figure 19 - Detail plan and section of site 2 -- tunnel N

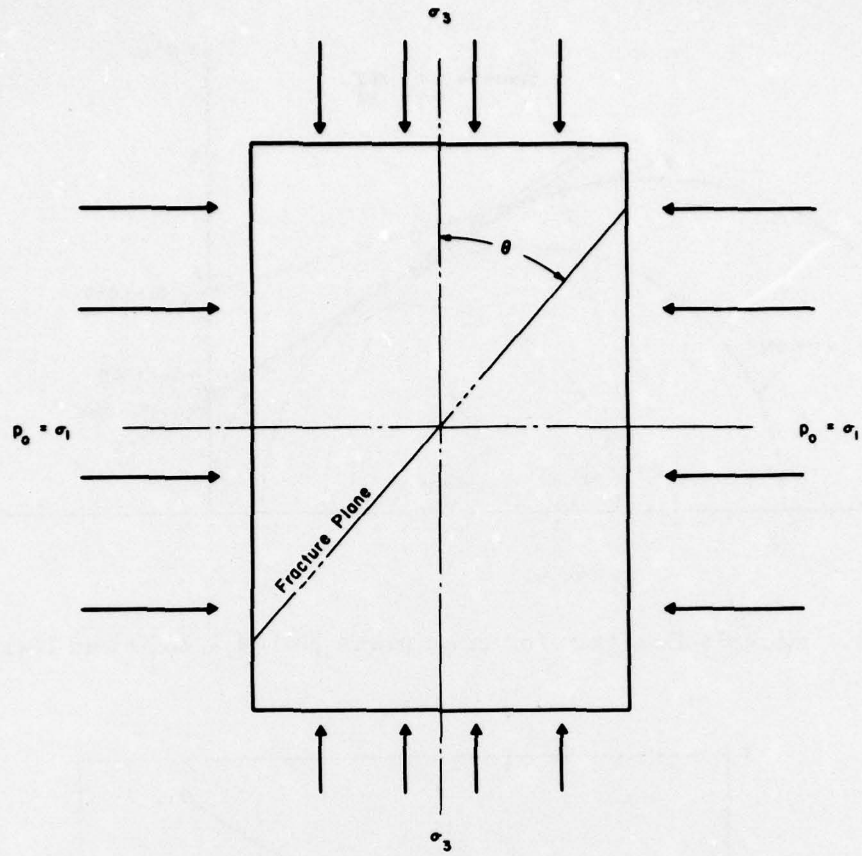

Figure 20 - Nomenclature for triaxial test

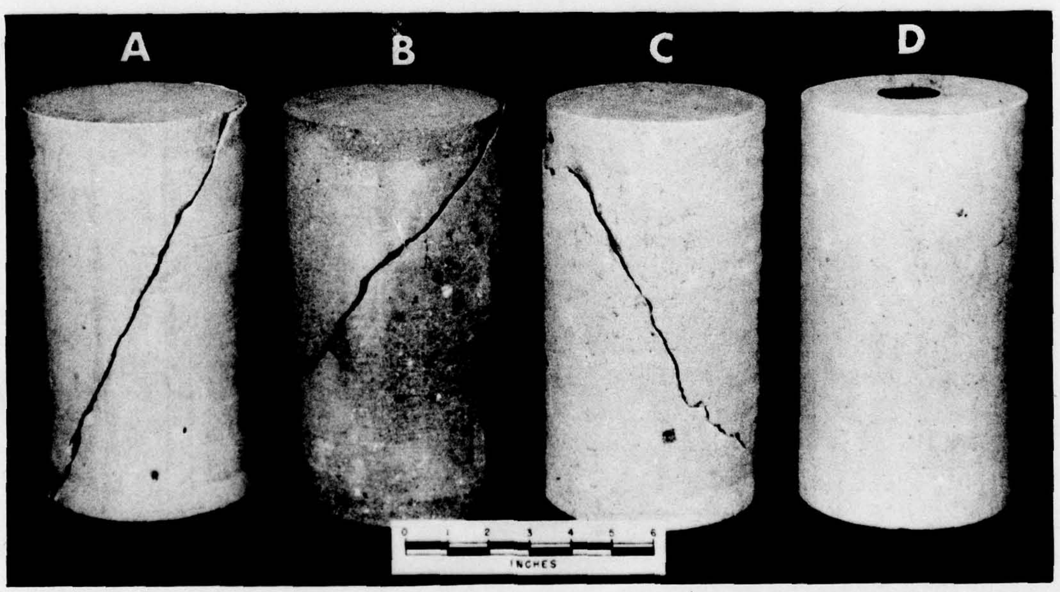

Figure 21 - Mechanical property test specimens

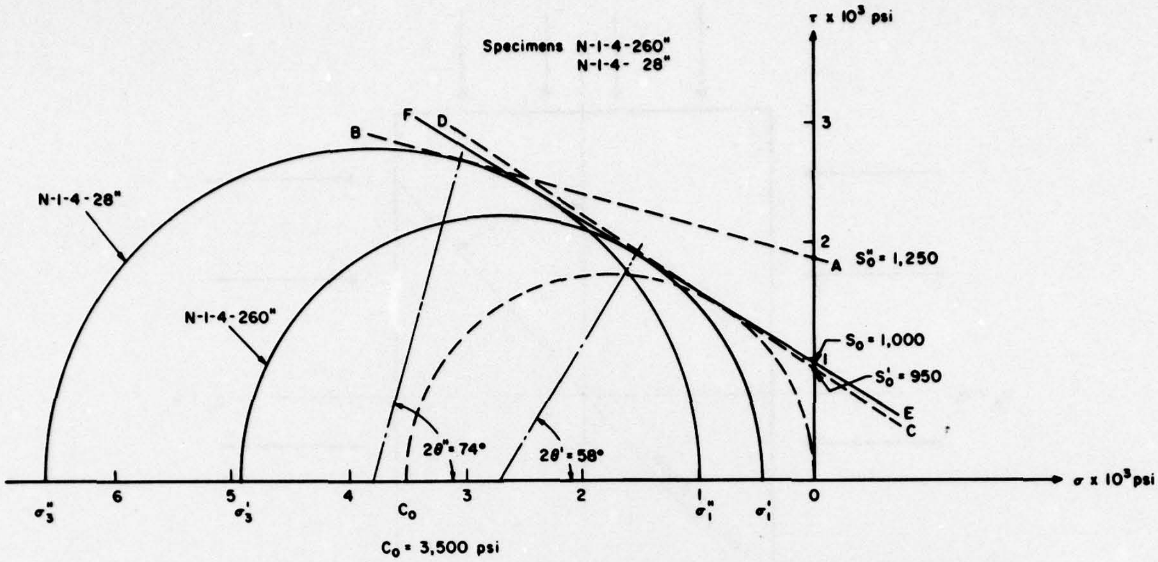

Figure 22 - Mohr's Diagram for specimens N-1-4 - 260" and N-1-4 - 28"

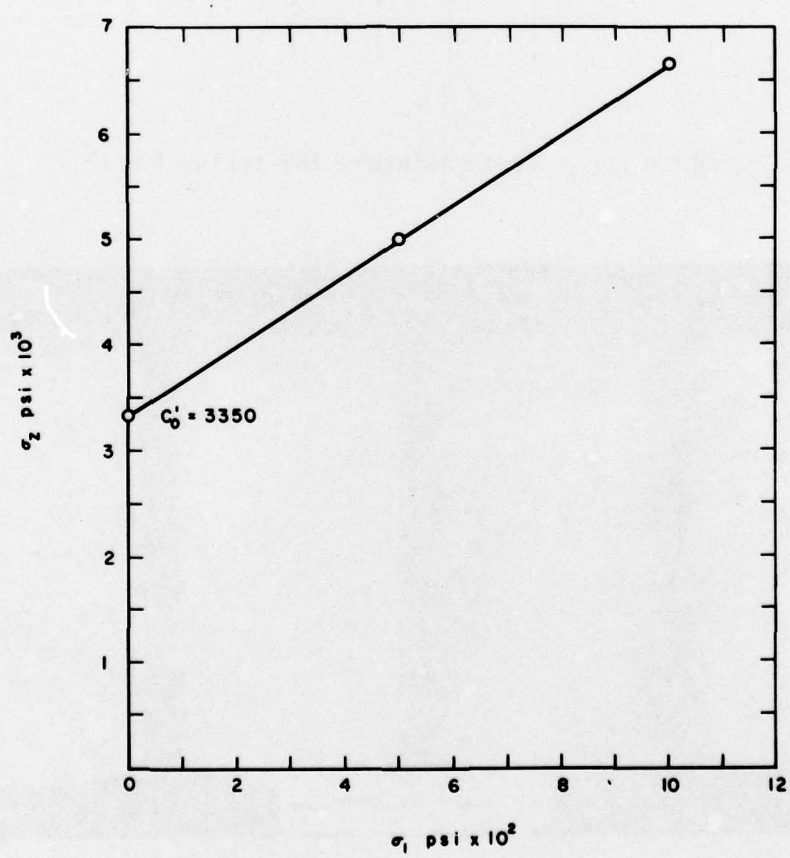

Figure 23 - Triaxial compressive strength of specimens from hole N-1-4

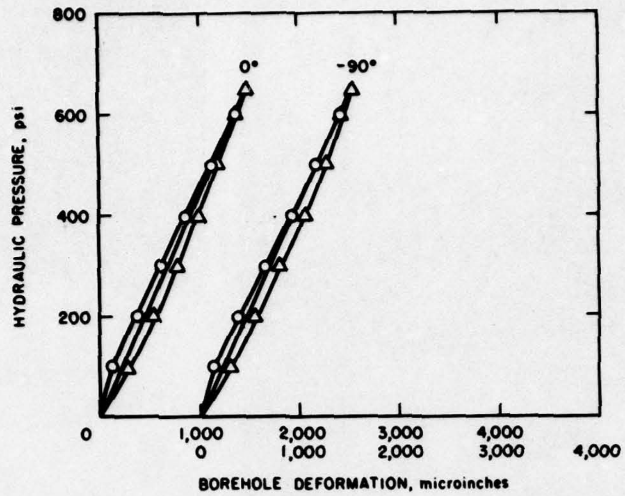

Figure 24 - Linear axial stress versus borehole deformation curves, biaxial method - specimen G-1-2 - 71"

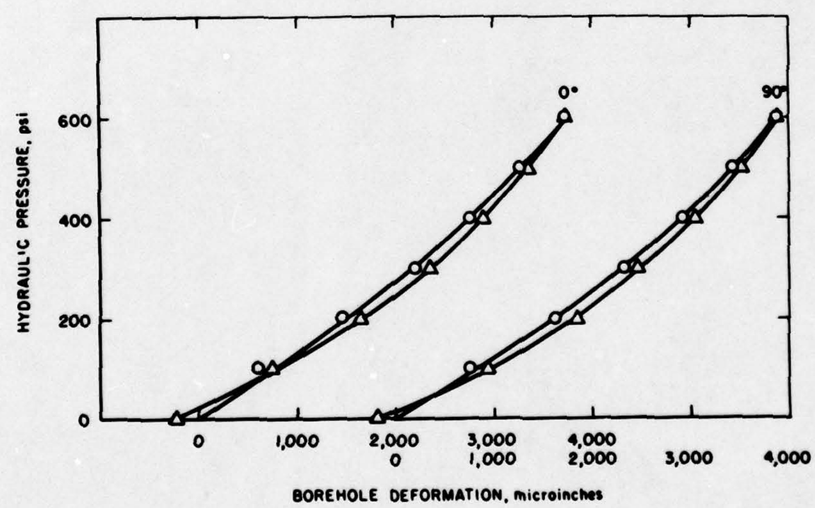

Figure 25 - Non-linear axial stress versus borehole deformation curve, biaxial method - specimen E-1-5 - 212"

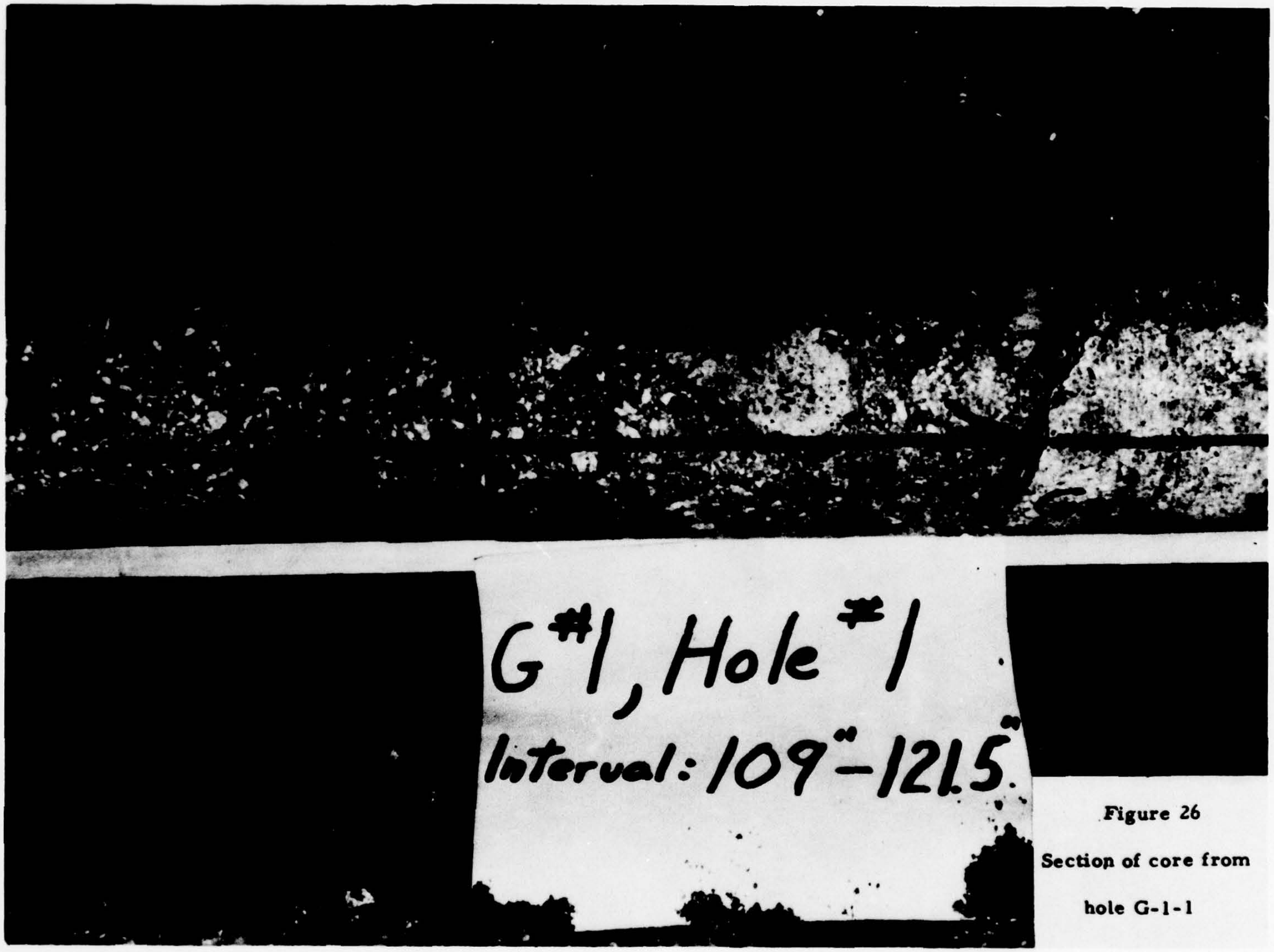

Figure 26

Section of core from hole G-1-1

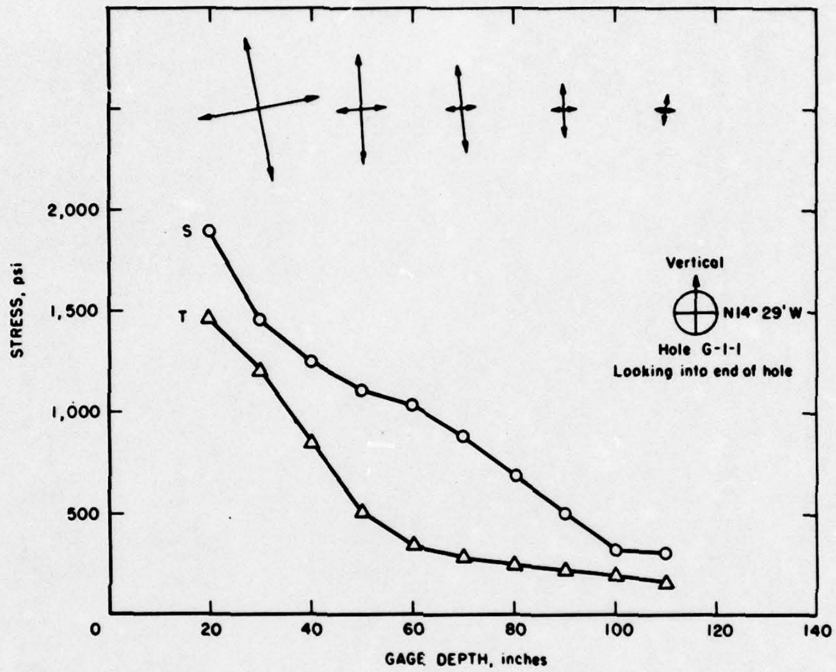

Figure 27 - Stress versus distance from face - hole G-1-1

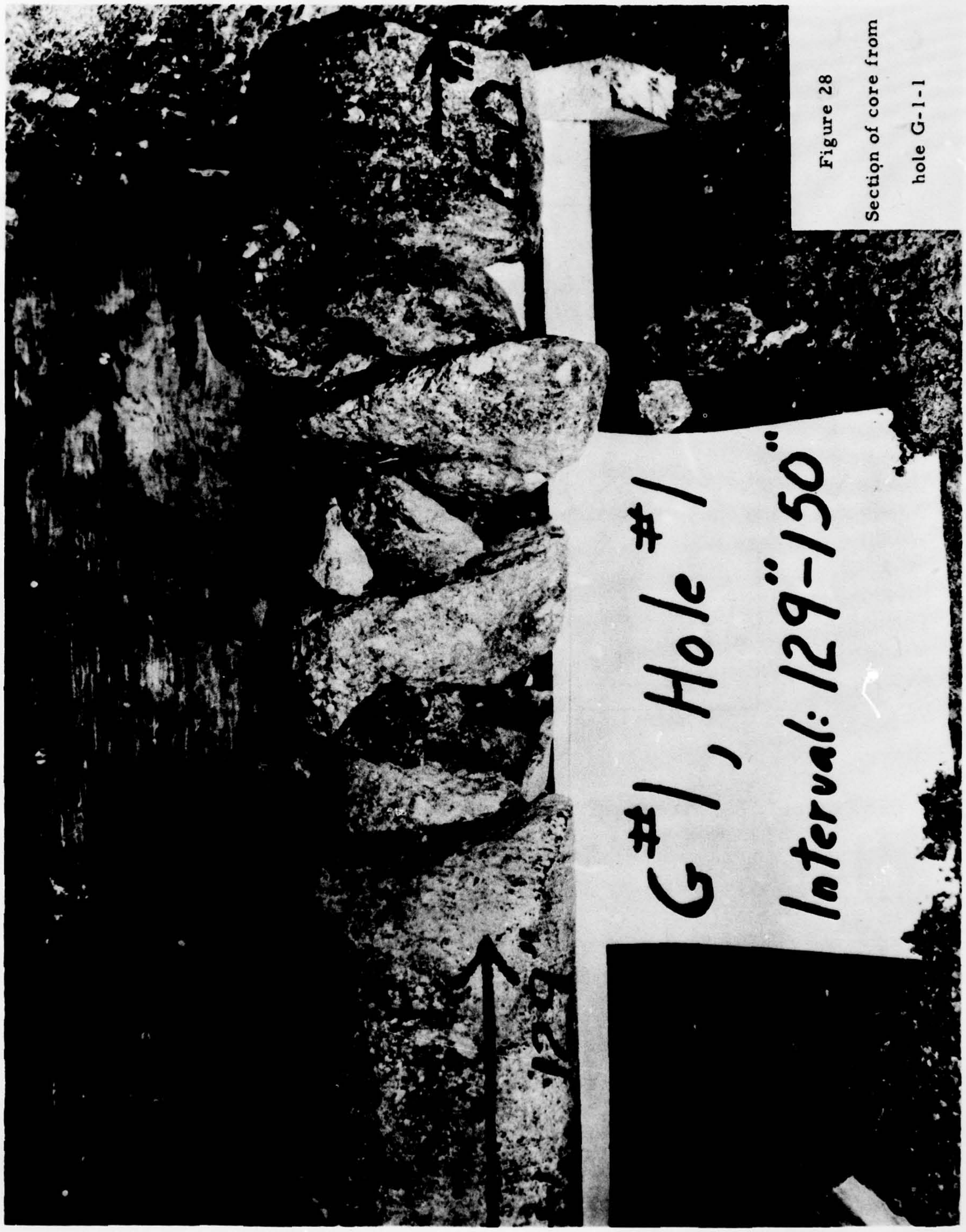

Figure 28
Section of core from
hole G-1-1

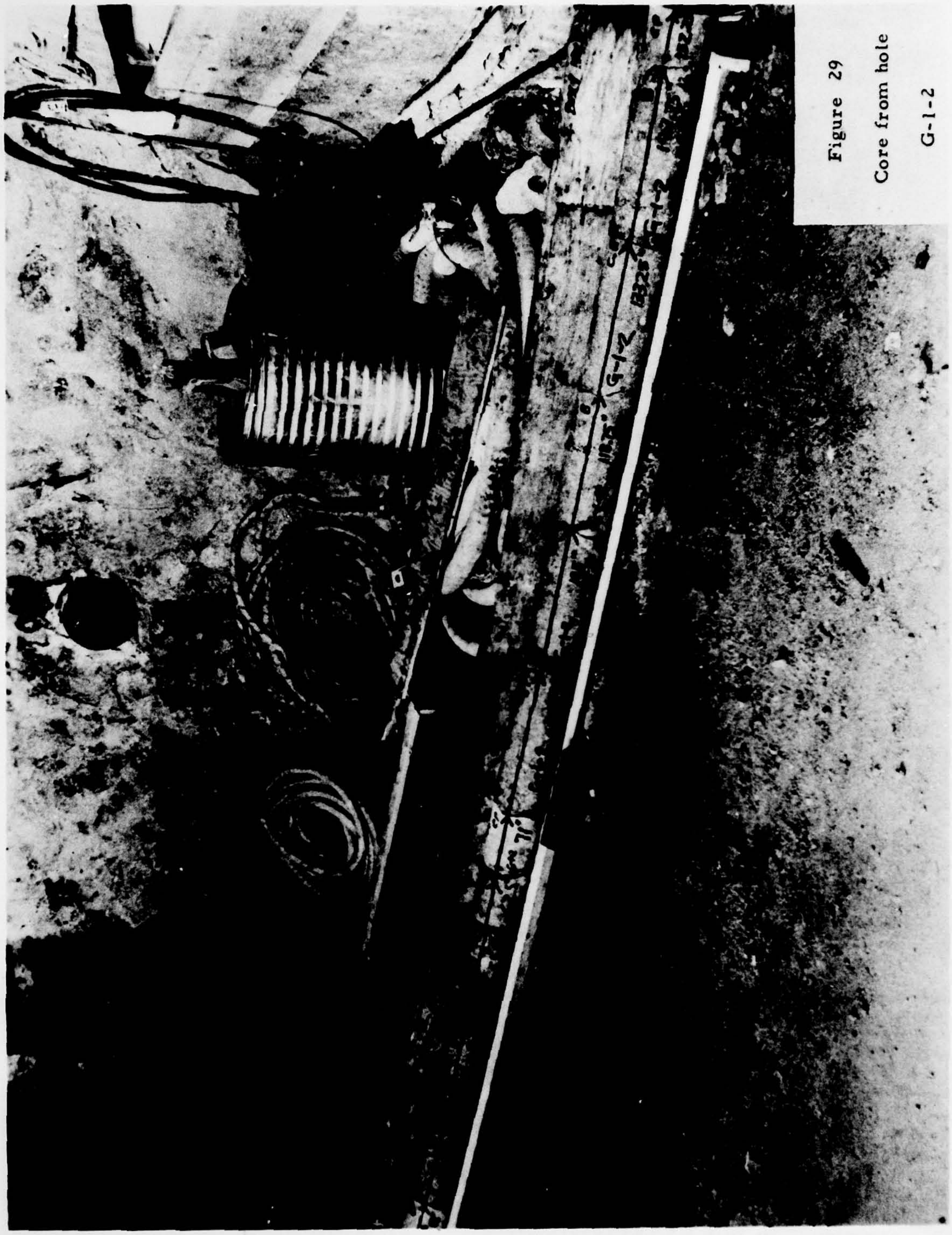

Figure 29
Core from hole
G-1-2

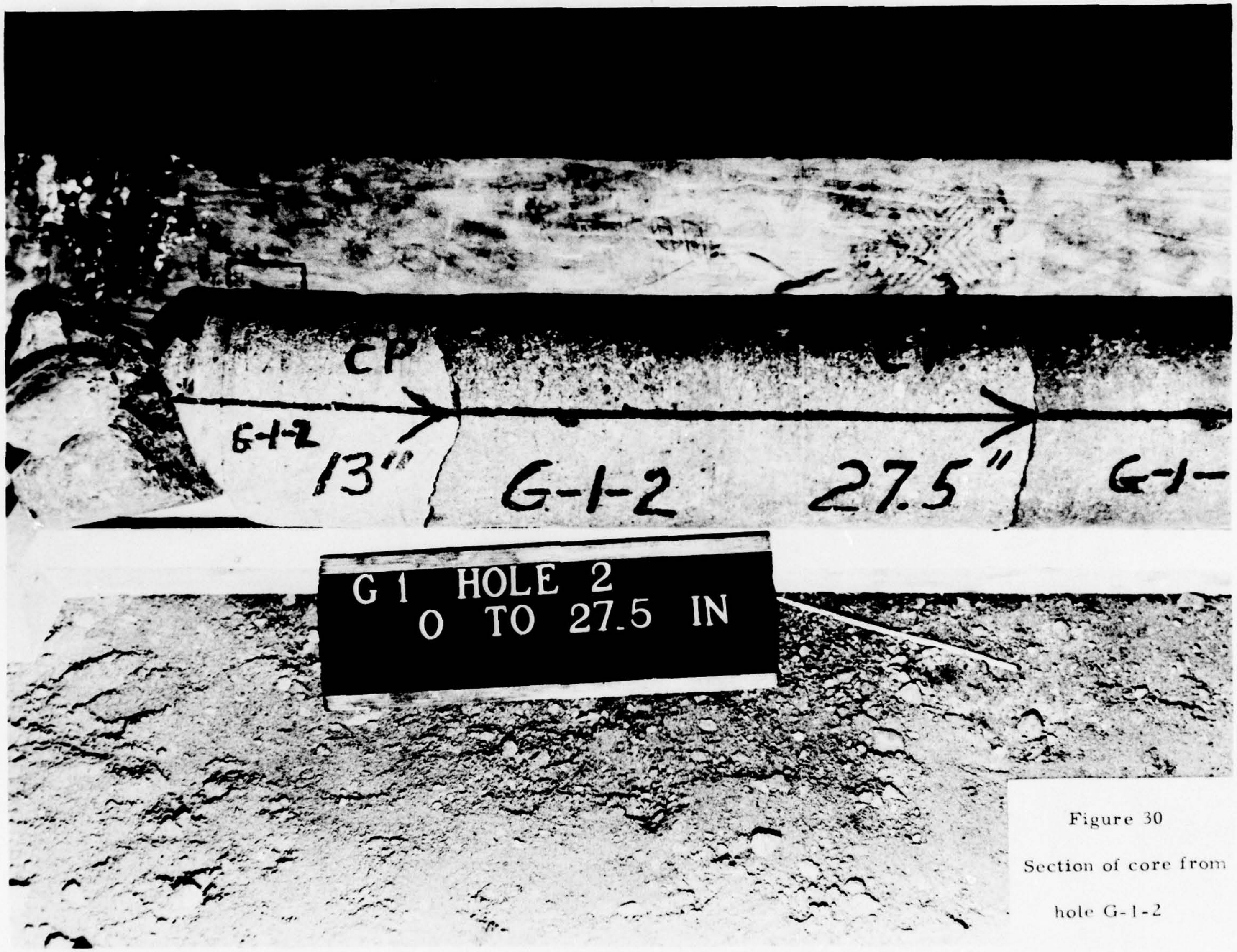

Figure 30

Section of core from hole G-1-2

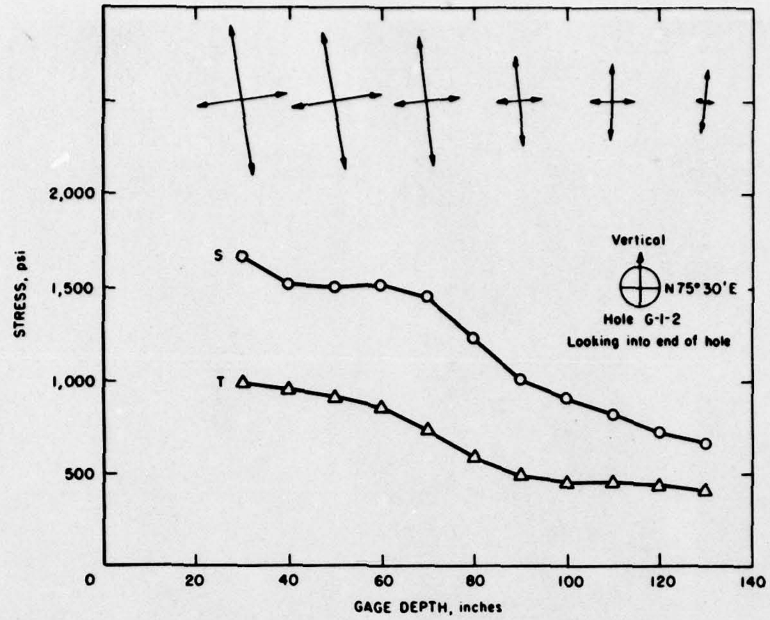

Figure 31 - Stress versus distance from face - hole G-1-2

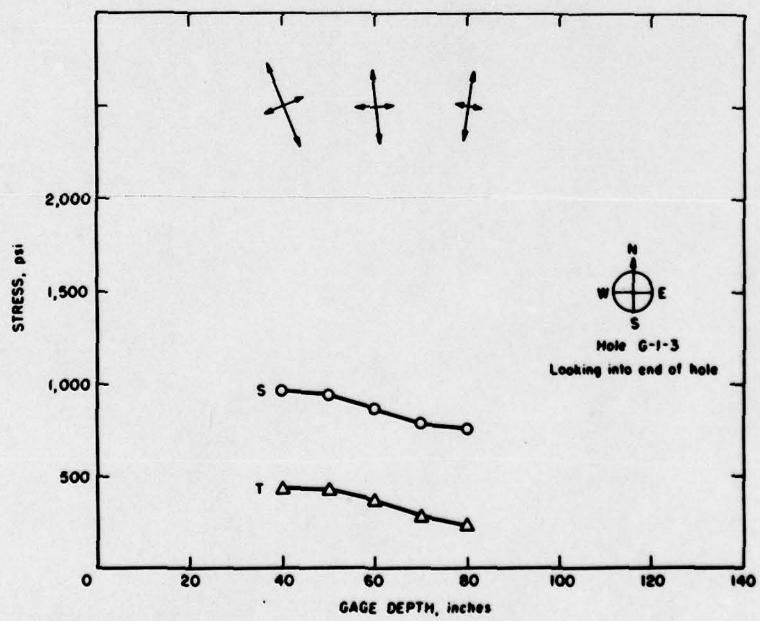

Figure 32 - Stress versus distance from face - hole G-1-3

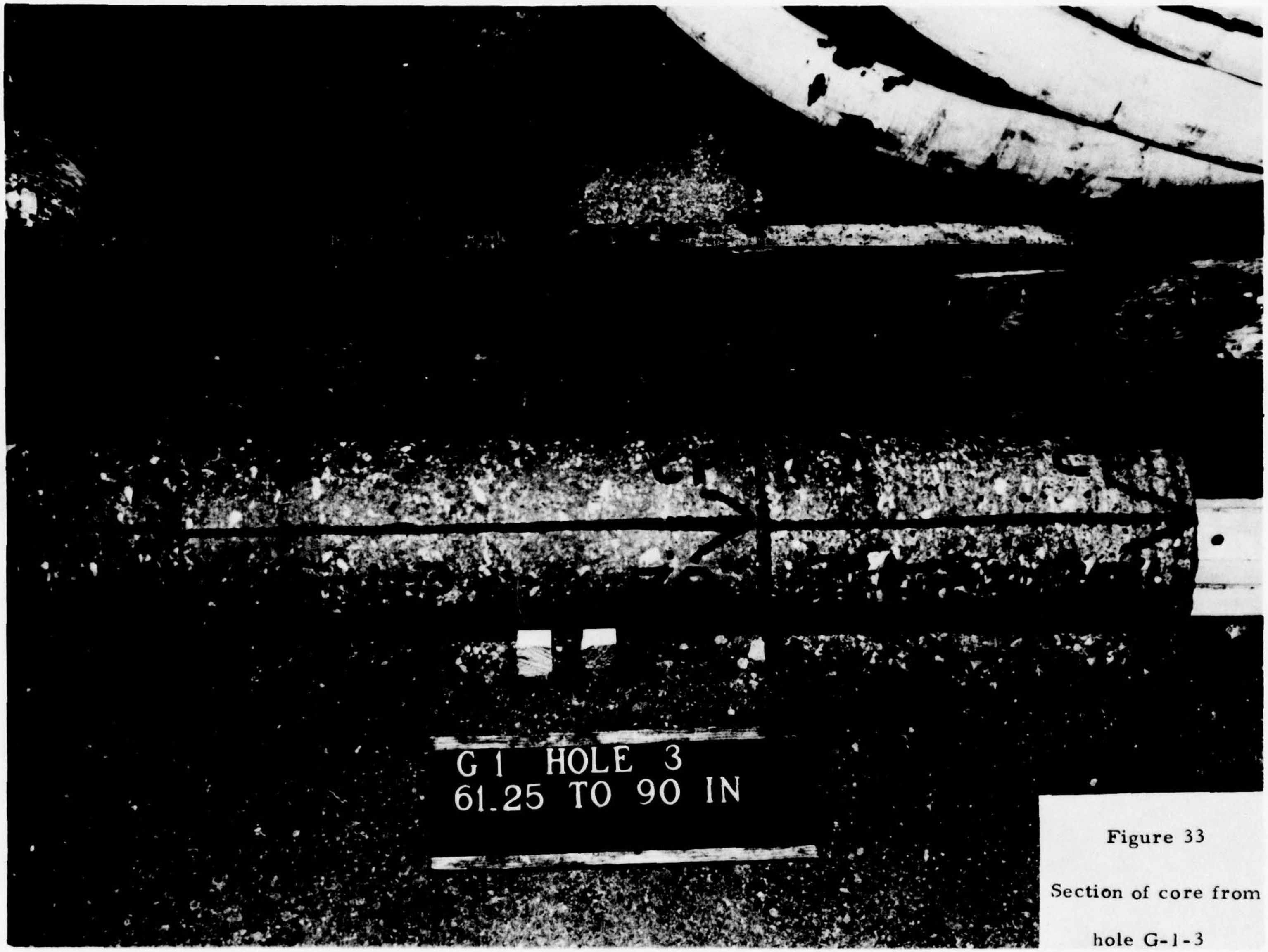

Figure 33

Section of core from hole G-1-3

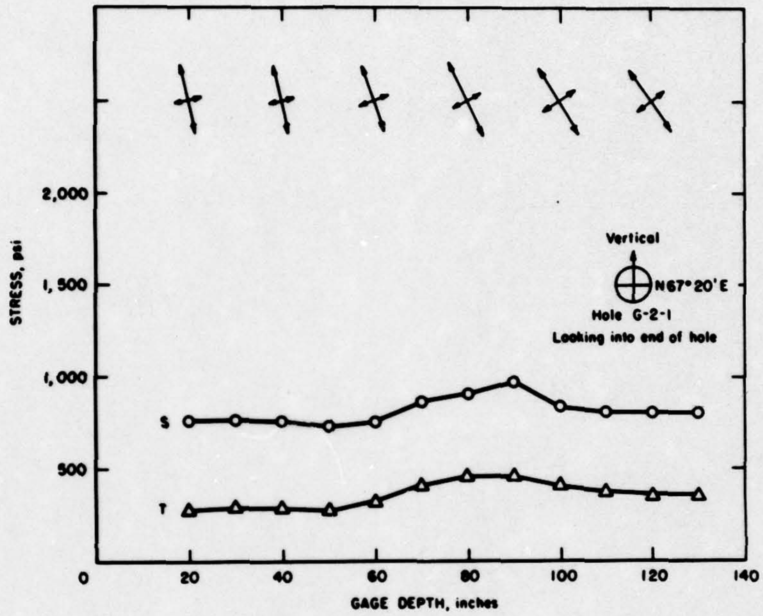

Figure 34 - Stress versus distance from face - hole G-2-1

Figure 35
Core from hole
G-2-1

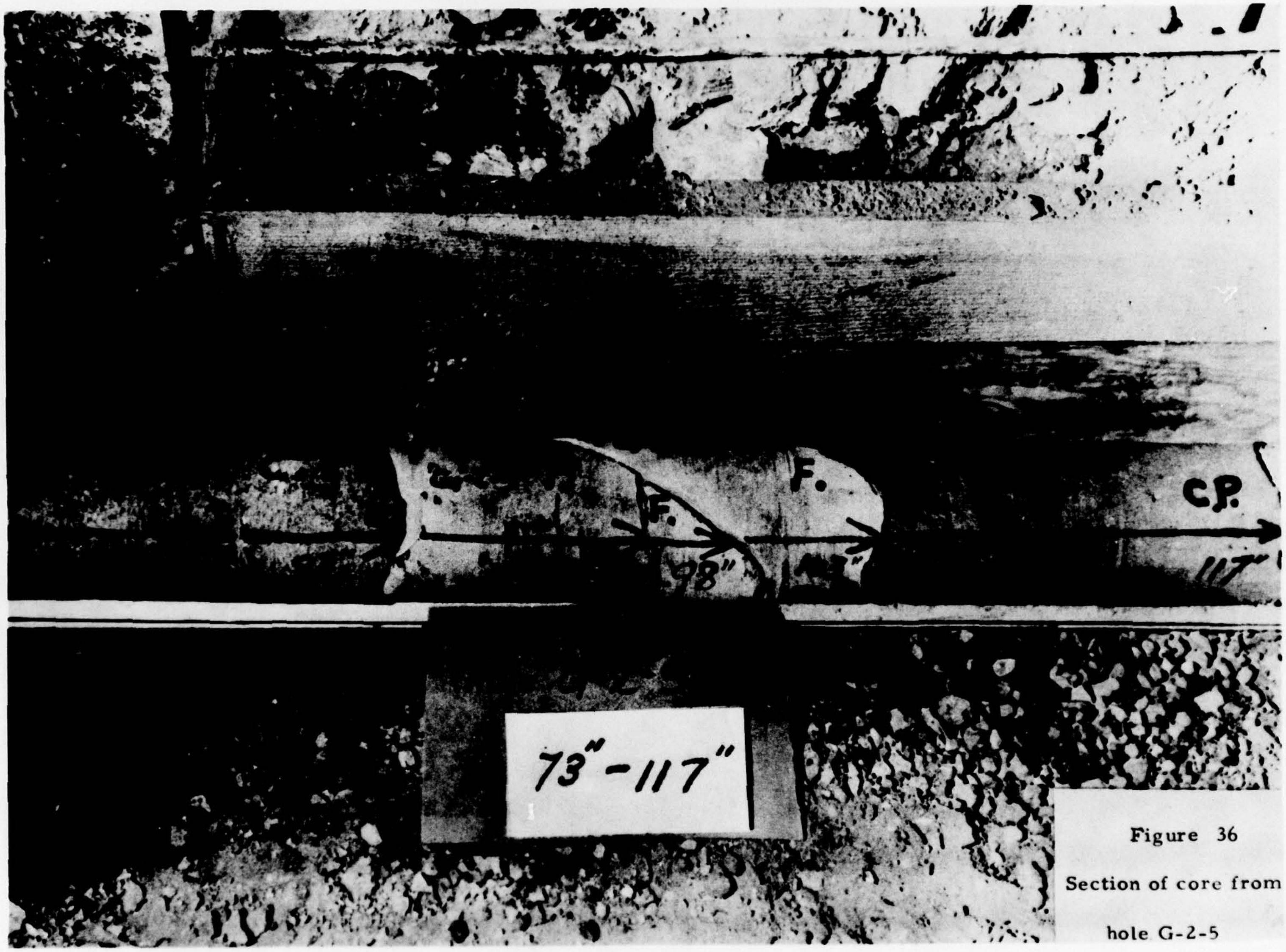

Figure 36

Section of core from hole G-2-5

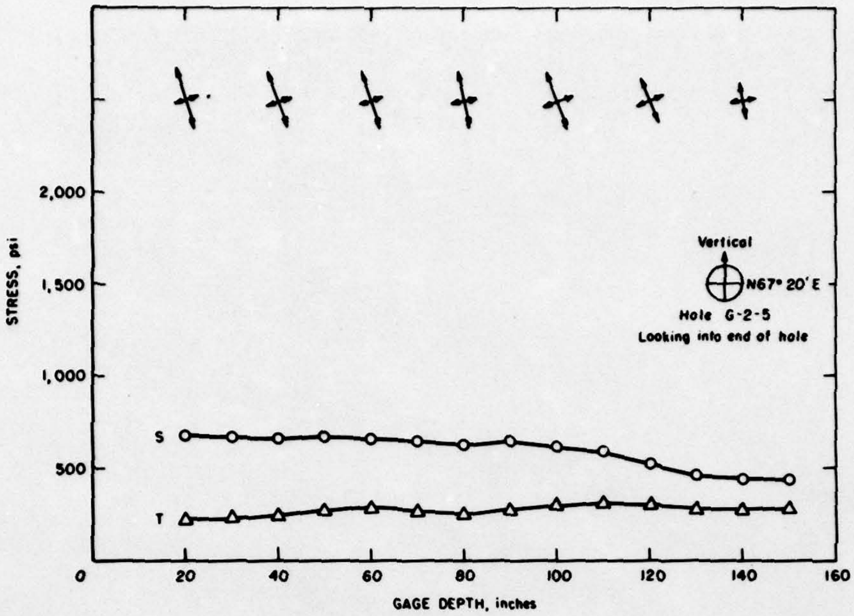

Figure 37 - Stress versus distance from face - hole G-2-5

Figure 38
Section of core from
hole G-2-4

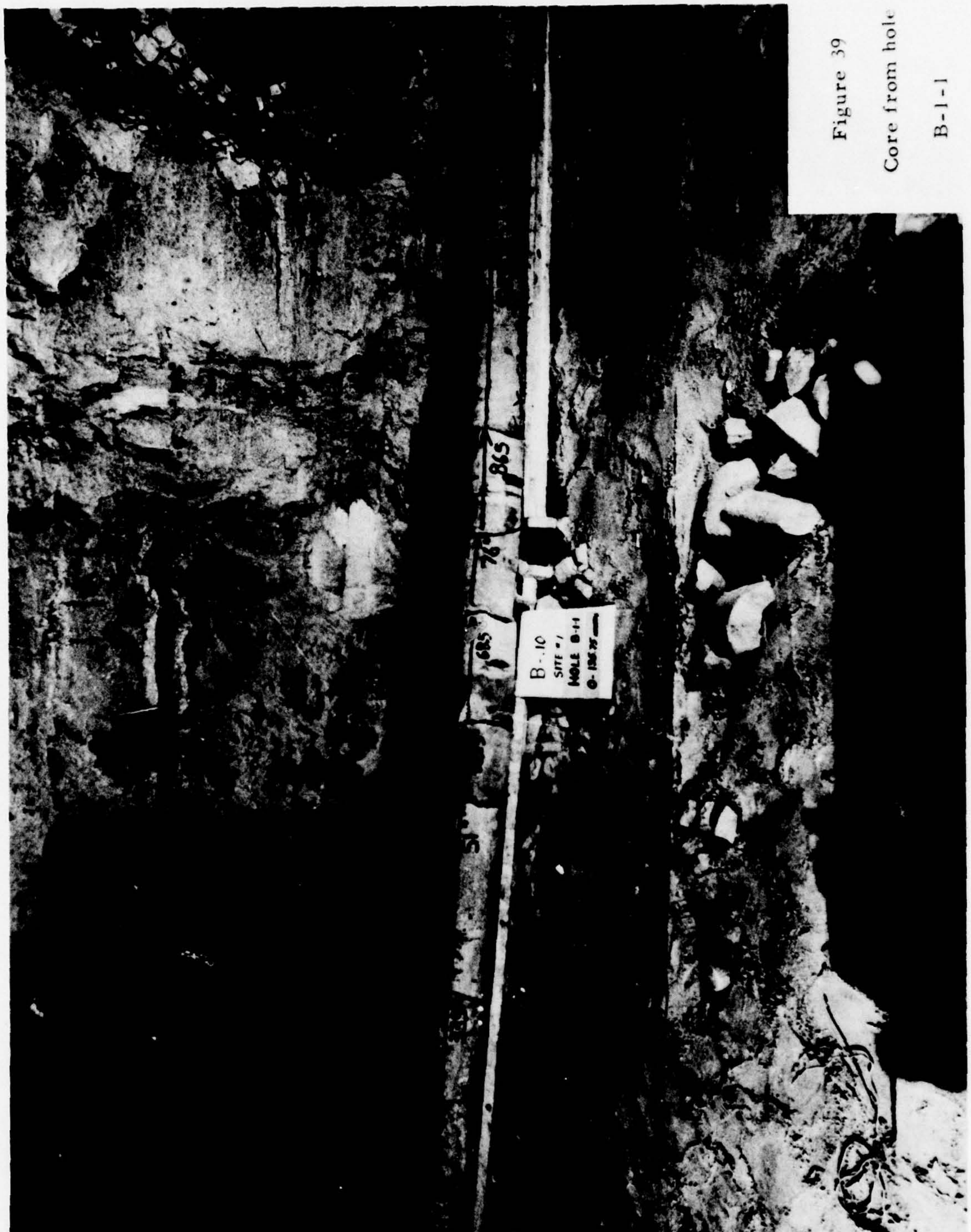

Figure 39
Core from hole
B-1-1

Figure 40

Section of core from hole B-1-1

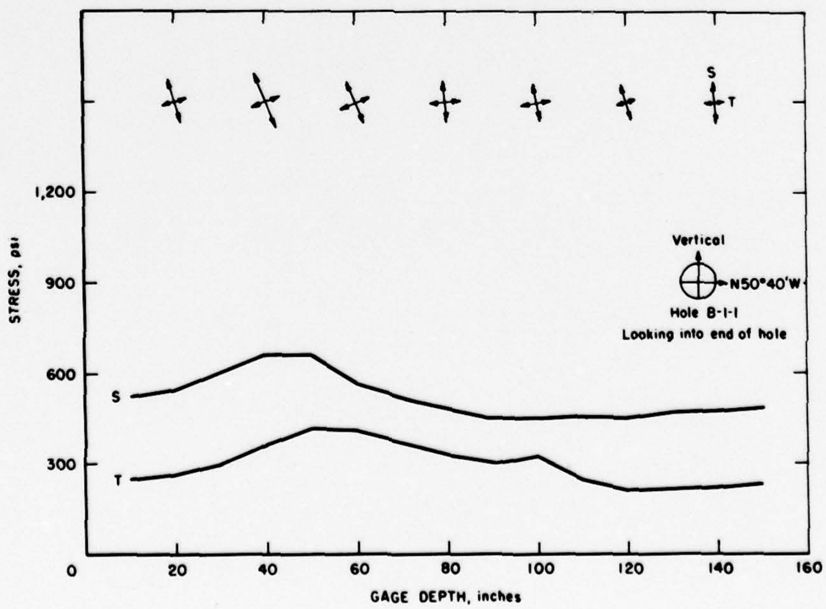

Figure 41 - **Stress versus distance from face - hole B-1-1**

Figure 42

Section of core from

hole B-1-2

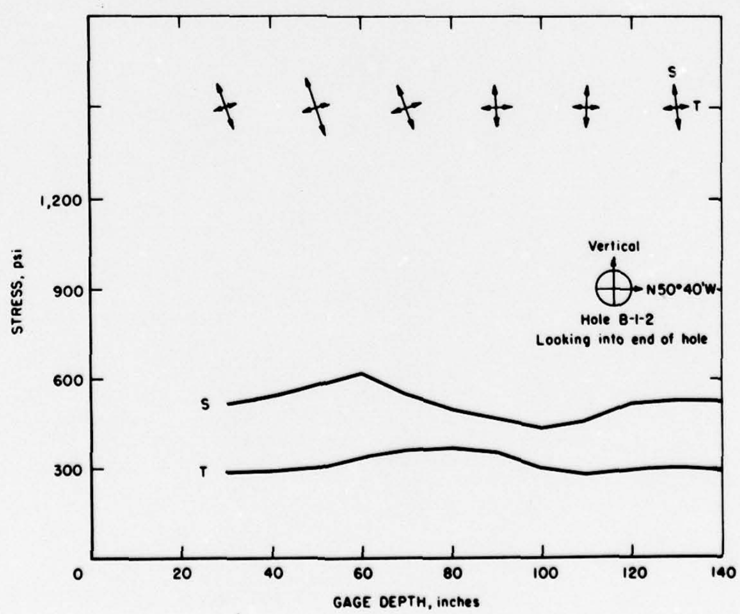

Figure 43 - Stress versus distance from face - hole B-1-2

Figure 44

Core from hole

B-1-4

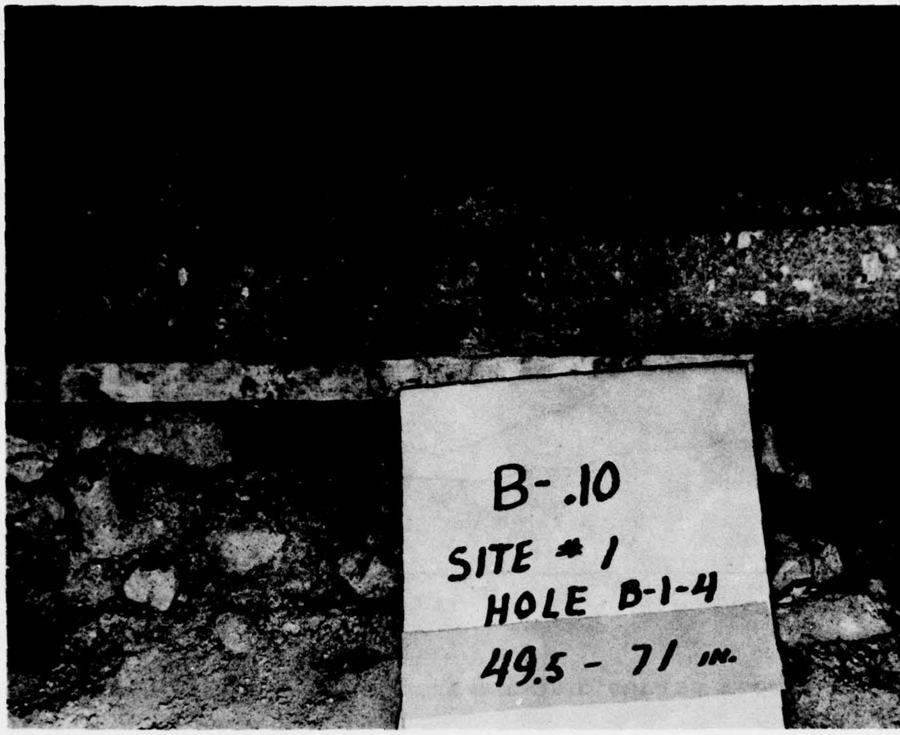

Figure 45
Section of core from
hole B-1-4

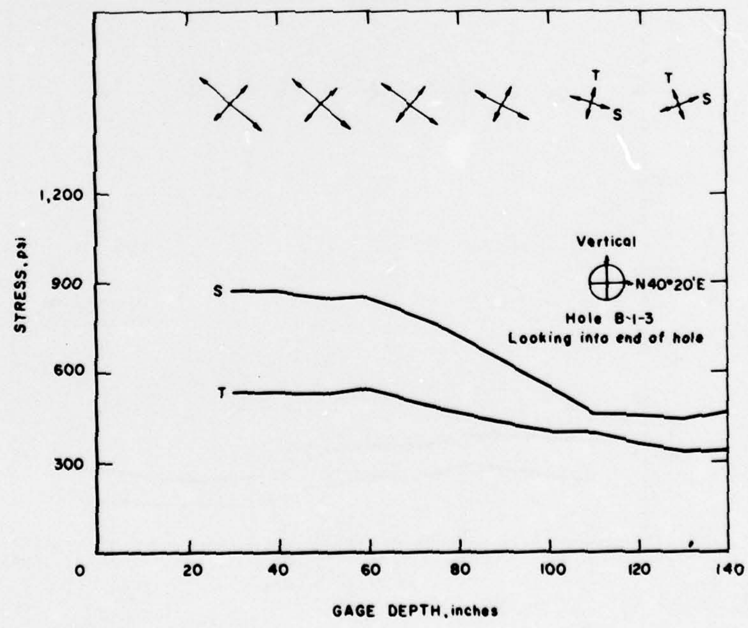

Figure 46 - Stress versus distance from face - hole B-1-3

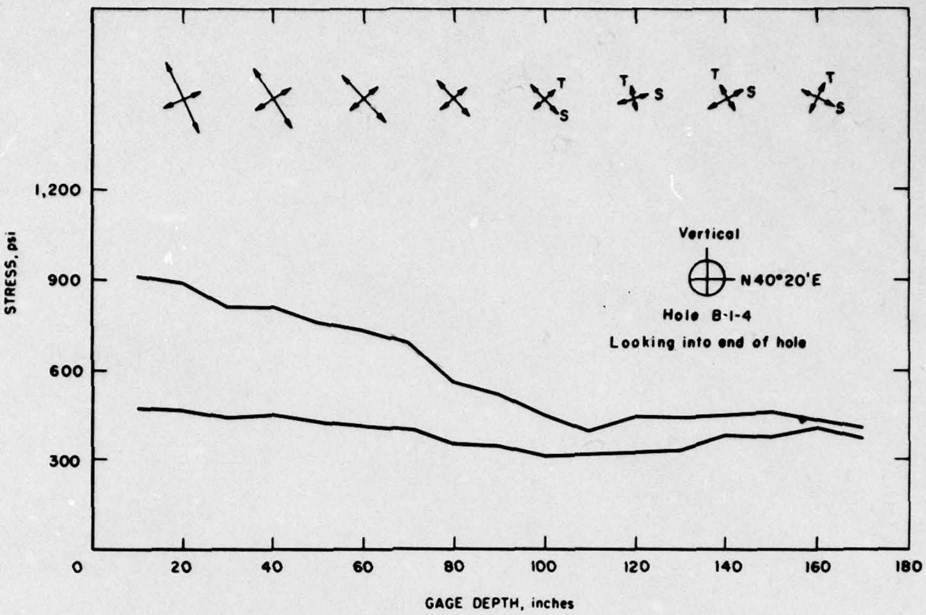

Figure 47 - Stress versus distance from face - hole B-1-4

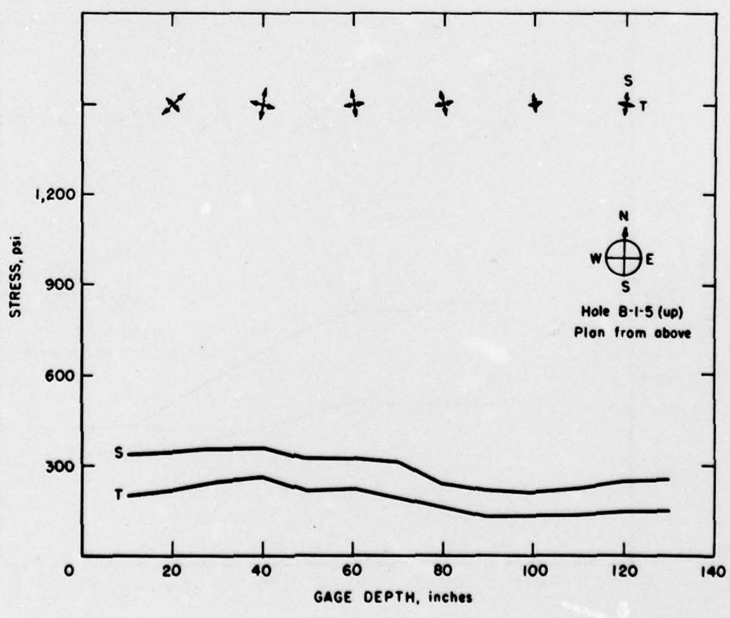

Figure 48 - Stress versus distance from face - hole B-1-5 (up)

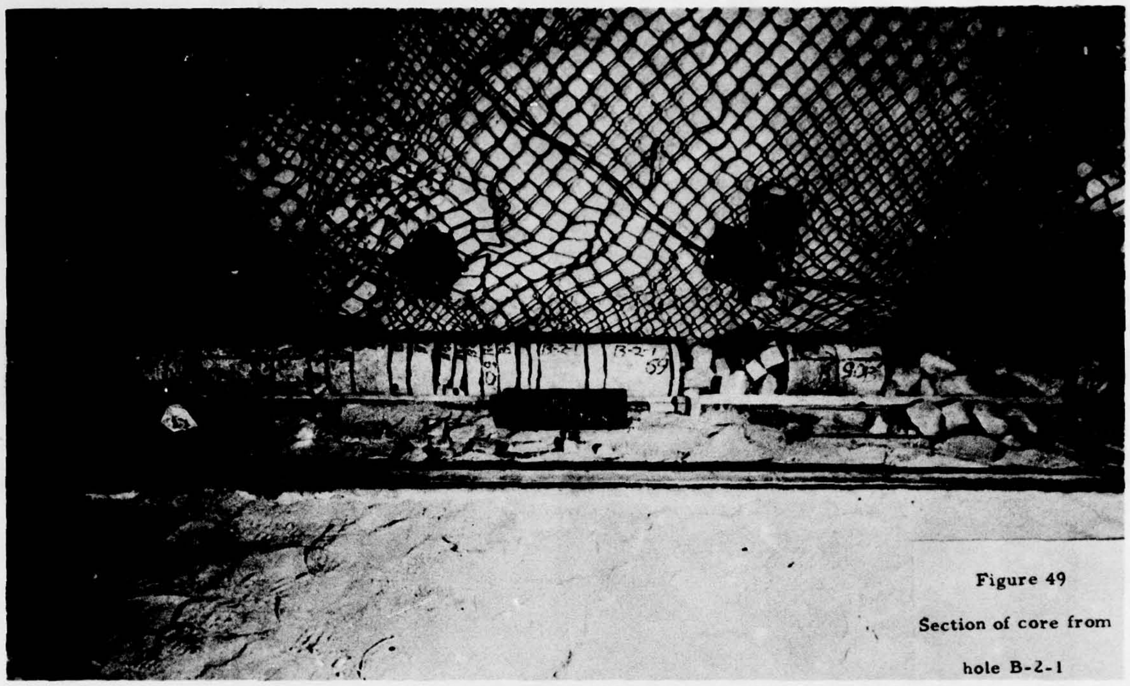

Figure 49

Section of core from

hole B-2-1

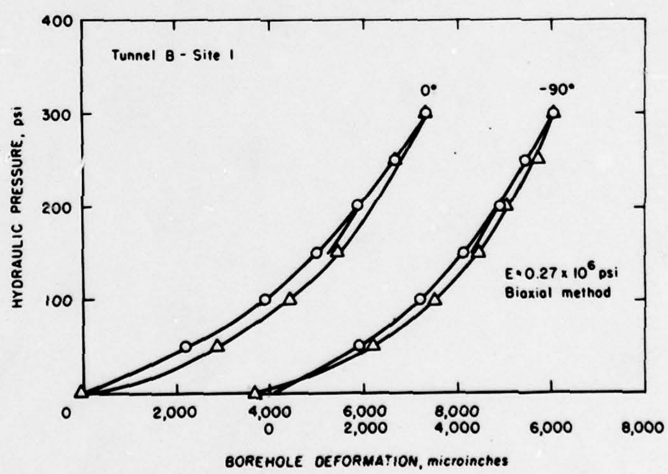

Figure 50 - **Data for modulus of elasticity at 140" depth - hole 1**

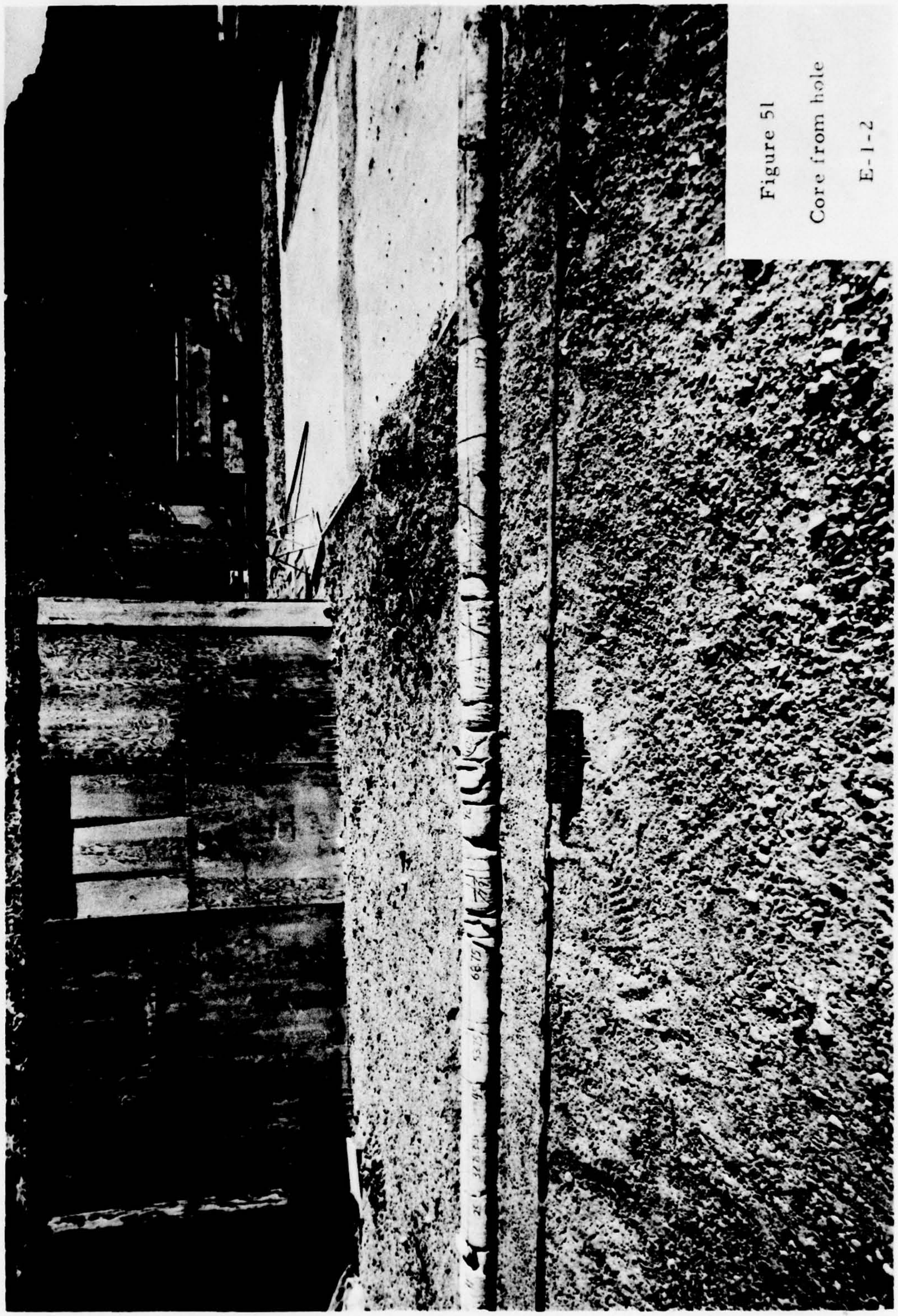

Figure 51

Core from hole

E-1-2

Figure 52

Core from hole

E-1-5

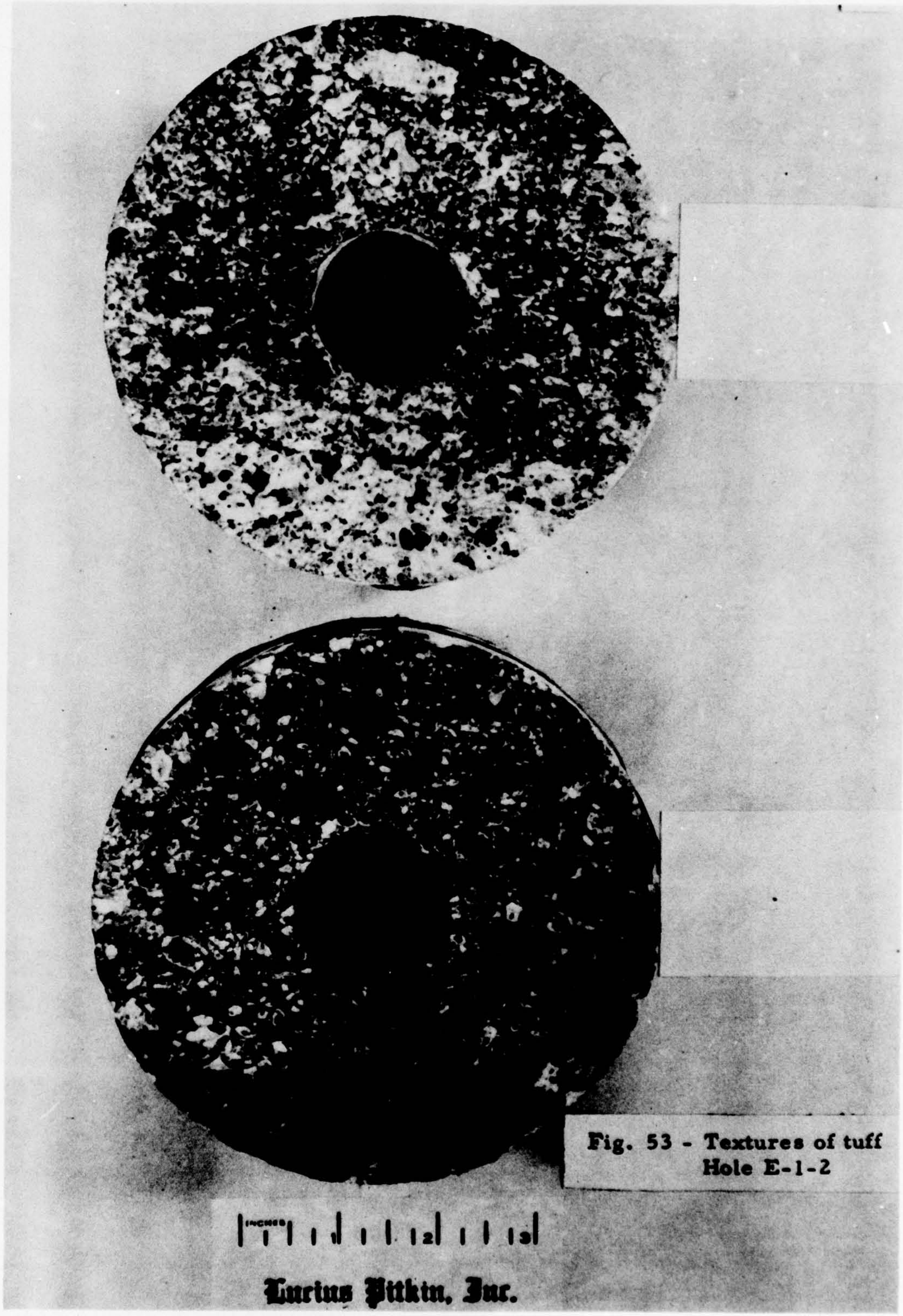

Fig. 53 - Textures of tuff
Hole E-1-2

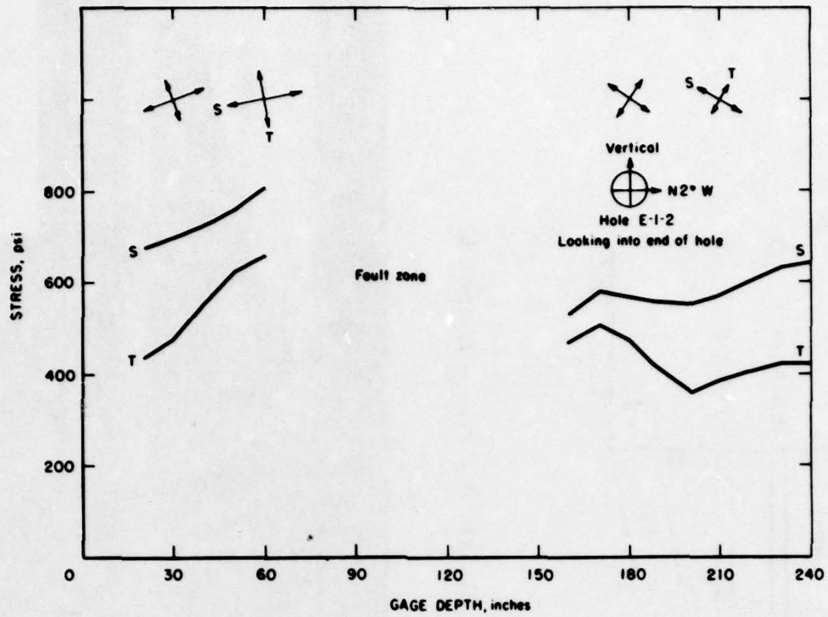

Figure 54 - Stress versus distance from face - hole E-1-2

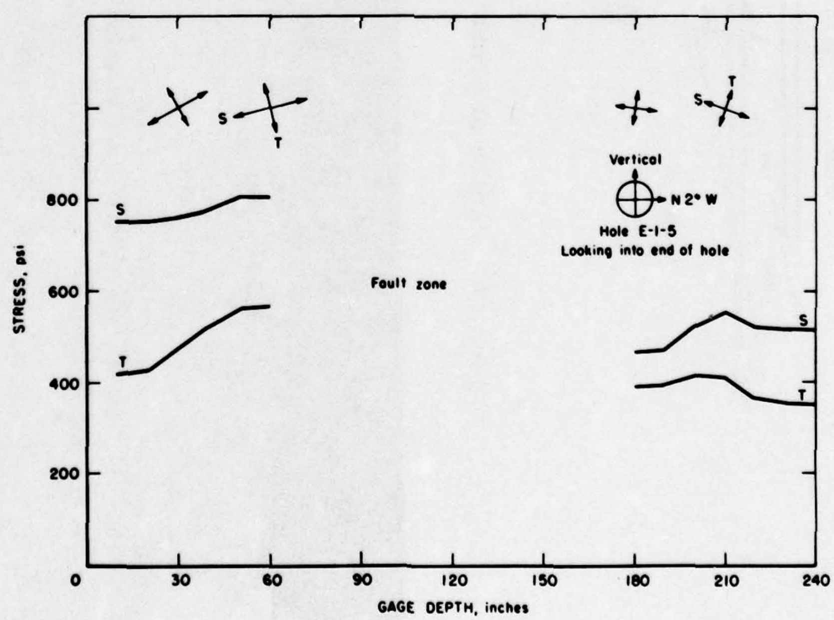

Figure 55 - Stress versus distance from face - hole E-1-5

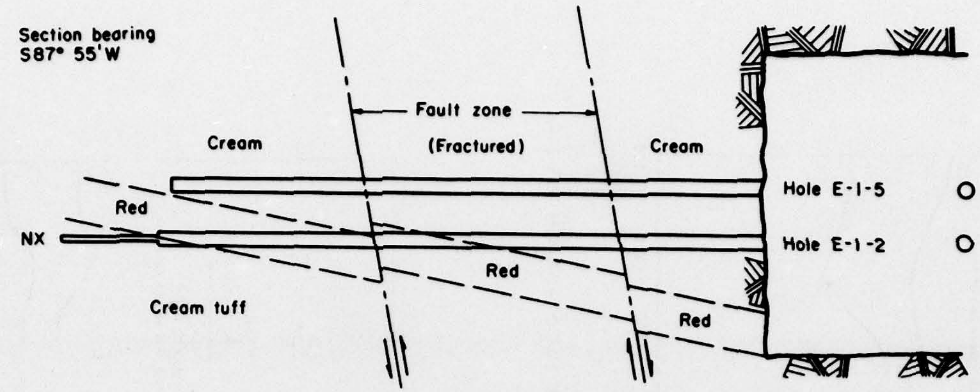

Elevation

Figure 56 - Sketch of probable structure at drilling site - tunnel E

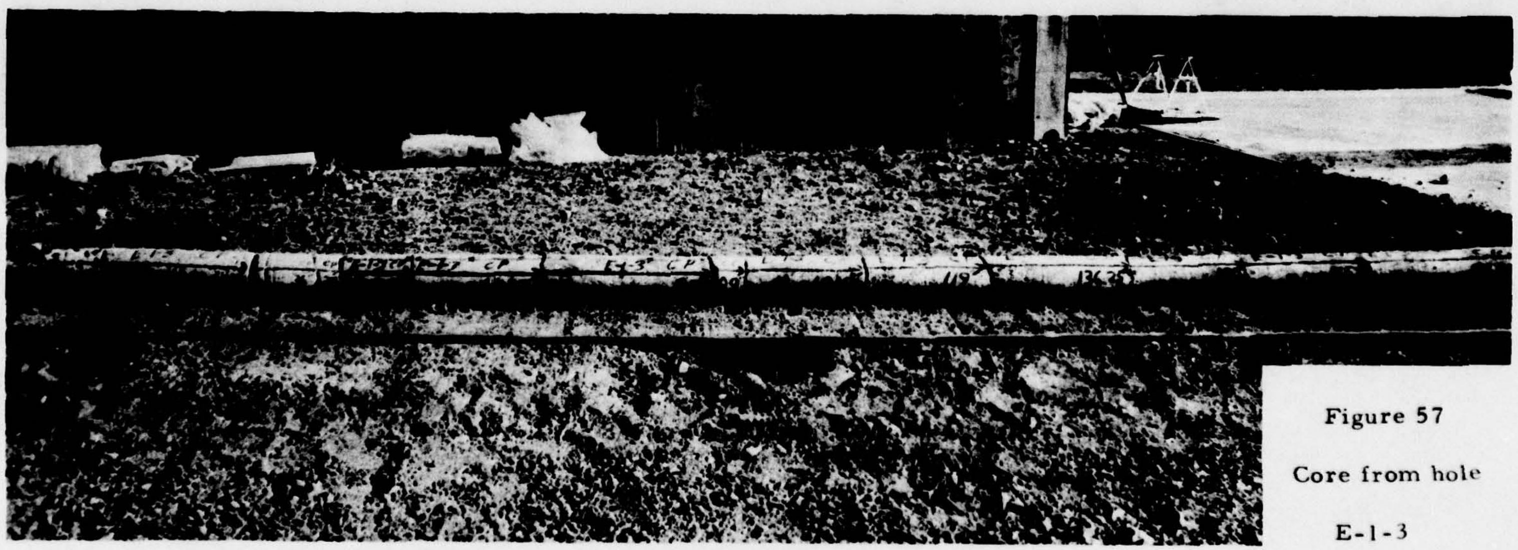

Figure 57

Core from hole

E-1-3

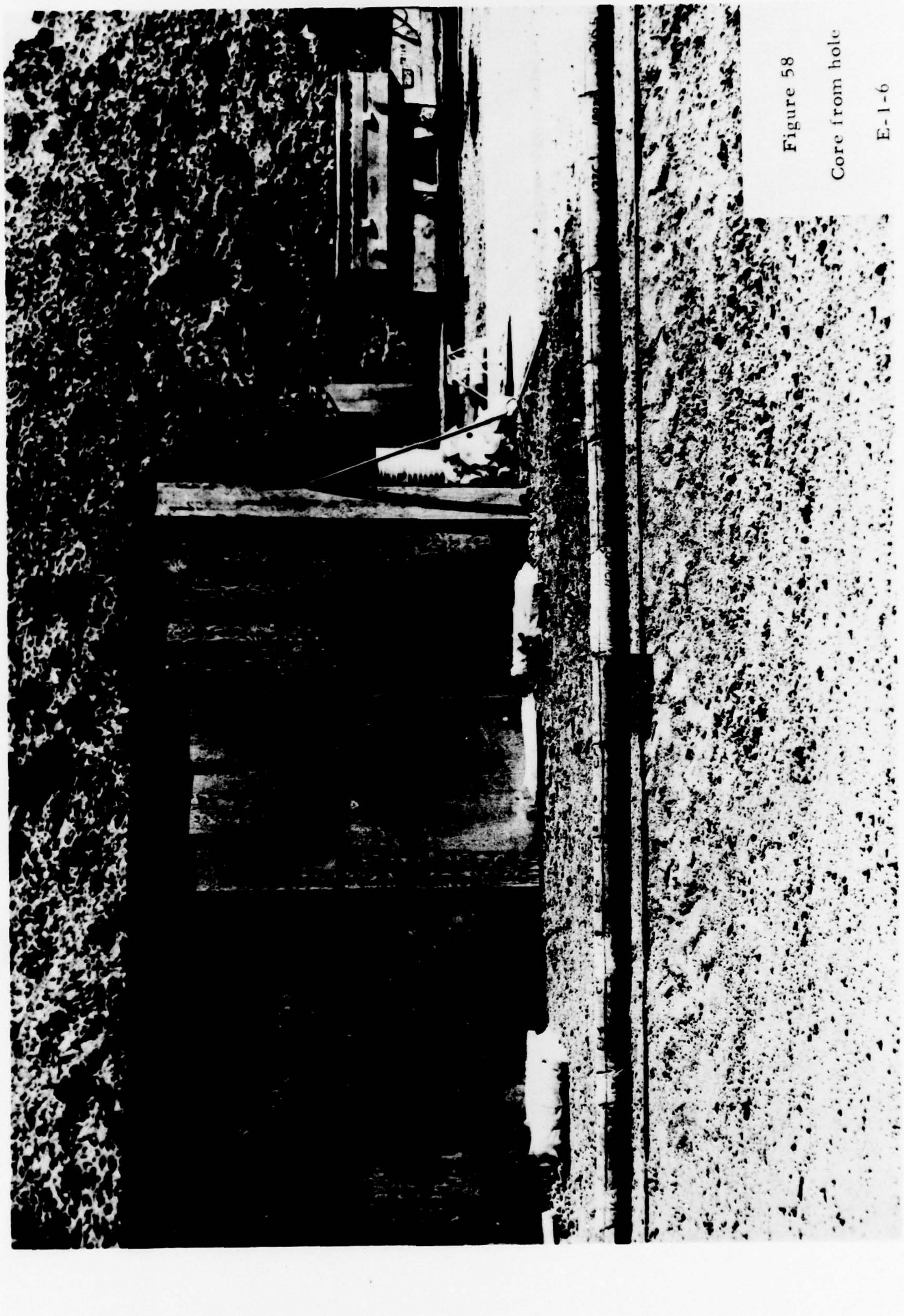

Figure 58

Core from hole

E-1-6

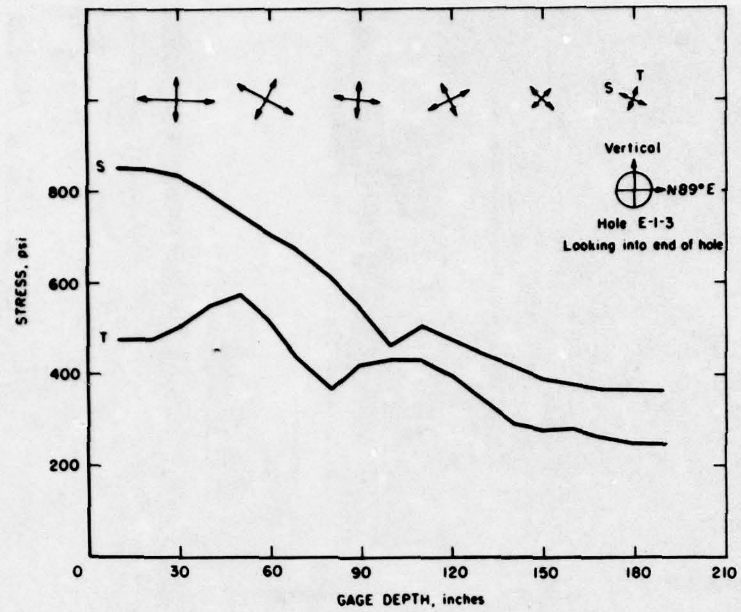

Figure 59 - Stress versus distance from face -- hole E-1-3

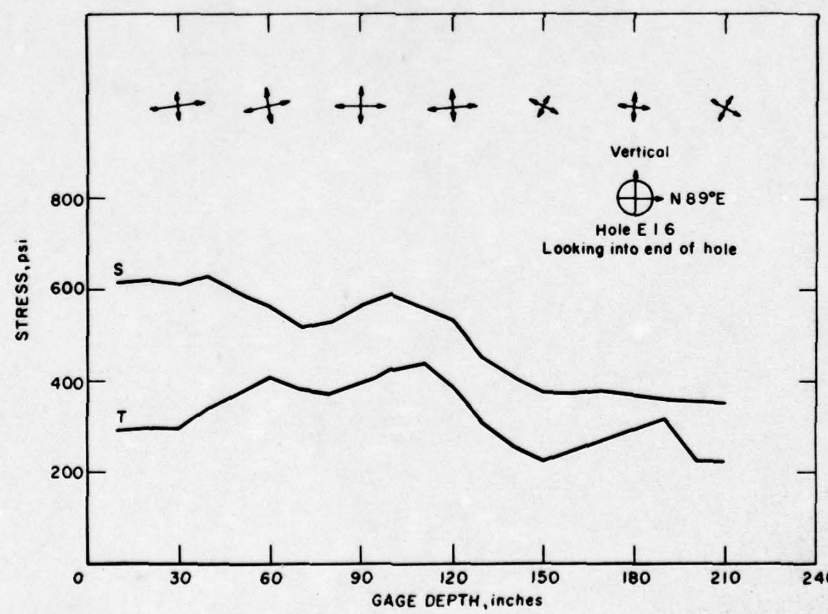

Figure 60 - Stress versus distance from face - hole E-1-6

Figure 61

Core from hole

E-1-4

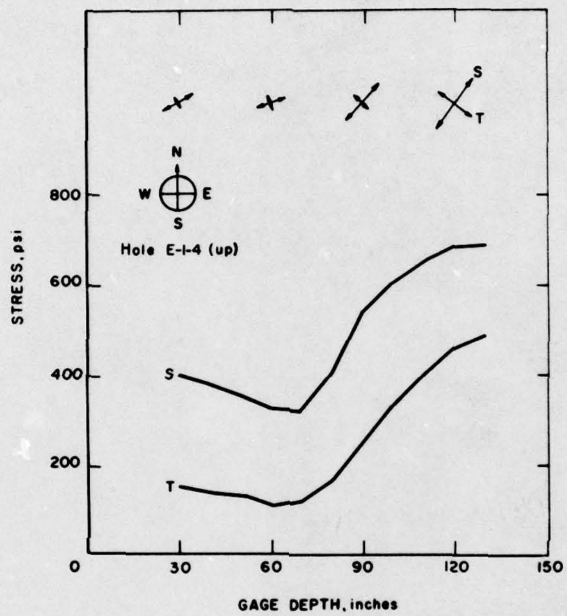

Figure 62 - Stress versus distance from face - hole E-1-4 (up)

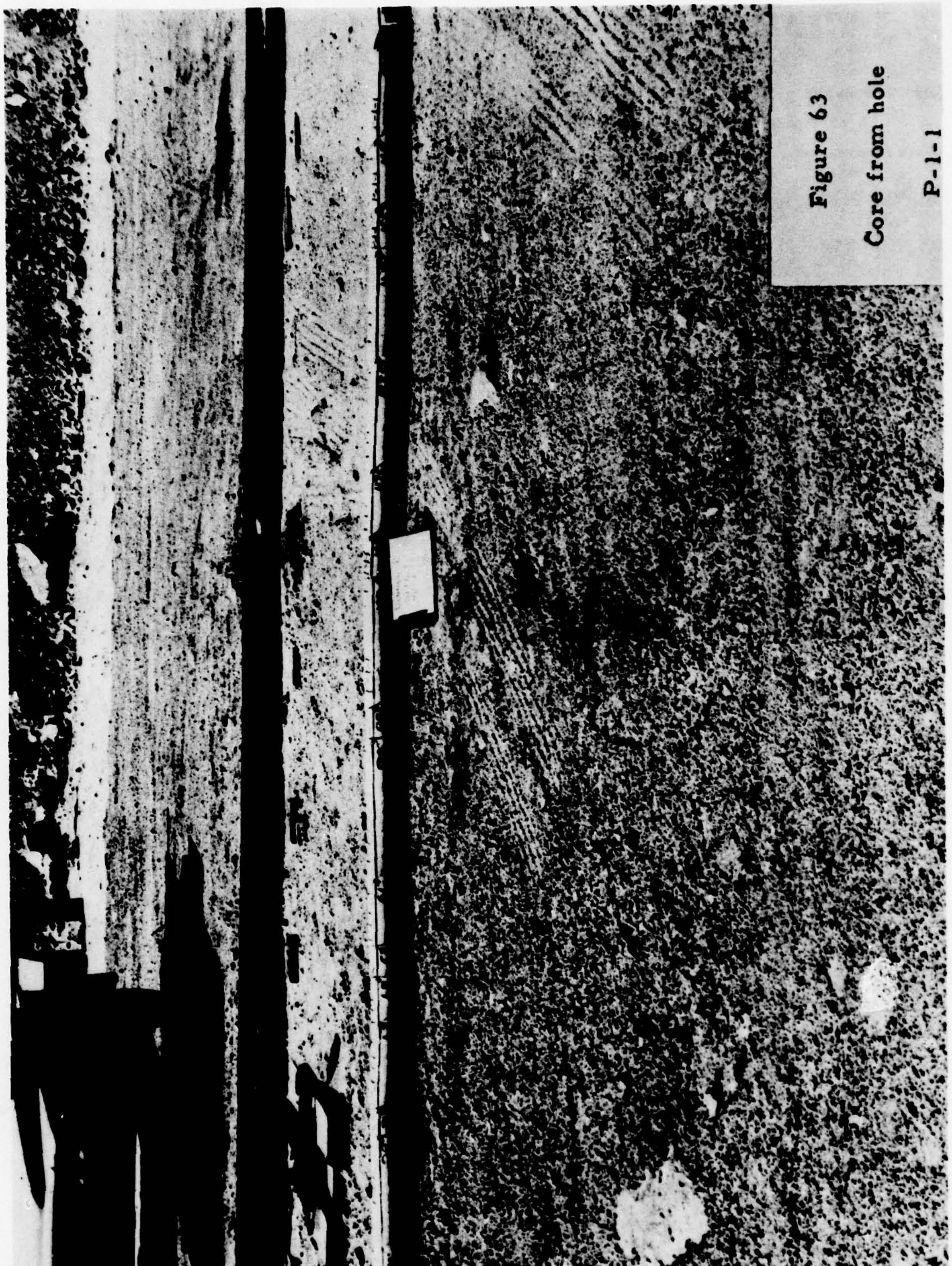

Figure 63
Core from hole
P-1-1

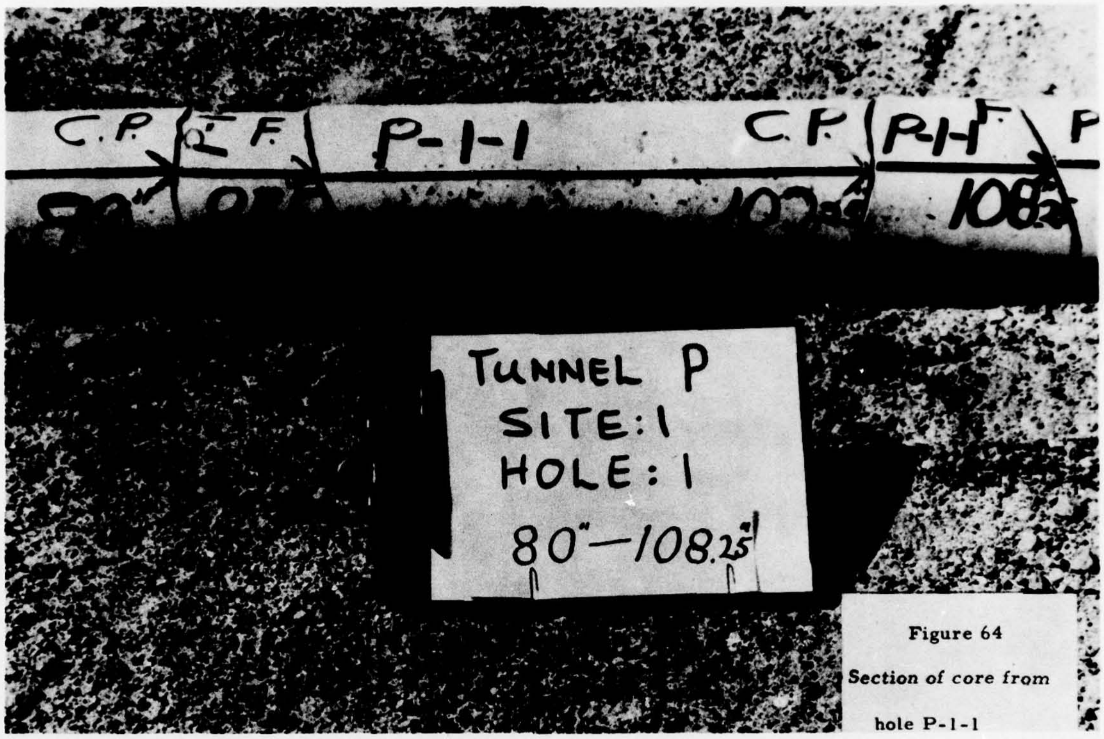

Figure 64

Section of core from

hole P-1-1

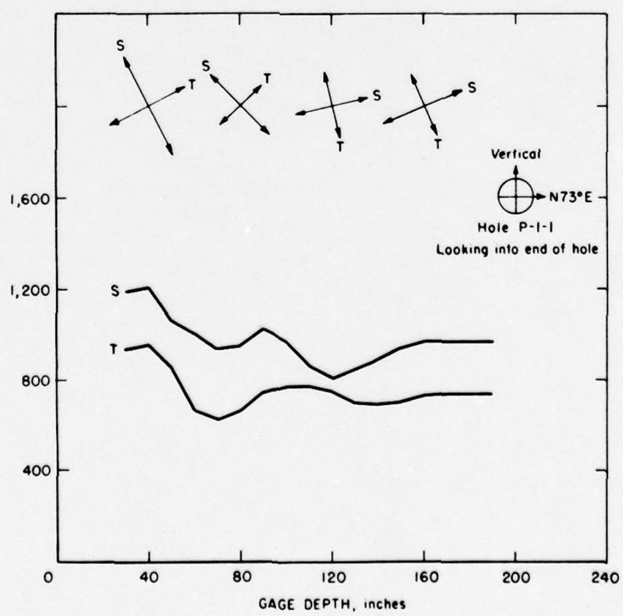

Figure 65 - **Stress versus distance from face - hole P-1-1**

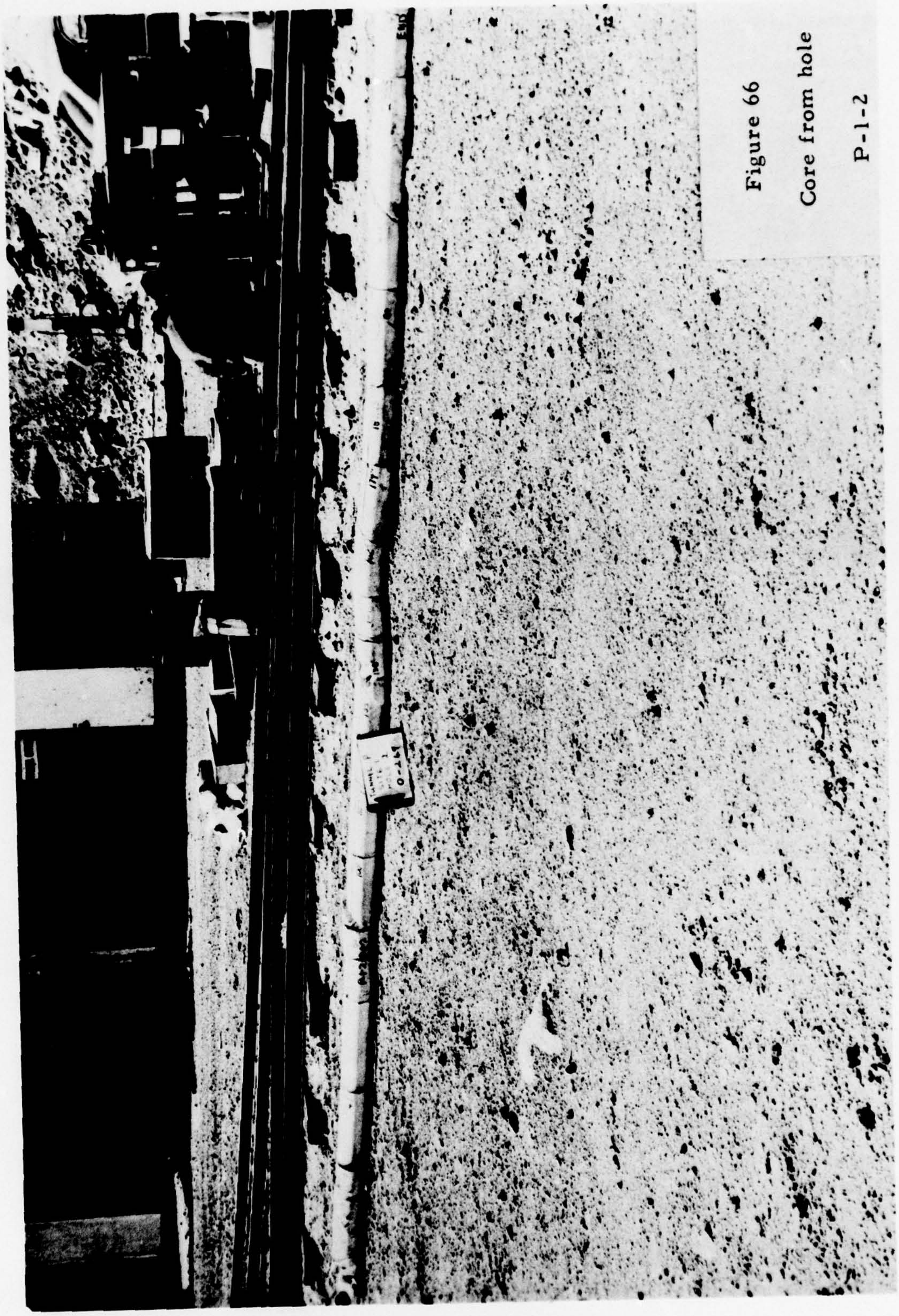

Figure 66
Core from hole
P-1-2

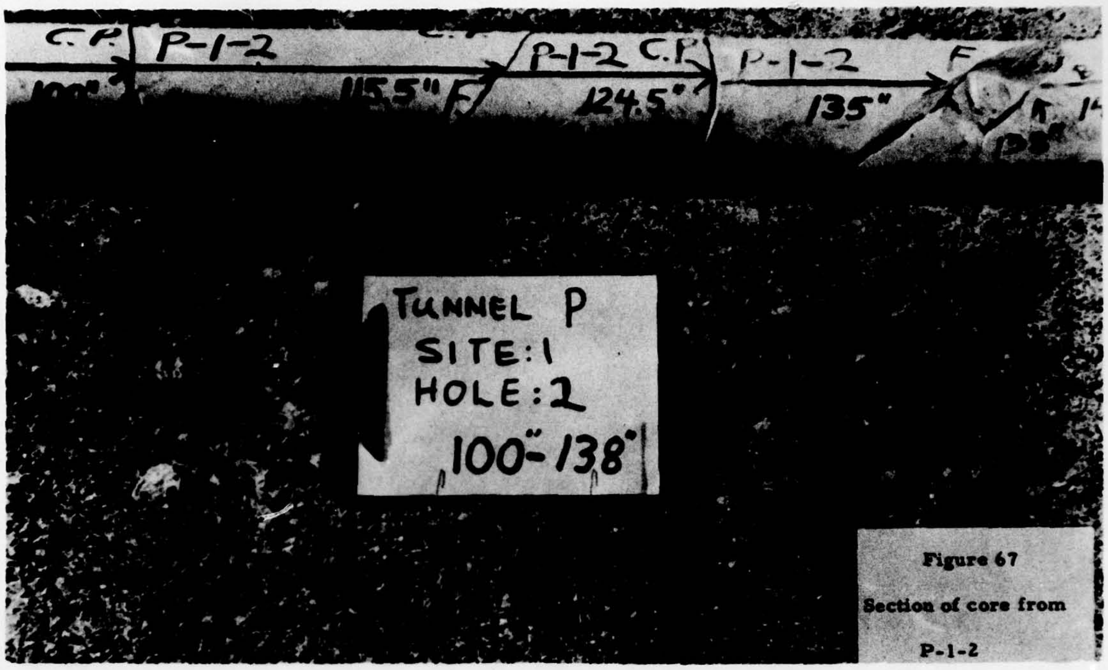

Figure 67

Section of core from

P-1-2

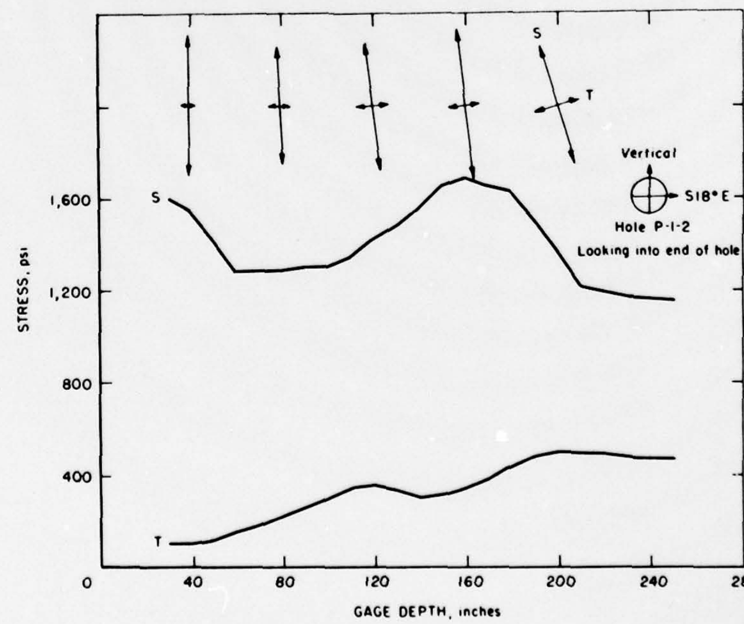

Figure 68 - **Stress versus distance from face - hole P-1-2**

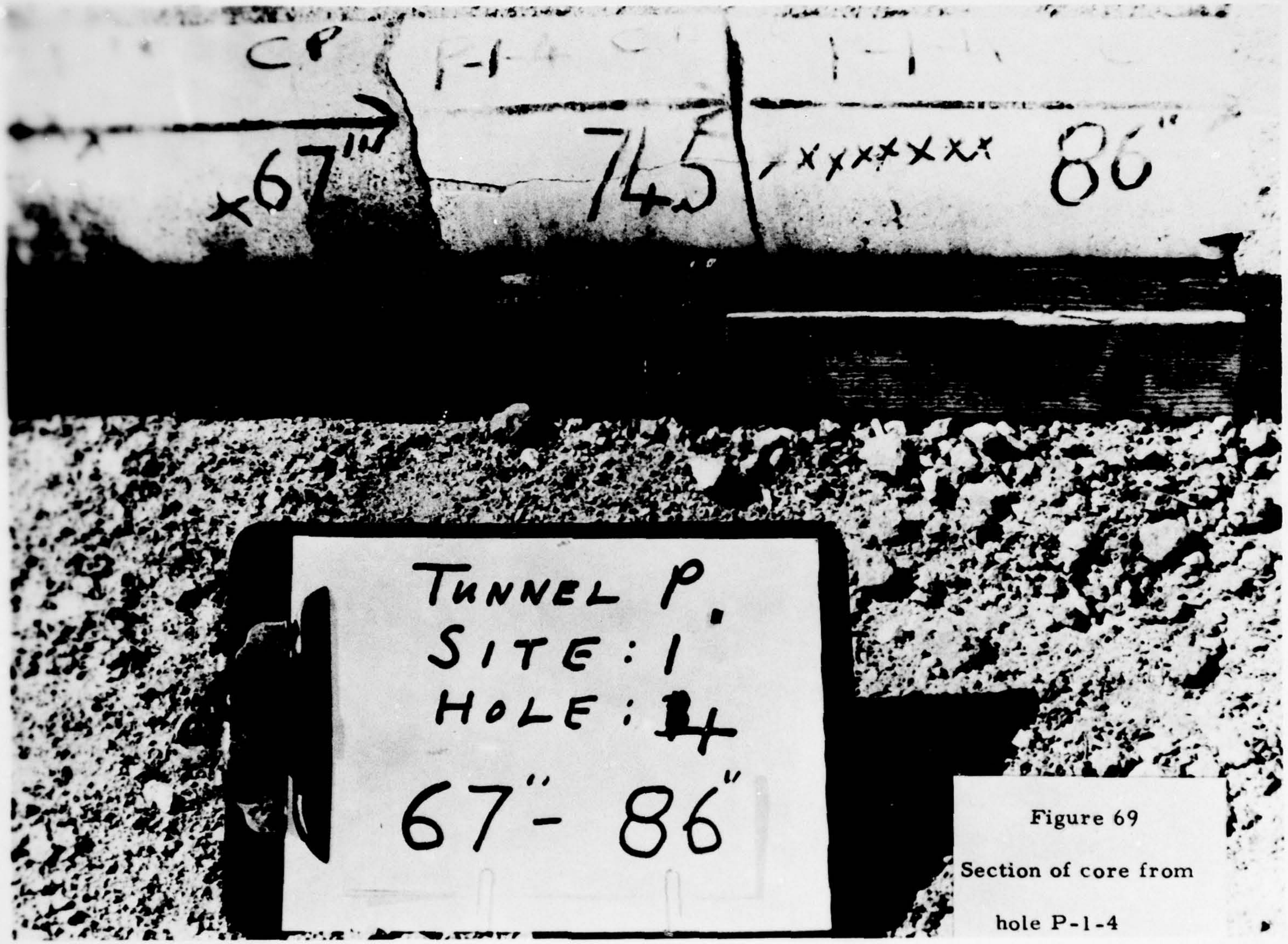

Figure 69

Section of core from

hole P-1-4

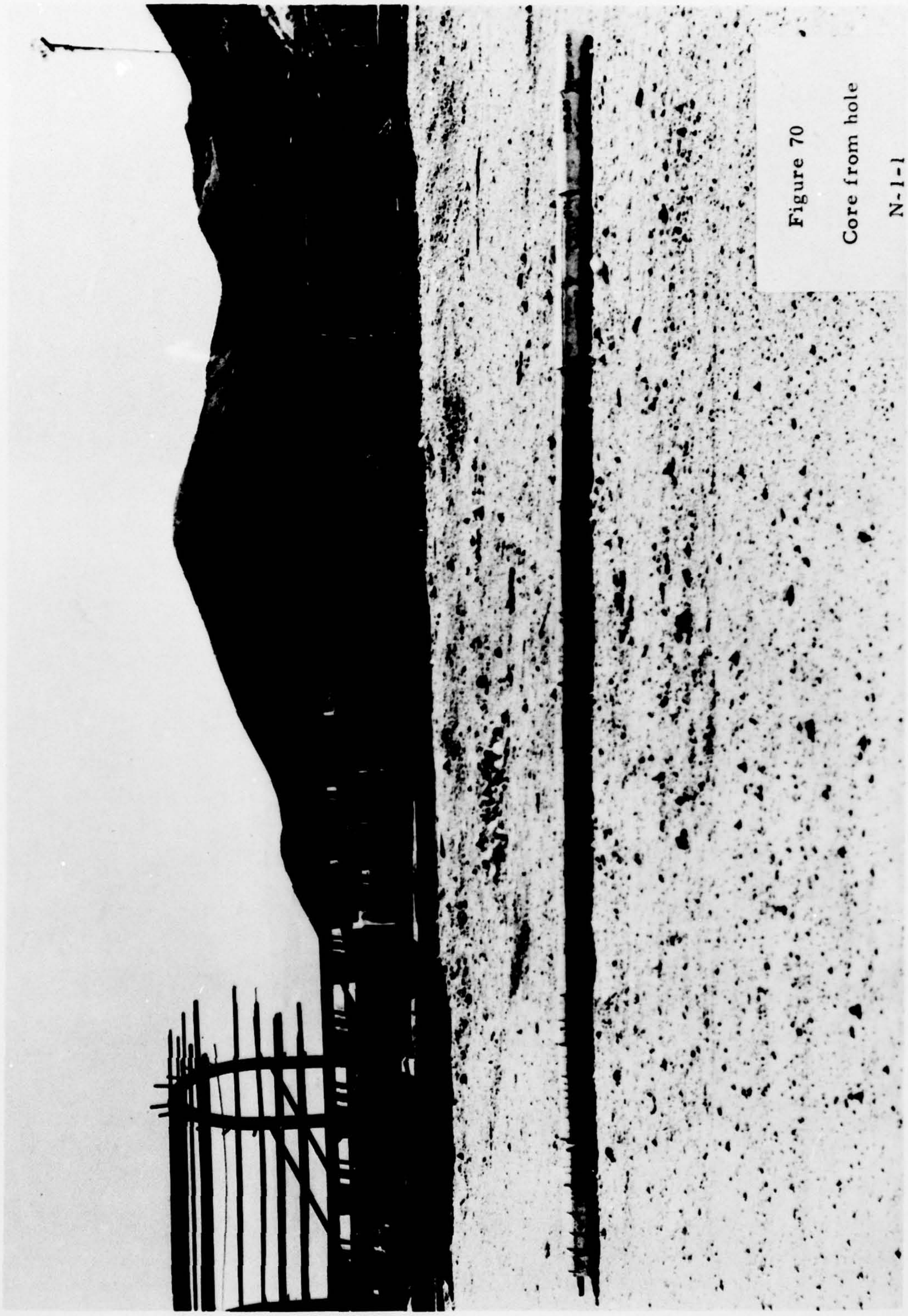

Figure 70

Core from hole

N-1-1

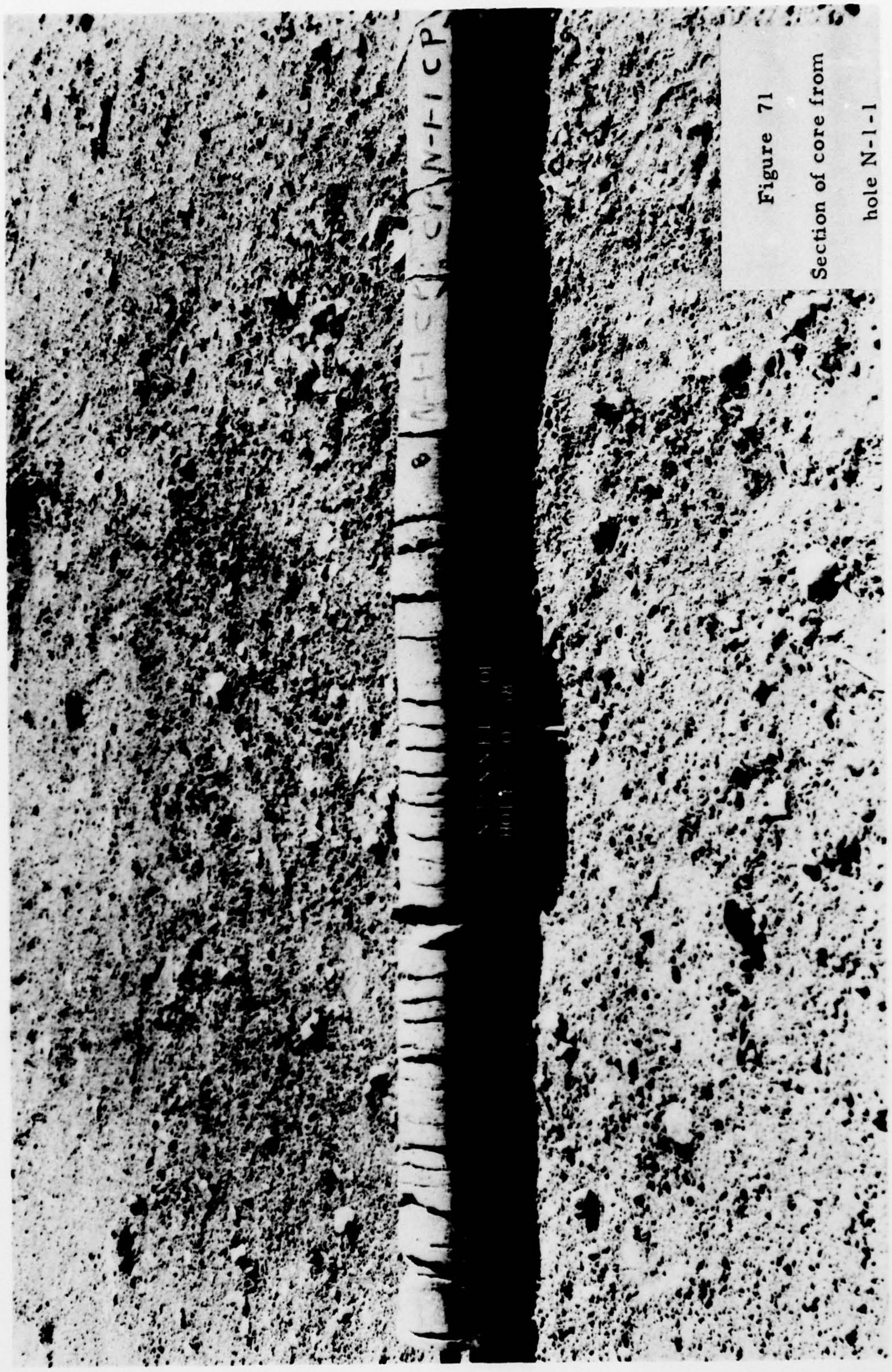

Figure 71
Section of core from hole N-1-1

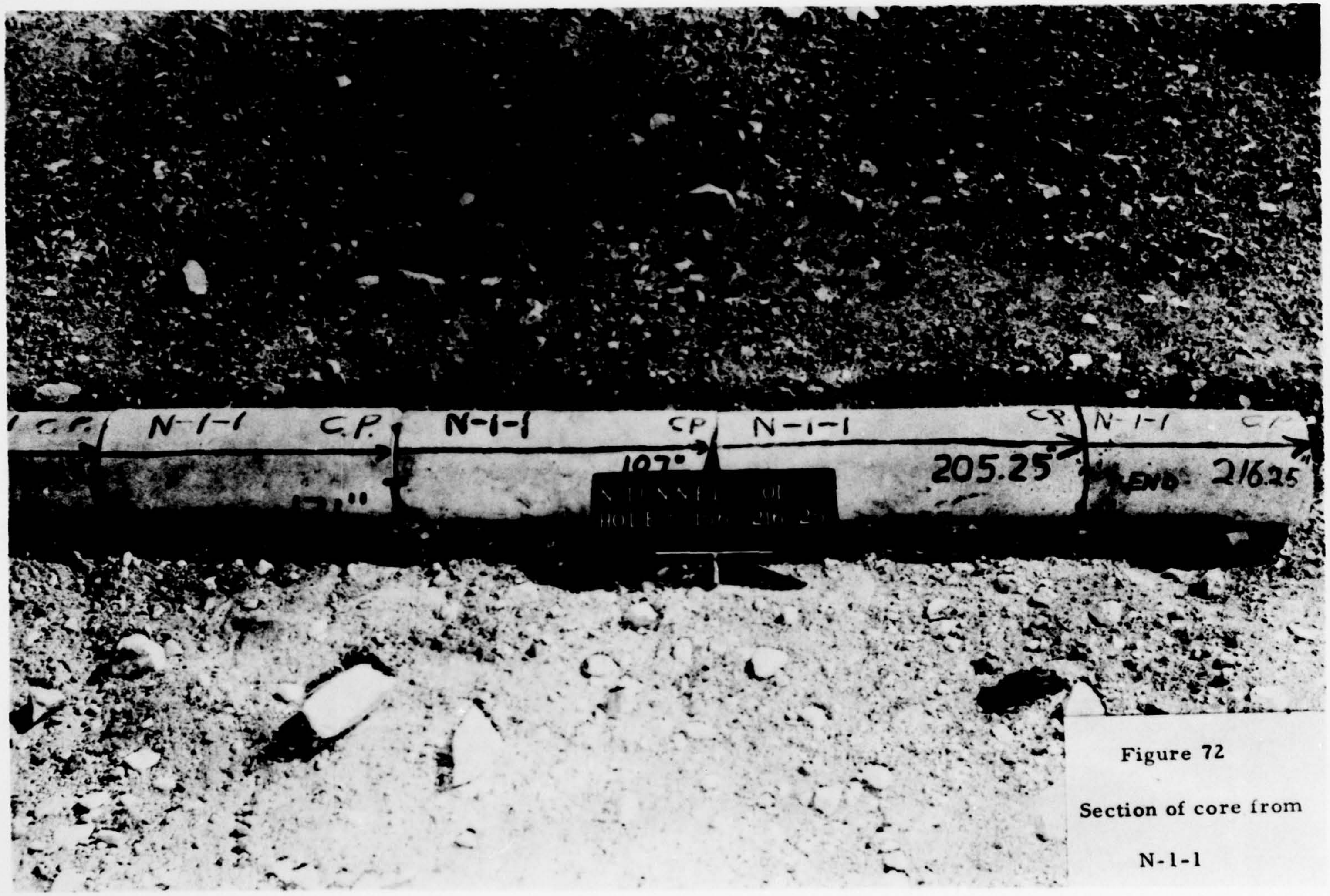

Figure 72

Section of core from

N-1-1

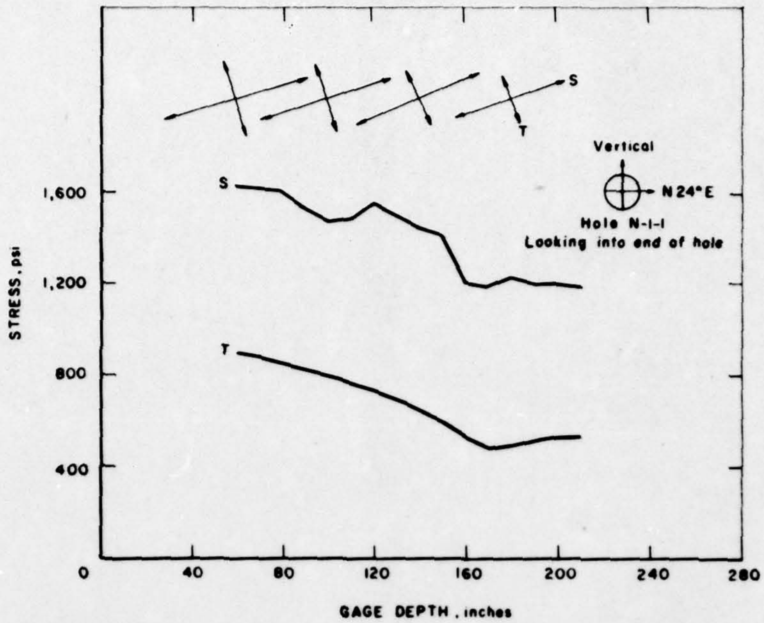

Figure 73 - **Stress versus distance from face - hole N-1-1**

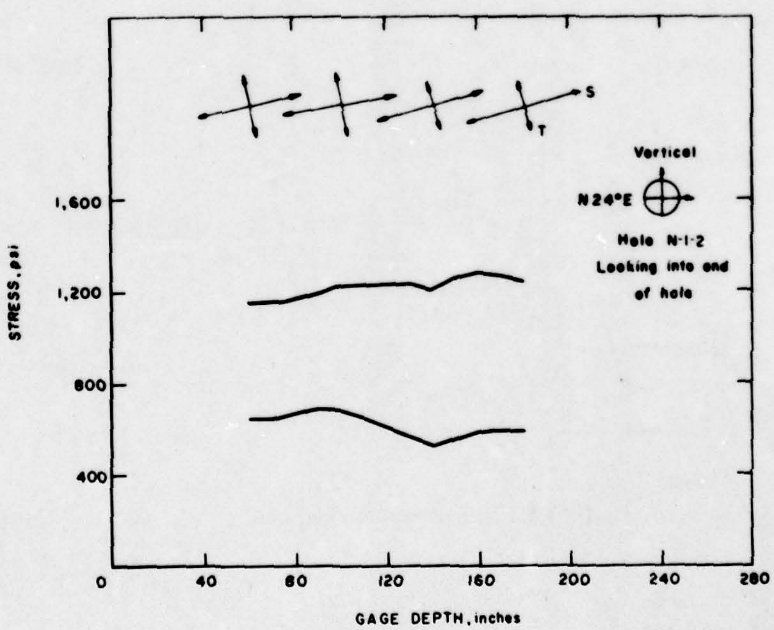

Figure 74 - **Stress versus distance from face - hole N-1-2**

Figure 75

Core from hole

N-1-4

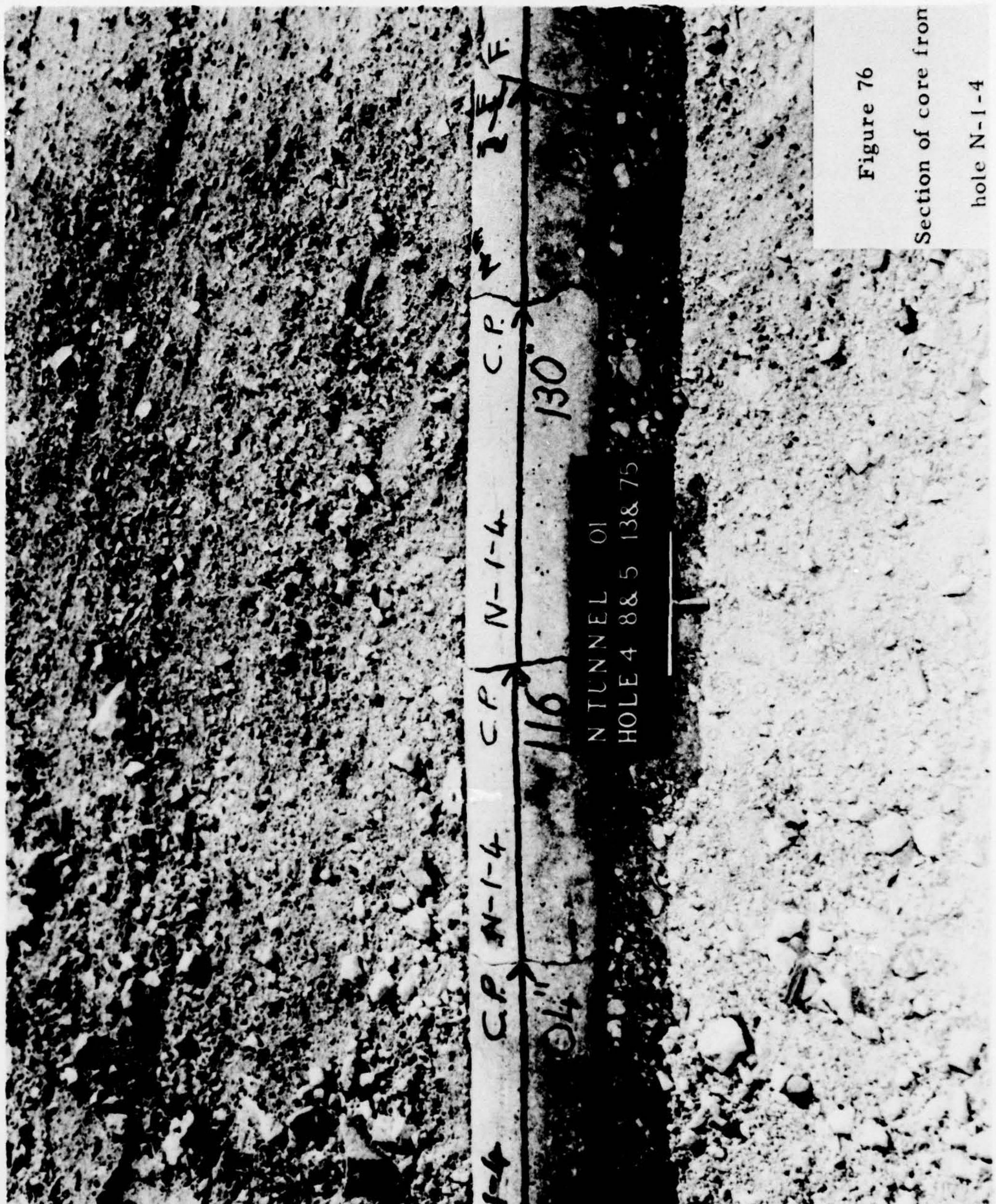

Figure 76
Section of core from
hole N-1-4

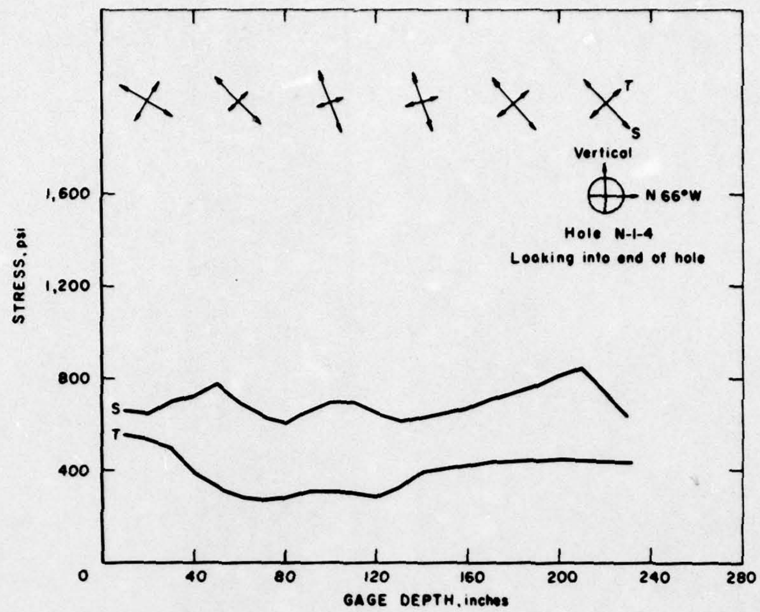

Figure 77 - Stress versus distance from face - hole N-1-4

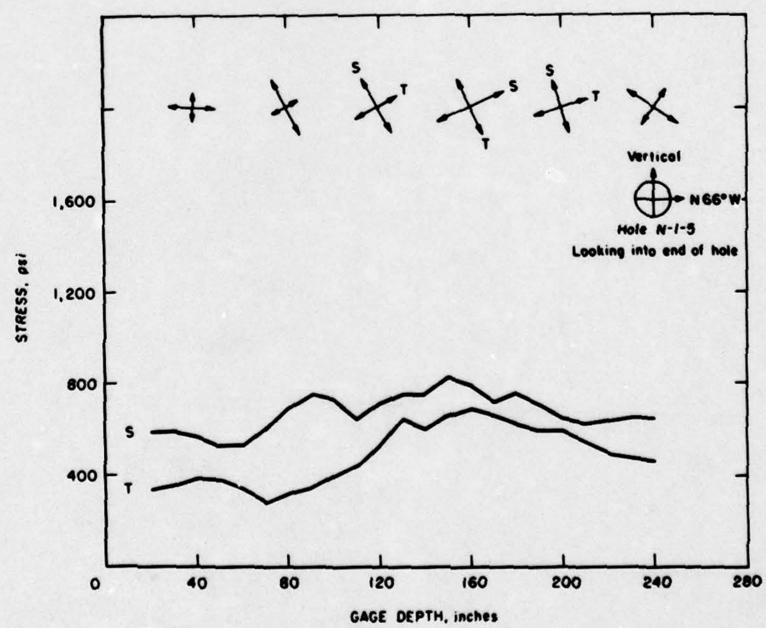

Figure 78 - Stress versus distance from face - hole N-1-5

Figure 79

Section of core from hole N-1-6

Figure 80

Section of core from hole N-2-1

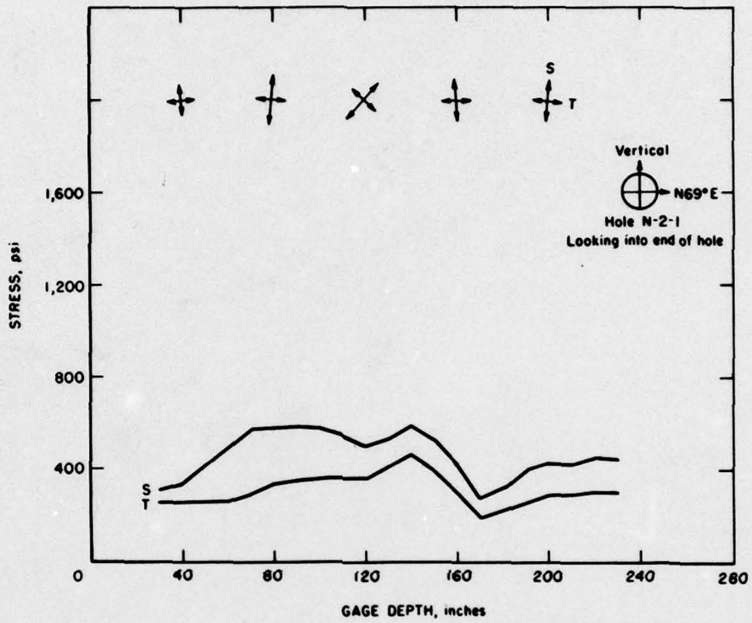

Figure 81 - Stress versus distance from face - hole N-2-1

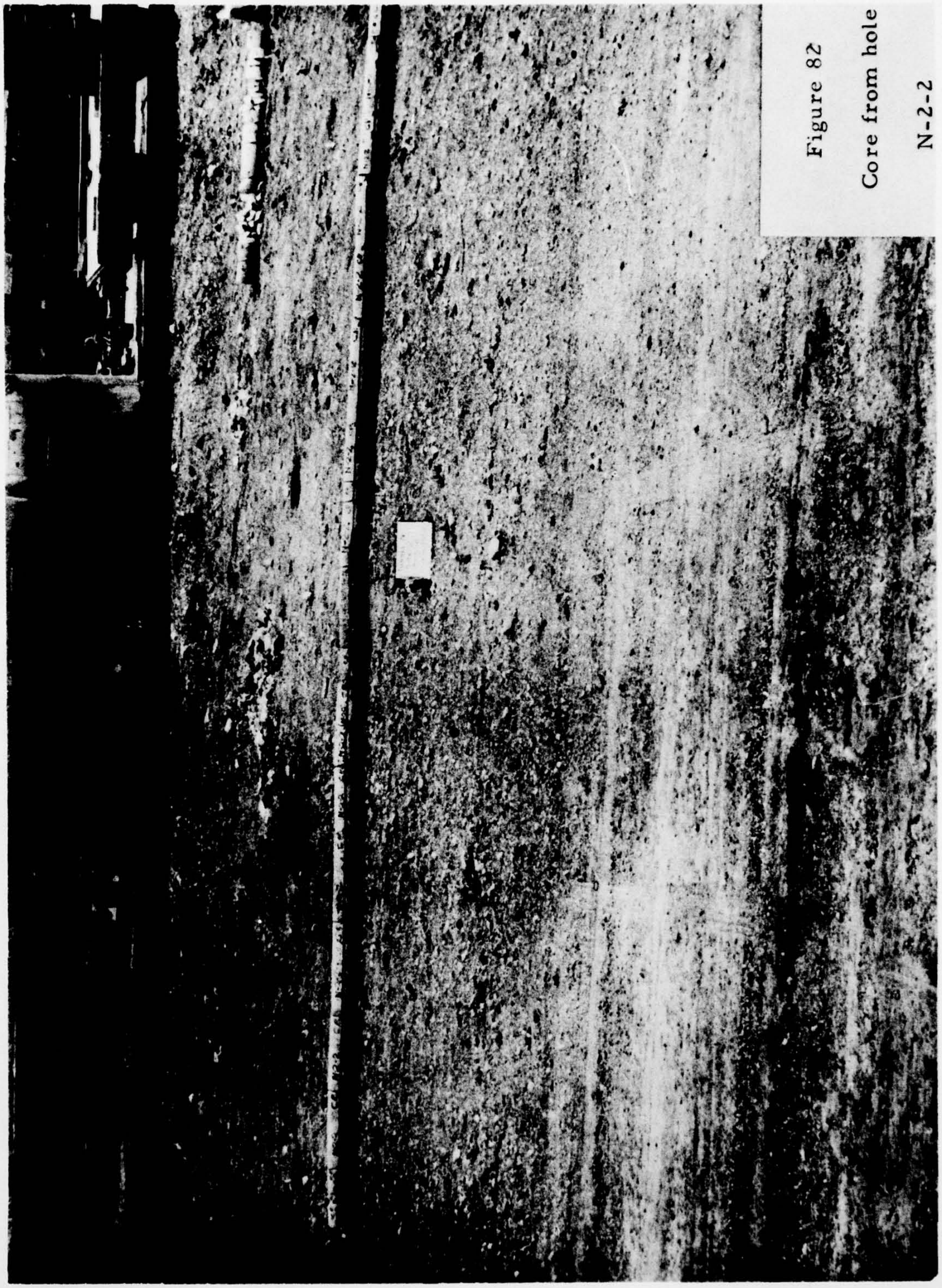

Figure 82

Core from hole

N-2-2

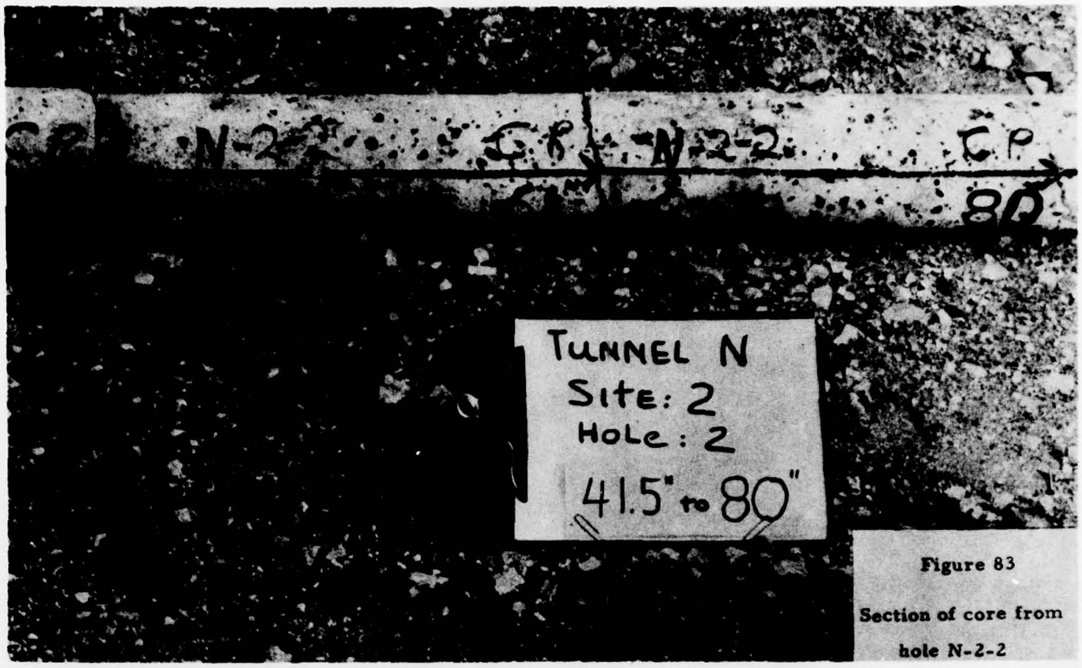

Figure 83

Section of core from hole N-2-2

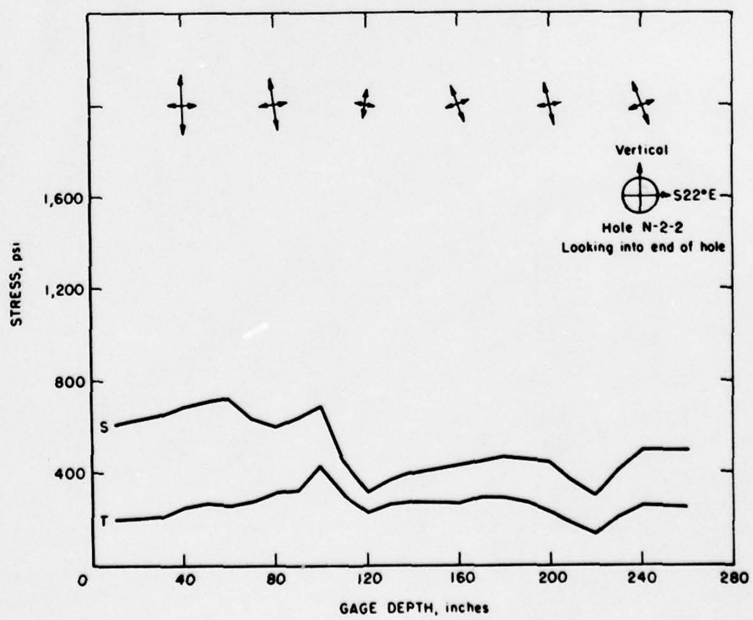

Figure 84 - Stress versus distance from face - hole N-2-2

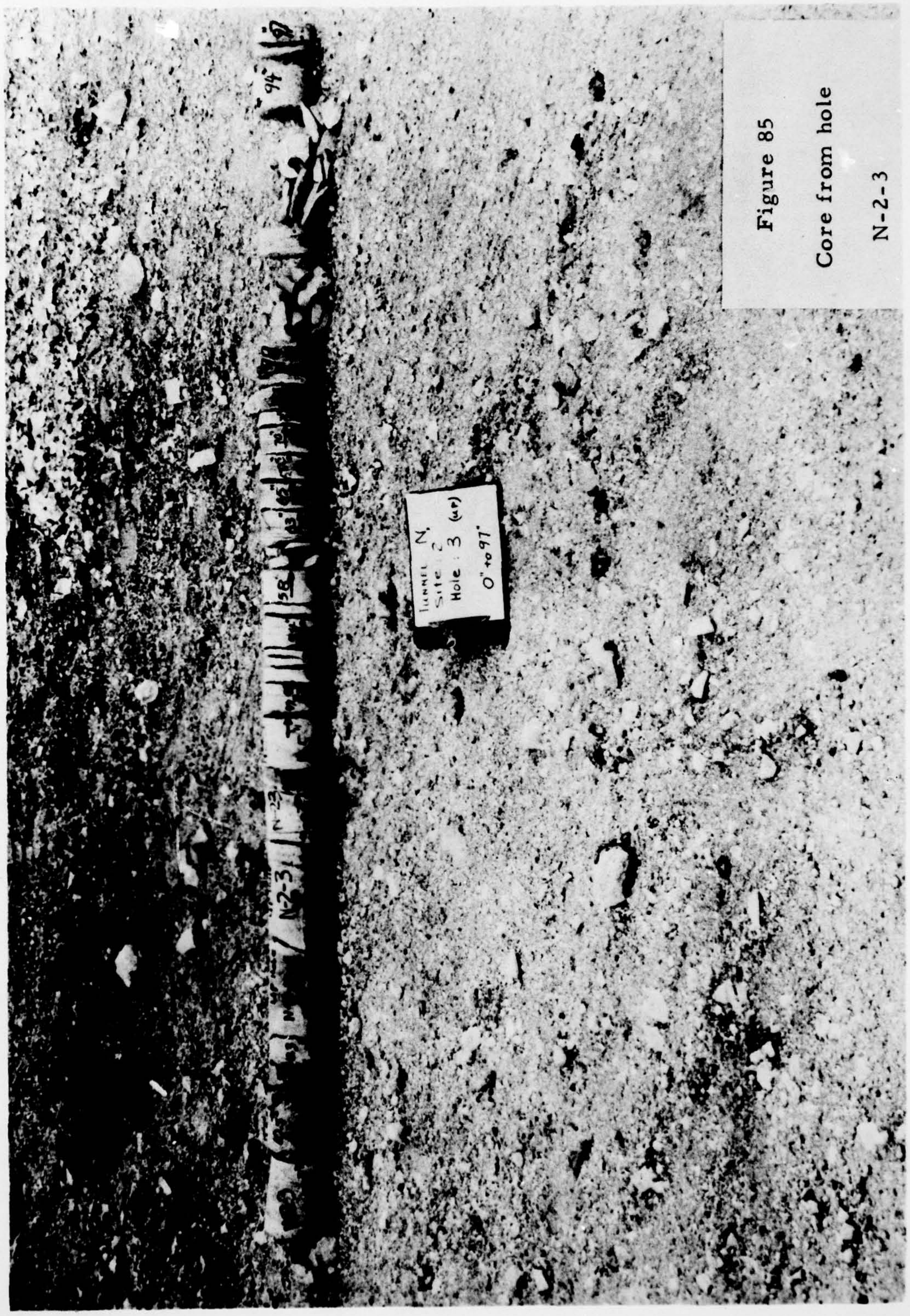

Figure 85
Core from hole
N-2-3

AD-A073 527 DEFENSE ATOMIC SUPPORT AGENCY WASHINGTON DC F/G 18/3
OPERATIONS NOUGAT AND STORAX IN SITU STRESSES IN ROCK, RAINIER --ETC(U)
SEP 64 L OBERT
UNCLASSIFIED DASA-WT-1869 NL

2 OF 2
AD A073527

END
DATE
FILMED
10-79
DDC

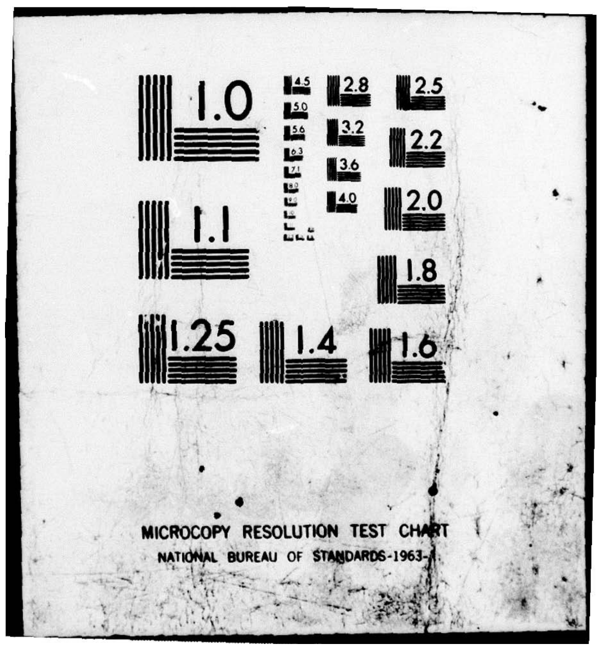
1.0
4.5
5.0
5.6
6.3
7.1
2.8
3.2
3.6
4.0
2.5
2.2
2.0
1.1
1.8
1.25
1.4
1.6
MICROCOPY RESOLUTION TEST CHART
NATIONAL BUREAU OF STANDARDS-1963-A

Table 1. Test sites - Madison and Yuba Tunnels

Tunnel	Site	Drift designation	Coordinates	Floor elevation feet	Overburden depth-feet
G	1	U12g .01	N 880,671-E 634,262	6,159	1,300
G	2	Main tunnel	N 882,075-E 635,205	6,142	640
B	1	U12b .10	N 890,643-E 633,073	6,635	780
B	2	U12t .10	N 890,944-E 633,905	6,635	790
B	3	U12b Bypass	N 891,106-E 633,855	6,635	785
E	1	U12e .06	N 885,103-E 631,912	6,175	1,425
P	1	U12p	N 904,212-E 648,212	5,414	780
N	1	L.O.S. No2	N 893,295-E 635,630	6,057	1,180
N	2	U12n	N 893,560-E 635,650	6,045	695

Table 2. Designation and bearing of stress-relief holes

Tunnel	Site	Hole	Bearing of hole		Comments
G	1	G-1-1	Horizontal	S 75° 31' W	
		G-1-2	Horizontal	N 14° 30' W	
		G-1-3	Vertical (down)	S 75° 31' W(U_1)	
	2	G-2-1a	Horizontal	N 22° 40' W	Non-feasible
		G-2-1	Horizontal	N 22° 40' W	
		G-2-2	Horizontal	N 66° 50' W	Non-feasible
		G-2-3	Vertical (down)	N 22° 40' W(U_1)	Non-feasible
		G-2-4	Horizontal	N 66° 50' E	Non-feasible
		G-2-5	Horizontal	N 22° 40' W	
		G-2-6	Vertical (down)	N 22° 30' W(U_1)	Non-feasible
B	1	B-1-1	Horizontal	S 39° 20' W	
		B-1-2	Horizontal	S 39° 20' W	
		B-1-3	Horizontal	N 49° 40' W	
		B-1-4	Horizontal	N 49° 40' W	
		B-1-5	Vertical	S 39° 20' W(U_1)	
	2	B-2-1	Horizontal	N 63° 10' W	Non-feasible
	3	B-3-1	Horizontal	S 89° 30' W	Non-feasible
E	1	E-1-1	Horizontal	S 87° 55' W	Data insufficient
		E-1-2	Horizontal	S 87° 55' W	
		E-1-3	Horizontal	N 0° 44' W	
		E-1-4	Vertical (up)	S 87° 55' W(U_1)	
		E-1-5	Horizontal	S 87° 55' W	
		E-1-6	Horizontal	N 0° 45' W	
P	1	P-1-1	Horizontal	N 16° 57' W	
		P-1-2	Horizontal	N 71° 56' E	
		P-1-3	Vertical (up)	N 17° W(U_1)	Data insufficient
		P-1-4	Vertical (up)	N 17° W(U_1)	Data insufficient
N	1	N-1-1	Horizontal	N 66° 07' W	
		N-1-2	Horizontal	N 66° 07' W	
		N-1-3	Horizontal	N 24° 0 ' E	Non-feasible
		N-1-4	Horizontal	N 24° 0 ' E	
		N-1-5	Horizontal	N 24° 0 ' E	
		N-1-6	Vertical (up)		Non-feasible
		N-1-7	Vertical (down)		Non-feasible
	2	N-2-1	Horizontal	N 21° 46' W	
		N-2-2	Horizontal	N 68° 0 ' E	
		N-2-3	Vertical (down)		Non-feasible
		N-2-4	Vertical (up)		Non-feasible

Table 3. Uniaxial and triaxial strengths of tuff from Madison and Yuba sites [1/]

Hole	Depth inch	C_o [2/] psi	σ_3 psi	$p_o = \sigma_1$ psi	θ degrees	S_o psi	$S_o(Av)$ [3/] psi	C'_o psi	μ
G-1-1	21	-4,360							
G-1-2	31	-2,700							
G-1-3	68	-2,860							
G-2-1	31	-2,440							
G-2-1	65		-3,720	-500	36	1,000	900A	-3550	0.32
G-2-2	61		-5,663	-1,000	40	1,800			0.18
G-2-2	88	-2,775							
B-1-1	16	-423							
B-1-1	24	-402							
B-1-3	19	-414							
B-1-3	26	-560							
E-1-2	249	-3,870							
E-1-2	252	-3,540							
E-1-2	269		-3,638	-400	30	850			0.58
E-1-2	288		-2,852	-400	0				
E-1-3	188	-1,840							
E-1-3	191	-2,060							
E-1-3	205		-3,762	-400	33	950	750 A	-2670	0.44
E-1-3	245		-3,638	-200	22	550			1.04
E-1-4	14	-2,040							
E-1-4	17	-1,980							
P-1-1	36		-10,335	-250	27	2,450			0.73
P-1-1	59	-6,500							
P-1-1	61	-7,300							
P-1-2	66		-6,118	-250	17	600	800 A	-4900	1.48
P-1-2	113		-10,045	-250	16	1,000			1.60
P-1-2	144	-12,100							
P-1-2	146	-11,680							
N-1-1	263	-6,200							
N-1-1	265	-6,280							
N-1-1	237		-5,870	-500	33	1,500	1,175 A	-4500	0.44
N-1-1	257		-6,614	-400	22	850			1.04
N-1-4	284	-2,230							
N-1-4	287	-2,450							
N-1-4	29		-6,614	-1,000	37	1,850	1,000 E	-3350	0.29
N-1-4	260		-4,961	-500	29	950	1,400 A		0.62
N-2-1	40	-4,880							
N-2-1	51	-3,910							
N-2-1	43		-3,286	-500	31	600	750 E	-2100	0.53
N-2-1	65		-4,444	-1,000	27	200	400 A		0.73
N-2-2	48	-2,400							
N-2-2	50	-2,200							

1/ Definition of symbols

C_o = Uniaxial compressive strength - 1D - NX specimen (psi) (Negative values indicate compression)

σ_3 = Axial load on 5-5/8 x 10-1/2-inch triaxial specimen (psi)

p_o = Radial pressure on 5-5/8 x 10-1/2-inch triaxial specimen (psi)

θ = Fracture angle with respect to σ_3, triaxial specimen (degrees)

S_o = Triaxial shear strength (from Mohr's envelope) (psi)

$S_o(Av)$= Average triaxial shear strength (psi)

C'_o = Triaxial compressive strength (from Mohr's envelope) (psi)

μ = Coefficient of internal friction cot 2θ.

2/ By LPI

3/ A designates $S_o(Av)$ obtained from average of S_o.

E designates $S_o(Av)$ obtained from Mohr's envelope for 2 specimens.

Table 4. Biaxial and triaxial elastic properties of tuff from Madison and Yuba sites

Hole	Depth from Collar-inch	Biaxial secant modulus of elasticity, psi, at gage orientation			Triaxial secant modulus of elasticity, psi by	
		0°	90°	Aver.	$\frac{\sigma_z}{\epsilon_z}$	$\frac{p_o}{U}$
G-1-1(NX)[1]	16	1.26				
G-1-1	25	1.27	1.27	1.27		
G-1-1	82				0.92	1.18
G-1-1	121	0.90	1.00	0.95		
G-1-2	28					0.76
G-1-2	71	1.41	1.37	1.39		
G-1-2	133	0.96	0.94	0.95		
G-1-3	37	0.86	0.83	0.85		
G-1-3	61	0.71	0.80	0.74		
G-1-3	78					0.72
G-2-1(NX)[1]	32	0.55				
G-2-1	34	0.79	0.60	0.70		
G-2-1	137	0.69	0.59	0.64		
G-2-2	29	0.55	0.40	0.48		
G-2-2	92	0.77	0.76	0.77		1.05
G-2-3	74	1.20	0.92	1.06	0.70	1.31
G-2-5	33				0.31	0.22
G-2-5	158	0.26	0.34	0.30	0.24	
G-2-5	171				0.36	0.21
B-1-1	10	0.26	0.27	0.26		
B-1-1a	33				0.27	
B-1-1	120				0.26	
B-1-1	140	0.26	0.28	0.27		
B-1-2	40	0.32	0.33	0.32		
B-1-2	97	0.29	0.35	0.32		
B-1-3	21	0.42	0.48	0.45		
B-1-3	113	0.43	0.45	0.44		
B-1-4	112	0.29	0.33	0.31		
B-1-5 [1]	66		0.99			
E-1-2	40	0.48	0.61	0.55		
E-1-2	184	0.85	0.64	0.75		
E-1-2	247				0.78	0.77
E-1-3	79	0.46	0.59	0.53		
E-1-3	170	0.62	0.68	0.65		
E-1-4	45				0.65	0.62
E-1-4	56	0.69	0.66	0.68		
E-1-4	109				0.67	0.69
E-1-4	113	0.52	0.54	0.53		
E-1-5	212	0.57	0.54	0.56		
E-1-6	57	0.40	0.42	0.41		
E-1-6	193	0.46	0.40	0.43		
P-1-1	9	1.37	1.48	1.43		
P-1-1	28				1.54	1.67
P-1-1	133				1.82	2.05
P-1-1	141	1.78	1.90	1.84		
P-1-2	38	1.65	1.72	1.71		
		1.78	1.68			

Table 4. Continued

Hole	Depth from Collar-inch	Biaxial secant modulus of elasticity, psi, at gage orientation			Triaxial secant modulus of elasticity, psi by	
		0^{o}	90^{o}	Aver.	$\frac{\sigma_z}{\varepsilon_z}$	$\frac{P_o}{U}$
P-1-2	70				1.73	1.86
P-1-2	210	2.15	2.06	2.08		
		2.15	1.94			
P-1-2	238					1.62
N-1-1	118	0.88	0.58	0.73		
N-1-1	146					0.93
N-1-1	193	0.74	0.53	0.64		
N-1-2	78	0.62	0.48	0.55		
N-1-2	131				0.70	0.93
N-1-2	156	0.69	0.54	0.62		
N-1-2	185					0.76
N-1-4	74					0.98
N-1-4	80	0.64	0.68	0.69		
		0.66	0.67			
N-1-5	99				0.45	0.58
N-1-5	137	0.74	0.77	0.77		
		0.75	0.81			
N-2-1	59	0.40	0.44	0.43		
		0.41	0.45			
N-2-1	89					0.45
N-2-1	195				0.29	0.21
N-2-1	198	0.11	0.14	0.13		
N-2-2	80				0.33	
N-2-2	85	0.47	0.54	0.52		
		0.48	0.56			
N-2-2	141	0.14	0.18	0.17		
		0.15	0.16			
N-2-2	233				0.27	
N-2-2	237	0.35	0.34	0.36		
		0.35	0.37			

1/ *Uniaxial*

Table 5 - Summary of stress measurements

Site	Hole	S_∞ psi	T_∞ psi	Direction 2/ with respect to vertical	S_{max} psi	Stress concentration	Stress Field: Gravity	Stress Field: Gravity plus tectonic
G-1	G-1-1	320	170	0°	1,900	6 (?)	X 1/	
"	G-1-2	670	410	0°	1,670	2.5	X 1/	
"	G-1-3(down)	750	240	NS	950	1.3	X 1/	
G-2	G-2-1	800	360	30°	--	0		X
"	G-2-5	440	280	15°	--	0		X
B-1	B-1-1	480	220	0°	660	1.4	X	
"	B-1-2	620	300	0°	530	1.2	X	
"	B-1-3	460	330	75°	850	1.8	X 1/	
"	B-1-4	400	370	75°	900	2.2	X 1/	
"	B-1-5(up)	260	150	NS	360	--	X 1/	
E-1	E-1-2	640	420	60°	800	1.2	X 1/	
"	E-1-5	515	350	70°	800	1.5	X 1/	
"	E-1-3	360	250	70°	850	2.4	X 1/	
"	E-1-6	360	220	70°	620	1.7	X 1/	
"	E-1-4(up)	680	480	N 30 E	680	0	X 1/	
P-1	P-1-1	960	740	70°	1,200	1.3		X
"	P-1-2	1,160	470	0°	1,680	1.4		X
N-1	N-1-1	1,180	520	70°	1,620	1.3		X
"	N-1-2	1,240	600	70°	1,240	0		X
"	N-1-4	640	440	40°	840	0		X
"	N-1-5	640	450	50°	810	0		X
N-2	N-2-1	440	250	0°	590	0	X	
"	N-2-2	480	250	15°	720	0	X	

1/ Apparently affected by local geology

2/ Excepting for up or down holes

REFERENCES

1. FITZPATRICK, J.; Biaxial Device for Determining the Modulus of Elasticity of Stress-Relief Cores, BuMines Rept. of Inv. 6128, 1962, 13 pp.

2. OBERT, L., W. I. Duvall, and S. L. Windes; Standardized Tests for Determining the Physical Properties of Mine Rock, BuMines Rept. of Inv. 3891, 1946, 67 pp.

3. OBERT, L.; An Inexpensive Apparatus for Testing Mine Rock, BuMines Rept. of Inv. 6332, 1963, 10 pp.

4. OBERT, L.; Triaxial Method for Determining the Elastic Constants of Stress Relief Cores, BuMines Rept. of Inv. (In press)

5. OBERT, L.; In Situ Determination of Stress in Rock, Mining Engineering, v. 14, No. 8, August 1962, pp 51-58.